ADAPT & OVERCOME: HYPOXIA RESISTANCE IS A NOVEL PHENOTYPE OF THE FLEXOR DIGITORUM BREVIS SKELETAL MUSCLE

by

Everett Charles Minchew

December 2023

Director of Dissertation: Espen E. Spangenburg

Major Department: Physiology

Abstract

Skeletal muscle comprises the largest mammalian organ system by mass that enables movement, respiration, and thermogenesis. Each of these processes requires the presence of molecular oxygen (O_2). Inadequate O_2 bioavailability (i.e., hypoxia) is detrimental to muscle contractile function and morphology, and in chronic cases can result in muscle wasting. Importantly, modern therapeutics and surgical approaches have proven largely ineffective to rescue skeletal muscle from hypoxic damage. Such a gap in the field is attributed predominantly to the fact that known skeletal muscles are highly susceptible to hypoxic insults. Thus, current knowledge of specific cellular properties that promote hypoxia resistance is sparse. However, our lab has identified a murine skeletal muscle that retains physiological function in the complete absence of O_2. Using models of *in vivo* hindlimb ischemia and *ex vivo* muscle hypoxia exposure, we observed the preservation of force production and plasma membrane stability in the flexor digitorum brevis (FDB). In contrast, the extensor digitorum longus (EDL) and soleus muscles suffered functional decline and structural damage following the same hypoxic insults.

A critical aspect of hypoxia resistance in the FDB is the ability to sustain energetic charge. Hypoxia decreases the mass action ratio of adenosine triphosphate ([ATP]) to adenosine

diphosphate ([ADP]), which determines the capacity of a cell to perform work. However, the [ATP]/[ADP] ratio is maintained by the hypoxic FDB. Contrary to the EDL and soleus, we found that the FDB does not depend upon the mitochondria but requires glycolysis to function during hypoxia. Furthermore, the hypoxic FDB preserves stability of the plasma membrane whereas hypoxia causes membrane damage in the EDL and soleus. Following an unbiased, discovery-based interrogation of muscle proteomes, we identified significantly higher expression of multiple protein targets in the FDB as compared to the EDL and soleus that related to our findings.

Due to the loss of force output in the FDB with inhibition of glycolysis, we selected the transmembrane glucose transporter GLUT1 as our first target. Loss- and gain-of-function experiments surrounding GLUT1 were employed to further characterize the FDB phenotype. Skeletal muscle-specific deletion of GLUT1 accelerated the loss of force output in the FDB during hypoxia exposure. Thus, to test the sufficiency of GLUT1 to attenuate hypoxia-induced damage in other skeletal muscles, we utilized an adeno-associated virus (AAV) to overexpress GLUT1 in the EDL. During these experiments we also manipulated concentrations of glucose and the oxidized form of ascorbic acid as these are the primary substrates that are transported by GLUT1. However, all conditions failed to prevent the loss of force production of the EDL during hypoxia exposure. Collectively, our results demonstrate that GLUT1 is necessary for the FDB phenotype, but insufficient to rescue other skeletal muscles from functional decline in a hypoxic environment.

Due to the preservation of structural integrity in the FDB during hypoxia, we selected the membrane repair protein Annexin A2 and the extracellular matrix protein Col5a1 as our second and third targets, respectively. In separate sets of experiments, FDBs lacking Annexin A2 and Col5a1 did not demonstrate increased susceptibility to hypoxic damage as compared to control muscles. Importantly, however, using the same experimental approach that revealed the FDB's ability to resist hypoxia, we have observed that the phenotype is adapted over time as opposed to an innate feature of the muscle. Hypoxic FDBs from young mice (4 weeks) exhibit a loss of force output and structural integrity in a manner that is similar to the hypoxic EDL. Following our

observation of this apparent adaptation, we employed a proteomic analysis of FDBs from adult and young mice to further characterize differences between age groups. We subsequently integrated this data with our initial discovery-based proteomics analysis of the FDB, EDL, and soleus with the goal of improving the precision of our future target selection. Collectively, the data suggest that the FDB's ability to survive hypoxia may be conferred by protection against structural damage via stabilization of the dystrophin-glycoprotein protein complex (DGC), which links the muscle plasma membrane to the extracellular matrix. In turn, structural protection likely promotes the maintenance of physiological function in the hypoxic FDB. Defining the FDB's unique ability to resist hypoxic damage remains of critical importance for the muscle biology field to develop novel therapeutic approaches that promote the survival of skeletal muscle during times of limited O_2 availability.

ADAPT & OVERCOME: HYPOXIA RESISTANCE IS A NOVEL PHENOTYPE OF THE FLEXOR DIGITORUM BREVIS SKELETAL MUSCLE

A Dissertation

Presented to the faculty of the Department of Physiology

East Carolina University

In Partial Fulfillment of the Requirements of the Degree of

Doctor of Philosophy in Physiology

by

Everett Charles Minchew

December 2023

ADAPT & OVERCOME: HYPOXIA RESISTANCE IS A NOVEL PHENOTYPE OF THE FLEXOR DIGITORUM BREVIS SKELETAL MUSCLE

by

Everett Charles Minchew

APPROVED BY:

DIRECTOR OF

DISSERTATION: _____

Espen E. Spangenburg, PhD

COMMITTEE MEMBER: _____

Joseph M. McClung, PhD

COMMITTEE MEMBER: _____

Johanna L. Hannan, PhD

COMMITTEE MEMBER: _____

Nicholas T. Broskey, PhD

CHAIR OF THE DEPARTMENT

OF PHYSIOLOGY: _____

Espen E. Spangenburg, PhD

DEAN OF THE

GRADUATE SCHOOL : _____

Kathleen T. Cox, PhD

ACKNOWLEDGEMENTS

First and foremost, I would like to express my heartfelt gratitude for my advisor, Dr. Espen Spangenburg, whose guidance has proven invaluable towards both my scientific and personal development. Despite the risk, you took a chance on a 22-year-old kid who had never held a pipet prior to setting foot in the lab. You remained patient, understanding, and supportive through various trials and tribulations. Your commitment to mentorship throughout a global pandemic and appointments to serve as the chair of two different academic departments is incredibly commendable. I am proud to have learned from you.

I would next like to thank the members of my dissertation committee – Dr. Joe McClung, Dr. Johanna Hannan, and Dr. Nick Broskey. The quality and rigor of this dissertation has benefitted tremendously from your knowledgeable insight. Alongside my committee, I would like to extend my deepest appreciation to the members of the Spangeburg Lab, both past and present, for their contributions to this research. Specifically, I would like to thank Dr. Adam Amorese and Dr. Mike Tarpey, whose instruction has molded my scientific competence, and my right hand man – Andrew Readyoff – whose assistance made this dissertation possible.

Last, but certainly not least, I would like to thank the two most important women in my life – my mother, Nancy, and my life partner, Jenny. Without your unwavering support and unconditional love, I would not be the man I am today. You have pushed me to be the best version of myself at all times. For these reasons and more, I am forever indebted to you both.

TABLE OF CONTENTS

LIST OF TABLES

CHAPTER 3

CHAPTER 4

LIST OF FIGURES

CHAPTER 3

CHAPTER 4

LIST OF SYMBOLS & ABBREVIATONS

ΔG_{ATP} – ATP-free energy

$\Delta\Psi$ – mitochondrial membrane potential

µg – microgram

µL – microliter

µm – micrometer

µM – micromolar

AAV – adeno-associated virus

ACh – acetylcholine

ADP – adenosine diphosphate

AMP – adenosine monophosphate

AP – action potential

ATP – adenosine triphosphate

BCA – Bicinchoninic acid

BrP – bromopyruvate

Ca^{2+} – calcium

$CaCl_2$ – calcium chloride

CHF – congestive heart failure

CK – creatine kinase

CO_2 – carbon dioxide

COPD – chronic obstructive pulmonary disease

CSA – cross-sectional area

DCG - dystrophin-glycoprotein complex

DHPR – dihydropyridine receptor

DMD – Duchenne muscular dystrophy

DNA – deoxyribonucleic acid

DTT – dithiothreitol

ECM – extracellular matrix

EDL – extensor digitorum longus

ETS – electron transport system

$FADH_2$ – flavin adenine dinucleotide

FDB – flexor digitorum brevis

GAPDH – glyceraldehyde 3-phosphate

GFP – green fluorescent protein

GLUT1 – glucose transporter 1

Gpx3 – glutathione peroxidase 3

GSH – glutathione

H&E – hematoxylin and eosin

HEPES – 4-(2-hydroxyethyl)-1-piperazineethanesulfonic acid

HLI – hindlimb ischemia

IAM – iodoacetamide

IMP – inosine monophosphate

JO_2 – mitochondrial oxygen consumption rate

KCl – potassium chloride

KCN – potassium cyanide

KH_2PO_4 – potassium phosphate

KO – knockout

KOH – potassium hydroxide

kPa – kilopascal

L_0 – optimal muscle length

LDPI – laser Doppler perfusion imaging

MEF – mitochondrial enrichment factor

mg – milligram

$MgCl_2$ – magnesium chloride

$MgSO_4$ – magnesium sulfate

MHC – myosin heavy chain

mins – minutes

mRNA – messenger ribonucleic acid

ms – millisecond

N/cm^2 – newtons per square centimeter

N_2 – nitrogen

$Na_4P_2O_7$ – tetrasodium pyrophosphate

NaCl – sodium chloride

NAD – nicotinamide adenine nucleotide

NADH – nicotinamide adenine nucleotide + hydrogen

NaF – sodium fluoride

$NaHCO_3$ – sodium bicarbonate

nm – nanometer

nM – nanomolar

nmol – nanomolar

O_2 – oxygen

OCT – optimal cutting temperature

P11 – protein S100A10

PAD – peripheral artery disease

PBS – phosphate buffered saline

PCA – perchloric acid

PCr – phosphocreatine

PMFB – permeabilized muscle fiber bundles

PMR – plasma membrane repair

PPP – pentose phosphate pathway

ROS – reactive oxygen species

RYR – ryanodine receptor

s – second

SERCA – sarco-endoplasmic reticulum calcium ATPase

shRNA – short hairpin ribonucleic acid

SLC2A1 – gene name for glucose transporter 1

SOD3 – superoxide dismutase 3

SR – sarcoplasmic reticulum

TFA – trifluoroacetic acid

TMRM – tetramethyl rhodamine methyl ester

UPLC – ultra-performance liquid chromatography

VO_2max – maximal rate of oxygen uptake

WGA – wheat germ agglutinin

WT – wildtype

CHAPTER 1: Introduction and Specific Aims

Introduction

The necessity of oxygen (O_2) for cell function and survival is a universal principle of mammalian biology. Therefore, maintaining O_2 homeostasis is critical for biological systems. Hypoxia is generally defined as compromised O_2 availability within a given system, which can occur due to environmental and/or pathological conditions. Hypoxia is detrimental to cell structure and function, especially within tissues that exhibit high energetic demands like skeletal muscle. Regardless of the mechanism by which hypoxia occurs, the insult must be transient to avoid muscle damage. If O_2 tension is not restored, a resulting decline in muscle mass and strength will decrease an individual's functional independence and increase mortality risk (Fitzgerald et al., 2004). Muscle quality (i.e., force produced per unit mass) is a critical indicator of morbidity and all-cause mortality in humans (Knowles et al., 2021; Li et al., 2018; Srikanthan & Karlamangla, 2014; Wang et al., 2019). Thus, it is necessary to identify mechanisms that tissues like skeletal muscle can utilize to survive hypoxia.

In a serendipitous fashion, our lab discovered that, contrary to other skeletal muscles, the murine flexor digitorum brevis (FDB) is capable of maintaining physiological function in the complete absence of O_2. We first identified the hypoxia-resistant phenotype of the FDB during contractile experiments following the induction of *in vivo* hindlimb ischemia (HLI). The HLI surgery involves ligation and transection of the femoral artery, which eliminates blood flow and O_2 delivery to distal tissue (Schmidt et al., 2018). Current dogma holds that the severity of tissue damage is greater in tissue located more distal to the site of an arterial occlusion as compared to more proximal tissue. Located at the bottom aspect of the foot, the FDB is among the most distal muscles from the occlusion site. However, in contrast to the more proximal extensor digitorum longus (EDL) and soleus muscles that suffer force loss following HLI, force output of the FDB remained unaltered despite the same loss of O_2 tension. Our *in vivo* findings were confirmed via *ex vivo* experiments during which muscles were exposed to hypoxia and stimulated maximally at

regular intervals within an isolated tissue bath system. Similar to HLI, the EDL and soleus exhibited a loss of force output whereas the FDB maintained force output for a significantly longer duration of time under the same hypoxic conditions.

In addition to preserved contractile function, the FDB maintains stability of the muscle plasma membrane (sarcolemma) during hypoxia. Sarcolemmal disruption is a consequence of hypoxia exposure that allows for the entry of extracellular molecules into the cell. Previous work has suggested that uncontrolled influx of extracellular Ca^{2+} is a contributing factor to sarcolemmal injury during hypoxia (Fredsted et al., 2005). Elevations in resting intracellular Ca^{2+} concentrations ($[Ca^{2+}]_i$) occur in various models that induce muscle hypoxia, and hypoxia-induced membrane damage can be attenuated by decreasing $[Ca^{2+}]$ in the incubation buffer (Jones et al., 1984). Our initial data suggest that protection of the FDB sarcolemma during hypoxia is associated with resistance to cytosolic Ca^{2+} overload. In skeletal muscles that are susceptible to hypoxia, Ca^{2+} influx induces a phenomenon called “excitotoxicity” which is a gradual rise in resting tension of the muscle. We have observed the development of excitotoxity in the hypoxic EDL and soleus, however resting tension of the FDB does not increase to the same degree as other skeletal muscles during hypoxia.

With the goal of defining the mechanisms that confer skeletal muscle hypoxia resistance, a set of specific aims has been developed to investigate the unique ability of the FDB to maintain force production and structural integrity during hypoxia.

Aim 1: To determine if unique bioenergetic programming promotes hypoxia resistance in the FDB. *Rationale:* O_2 serves as the terminal electron acceptor within the mitochondrial electron transport system, which synthesizes up to 90% of the ATP that is hydrolyzed to fuel myocellular work (Salin et al., 2015). Importantly, the extent to which the mass action ratio of ATP to ADP is displaced

from equilibrium determines the capacity of a cell to perform work (Fisher-Wellman et al., 2018; Nicholls, 2013). During hypoxia the [ATP]/[ADP] ratio moves closer to equilibrium in the EDL and soleus, which impairs ATP-consuming reactions like force production. In contrast, the [ATP]/[ADP] ratio is maintained by the hypoxic FDB. We found that the FDB does not depend upon the mitochondria to function during hypoxia, however glycolysis is indeed required for the FDB phenotype. Our proteomic analysis identified significantly higher expression of the glucose transporter GLUT1 in the FDB as compared to the EDL and soleus. Accordingly, we hypothesize that elevated GLUT1 content confers protection of the FDB by increasing glucose import for accelerated rates of glycolysis to sustain force production during hypoxia. In addition to glucose, GLUT1 is responsible for importing the oxidized form of the antioxidant ascorbic acid – dehydroascorbate. Thus, we hypothesize that elevated GLUT1 content defends the FDB from hypoxia-induced redox stress by importing high levels of dehydroascorbate.

Aim 2: To determine if unique structural protection promotes hypoxia resistance in the FDB.

Rationale: Hypoxia has been demonstrated to disrupt the plasma membrane of skeletal muscle cells (Fredsted et al., 2005). Histological analysis indicates that hypoxia also decreases expression of the sarcolemmal protein dystrophin in the EDL (Schmidt et al., 2018). Dystrophin is an integral component of the dystrophin-glycoprotein complex that links the cytoskeleton to the extracellular matrix (ECM) of skeletal muscle cells through the sarcolemma (Gao & McNally, 2015). Dystrophin loss not only leads to structural instability of the myocyte but also associates with functional impairments considering its role in facilitating the transmission of force production (Gao & McNally, 2015). Considering the lack of susceptibility to excitotoxicity in the anoxic FDB, we hypothesize that the muscle preserves dystrophin expression during hypoxia. To investigate the apparent protection of the FDB sarcolemma, we reviewed our proteomics analysis to identify proteins that are elevated in the FDB with known sarcolemmal functions. Our results identified

significantly higher expression of the sarcolemmal repair protein Annexin A2 and the Type V collagen isoform Col5a1 in the FDB as compared to the EDL and soleus. Annexin A2 interacts with the predominant membrane repair protein dysferlin to seal membrane lesions, such as those of which occur during hypoxia, while Col5a1 participates in fibrillogenesis – the formation of collagen fibrils within the ECM (Sun et al., 2011). We hypothesize that elevated Annexin A2 content protects the FDB by enabling the myocyte to repair membrane lesions prior to the induction of cell damage and/or death following hypoxia exposure. We also hypothesize that elevated Col5a1 content protects the FDB by promoting structural stability within the ECM to maintain the connection to the cytoskeleton via dystrophin.

CHAPTER 2: Review of the Literature

Molecular Oxygen – One Organism's Trash, Another Organism's Treasure

The development of biological life on Earth coincides with the emergence of oxygen – one of the planet's most abundant elements. At the time of Earth's formation ~4.5 billion years ago, O_2 levels were negligible. It was not until more than 2 billion years later during the 'great oxidation event' of the Proterozoic period that O_2 began to accumulate (Stamati et al., 2011). Through the replacement of hydrogen and sulfur with water as an electron donor for energy metabolism in cyanobacteria, the advent of oxygenic photosynthesis provided means of replenishing atmospheric O_2 (Lindahl, 2008). Oxygenic photosynthesis involves electrochemical activation of chlorophyll by light photons to a degree that energetically favors the enzymatic catalysis of water into waste products of O_2 and hydrogen (Allen & Martin, 2007). Due to the widespread expansion of aerobic respiration within existing organisms, elevated oxidation of oceanic iron led to substantial O_2 diffusion into the atmosphere (Lindahl, 2008). In turn, increased O_2 availability allowed for an exponentially greater number of metabolic reactions to occur, which ultimately gave rise to the biogenesis of multicellular eukaryotes and subsequent evolution of mammals.

The importance of O_2 to mammalian physiology lies predominantly with respect to the mitochondria. O_2 serves as the terminal electron acceptor in the mitochondrial electron transport system (ETS), which generates majority of the adenosine triphosphate (ATP) that is utilized to fuel cellular work (Salin et al., 2015). Tissues with high energetic demands (e.g., heart, skeletal muscle) are particularly reliant on O_2 to maintain sufficient ATP levels for endergonic reactions that would otherwise be thermodynamically unfavorable (Neufer, 2018). Overall, O_2 plays a central role in mammalian cellular bioenergetics.

Oxygen is Fundamental to Mammalian Skeletal Muscle Function

Comprising the largest mammalian organ system by mass, skeletal muscle is tasked primarily with generating force to enable locomotion and postural stability. Other key roles of

skeletal muscle include respiration and thermogenesis. Force production occurs via the contraction of hundreds to thousands of muscle fibers, which are activated by the central nervous system during a process known as excitation-contraction coupling. Briefly, an electrical stimulus called an action potential (AP) is initiated in the brain and transmitted along the motor unit, which is comprised of a motor neuron and the muscle fibers that the neuron innervates (Purves et al., 2001). Once the AP reaches the axon terminal, the neurotransmitter acetylcholine (ACh) is released into synaptic cleft and subsequently binds ligand-gated channels that are located on the muscle plasma membrane (i.e. the sarcolemma) (Shishmarev, 2020). The binding of ACh to its receptors propagates the AP from the sarcolemma to membrane invaginations called T-tubules (Calderón et al., 2014). Present within the T-tubule system are voltage-gated dihydropyridine receptors (DHPRs) that sense changes in membrane potential and undergo conformational shape changes when the membrane is depolarized (Calderón et al., 2014). Mechanically coupled with DHPRs are ryanodine receptors (RyRs), which are signaled to open upon DHPR shape changes. RYRs are linked to the sarcoplasmic reticulum – the predominant calcium (Ca^{2+}) storage site in skeletal muscle (Frontera & Ochala, 2015) – thus their opening leads to a release of Ca^{2+} from the SR into the cytosol, which results in an increase of the intracellular Ca^{2+} concentration ($[Ca^{2+}]_i$) from nM to μM levels. (Rebbeck et al., 2014).

Once present within the cytosol, Ca^{2+} binds a regulatory protein located on the thin actin filament called troponin C. Subsequently, another actin-binding protein called tropomyosin undergoes a conformational shape change that uncovers actin's binding site for the thick myosin filament. The binding of myosin to actin forms a "crossbridge," initiating a series of molecular events known as the 'sliding filament theory.' Here, the filaments interact in a manner that involves sliding past one another, which shortens the functional unit of the myofiber – the sarcomere – and ultimately results in contraction of the muscle (Hitchcock-DeGregori & Irving, 2014). Following contraction, $[Ca^{2+}]_i$ is returned to basal conditions via the sarco-/endoplasmic reticulum Ca^{2+}

ATPase (SERCA), which drives Ca^{2+} across a >10,000-fold gradient from the cytosol back into the SR (Berchtold et al., 2000; Neufer, 2018).

Like contraction and relaxation, many skeletal muscle processes require substantial cellular free energy, which is derived by the hydrolysis of ATP into adenosine diphosphate (ADP) and an inorganic phosphate molecule (Neufer, 2018). Importantly, the extent to which the mass action ratio of [ATP] to [ADP] is displaced from equilibrium determines the capacity of a cell to perform work (Fisher-Wellman et al., 2018; Nicholls, 2013). Skeletal muscle tightly maintains a high [ATP]/[ADP] ratio to ensure that ATP-free energy (ΔG_{ATP}) availability is sufficient to carry out enzymatic reactions that are critical for physiological function of the muscle. Conditions of limited O_2 (i.e., hypoxia) increase the possibility of the mass action ratio moving closer to equilibrium due to decreased ATP production and, subsequently, increased [ADP]. Hypoxic skeletal muscle function is compromised not only by the overall reduction in ΔG_{ATP} that hinders ATP-consuming reactions, but also due to the specific effects of hypoxia on key components of muscle function. For example, redox stress has been demonstrated to decrease SERCA activity (Xu & Van Remmen, 2021), limiting the ability to drive Ca^{2+} across the concentration gradient between the cytosol and the SR. The consequent dysregulation of Ca^{2+} homeostasis impairs muscle relaxation, which leads to subsequent defects within the ECC system and ultimately results in contractile failure (Qaisar et al., 2018).

Skeletal Muscle Hypoxia Overview

The term “hypoxia” is nuanced. Highlighted by Donnelly et al. (2022), the cellular O_2 tension required to sustain proper function of a biological system is variable and system-specific. For example, skeletal muscle operates between 6 kPa (at rest) and 0.5 kPa (at VO_2max) as a function of the energetic demands that are placed on the tissue (Donnelly et al., 2022). Considering that normoxia is best viewed as a reference state as opposed to a static value of O_2 availability, hypoxia must be viewed in a similar manner as different conditions of hypoxia can elicit variable responses within skeletal muscle.

Despite a broad spectrum of definitions, hypoxia can be categorized in two forms from a cellular perspective. The first involves limited O_2 levels that impair (but do not inhibit) aerobic metabolism due to compensatory adaptations that sustain aerobic ATP production (Clanton & Klawitter, 2001). The second is characterized by O_2 deprivation to an extent that flux of the mitochondrial electron transport system (ETS) cannot be supported due to the inability of mitochondrial cytochromes to reduce O_2 to H_2O (Clanton & Klawitter, 2001). The latter form can result in cell dysfunction and/or death given sufficient duration of the hypoxic stimulus.

Hypoxia can arise from various conditions. In non-experimental and healthy settings hypoxia most often occurs in the form of altitude exposure. This type of insult is termed “hypobaric hypoxia” during which the fraction of inspired O_2 decreases proportionally with the barometric pressure (Grocott et al., 2007). Hypoxia can be modeled in both human and rodent tissue using laboratory hypoxia chambers and can also be induced using *ex vivo* or *in vivo* animal models. In *ex vivo* settings, O_2 concentrations can be altered within the incubation media of isolated rodent muscle experiments. For example, our lab’s hypoxia protocol employs 95% N_2/5% CO_2 in our tissue bath system (Amorese & Minchew et al., 2023). Hypoxia also occurs within pre-clinical models of ischemia such as hindlimb ischemia (HLI) where blood supply and O_2 delivery to peripheral skeletal muscles are reduced by femoral artery ligation and transection (Schmidt et al., 2018). Examples of hypoxic insults within skeletal muscle include decreased O_2 tension in arterial blood, impaired O_2 binding and/or transport, and reduced tissue perfusion among others (Collins et al., 2015; Pittman, 2011). Regardless of the mechanism by which hypoxia occurs, a common factor of hypoxic damage is the loss of force-producing capacity within the affected muscle.

Physiological Consequences of Acute Hypoxia on Skeletal Muscle Function

i. Bioenergetic failure

O_2 is a necessary substrate for mitochondrial oxidative phosphorylation, which generates up to 90% of the ATP that is utilized to fuel myocellular work (Salin et al., 2015). Mitochondrial

ATP production is critical to maintaining the mass action ratio of [ATP] to [ADP] at ~10 orders of magnitude away from equilibrium to establish the capacity of a muscle cell to perform work (Fisher-Wellman et al., 2018; Nicholls, 2013). Accordingly, O_2 is necessary for skeletal muscle bioenergetics.

Oxidative phosphorylation occurs via a series of redox reactions within the electron transport system (ETS) that couples ATP synthesis with electron flow across respiratory complexes embedded within the inner membrane. The movement of protons from the inner mitochondrial space to the matrix generates the mitochondrial membrane potential, which provides the driving force of electron flow to the final complex – ATP synthase (Schmidt et al., 2021). Following 5 hours of a hypoxic insult, decreased oxidative capacity of complexes I, II, and IV lead to a reduction in mitochondrial ATP synthesis (Thaveau et al., 2007), which would contribute to increased ADP content. Similarly, mitochondria isolated from hindlimb muscles of male mice exposed to 48 h of severe hypobaric hypoxia (pressure equivalent of 8500 m altitude) exhibited significantly lower respiration when compared to age-matched control mice (Magalhães et al., 2005). Respiratory deficits were accompanied by increased oxidative stress as demonstrated by greater levels of superoxide and protein oxidation (Magalhães et al., 2005). During hypoxia, O_2 depletion exerts an inhibitory effect on the ETS that results in the accumulation of reducing equivalents (i.e., NADH, $FADH_2$) and increases the availability of electrons for reactive oxygen species (ROS) formation (Baudry et al., 2008; Clanton, 2007). As mentioned previously, the concurrent reduction of ATP-free energy that occurs due to the movement of the [ATP]/[ADP] ratio towards equilibrium inhibits ATP-consuming reactions.

ii. Structural disruption

Skeletal muscle contractile impairments during hypoxia are accompanied by various structural disruptions such as blurred z-lines, swollen mitochondria, and damaged myofilaments (Harman, 1947; McCall & Duncan, 1989; Shamsadeen & Duncan, 1989). The muscle plasma membrane (sarcolemma) is another major site of hypoxic damage. Even under normoxic

conditions the sarcolemma is susceptible to disruption from mechanical stress, however the muscle contains multiple membrane repair systems to address this type of injury. Hypoxia not only impedes the process of repairing regular damage but also induces a secondary source of damage that may be mediated in part by activation of calpains. Calpains are a family of cysteine proteases (Huang & Forsberg, 1998) that disrupt various components of the myofiber through protein shuttling to the ubiquitin-proteosome system (Pandurangan & Hwang, 2012; Smith et al., 2008). Elevations in free intracellular Ca^{2+} occurs due to impaired SERCA activity and/or hypoxia-induced sarcolemmal lesions allowing for the entry of extracellular Ca^{2+} (among other molecules) into the cytosol (Fredsted et al., 2005). Cytosolic Ca^{2+} overload is a common signature of hypoxic muscle damage that can activate a variety of catabolic pathways (Orrenius et al., 2003) including calpain translocation to the sarcolemma where various structural proteins are degraded (Inserte et al., 2012). $[Ca^{2+}]_i$ is also elevated in response to hypoxia-induced acidosis. More specifically, a reduction in intracellular pH activates sarcolemmal $Na^{+/}H^{+}$ channels leading to Na^{+} import (Paradis et al., 2016) and reversal of $Na^{+/}Ca^{2+}$ exchangers, which further increases Ca^{2+} accumulation and calpain activation (Eliason & Wakefield, 2009; Ivanics et al., 2000).

Previous research has demonstrated that hypoxia decreases the expression of dystrophin (Schmidt et al., 2018), which is an integral component of the dystrophin-glycoprotein complex that links the sarcolemma to the extracellular matrix (ECM) and participates in force transmission throughout the cell (Gao & McNally, 2015). Considering its multifaceted role within skeletal muscle physiology, dystrophin loss is a major insult to the system. Hypoxia-induced loss of dystrophin expression likely occurs due to calpain-mediated degradation, and ultimately compromises the structural integrity of the cell. Prolonged structural fragility weakens the myocyte's ability to partition the intracellular and extracellular environments, which can result in cell death.

Requirements of Mammalian Skeletal Muscle to Survive Acute Hypoxia

i. Bioenergetic reprogramming

A critical requirement of the myocyte to survive a hypoxic insult is the ability to maintain energetic function in both the presence and absence of O_2. Specifically, the concept would be reflected in the cellular system either being able to meet the energetic demand of the cell through non-mitochondrial sources or reducing the energetic demand placed on the cell. For example, muscle samples from indigenous mountain populations and mountaineers returning from the Himalayas exhibit lower mitochondrial content, but more efficient coupling between ATP demand and supply as compared to sea-level counterparts (Hoppeler et al., 2003). Assuming a constant ATP demand, decreasing a muscle's reliance on the mitochondrial network would require an acute ability to increase flux of glycolysis and/or the phosphocreatine (PCr) system to ensure that ADP levels remain low. In addition to greater content of glycolytic enzymes, accelerated glycolytic flux would require greater availability of glycogen and NAD^+, the latter of which is regenerated from NADH via the conversion pyruvate to lactate (Melkonian & Schury, 2022). Upregulation of PCr content may not necessarily benefit the system, however creatine kinase (CK) has been demonstrated to localize near muscle ATPase sites for rapid ATP recycling (Guimarães-Ferreira, 2014). Thus, it is possible that increasing glycolytic flux and efficient localization of the PCr system could prevent energetic compromise during hypoxia.

It is also necessary to consider the energetic demand on the skeletal muscle cell. If the systems catabolizing ATP to ADP were downregulated, the requirement of the mitochondria to buffer increases in ADP content would be reduced. For example, if the muscle cell could reduce rates of protein synthesis or actin treadmilling when faced with a hypoxic insult, it might be possible to maintain lower ADP content. Decreased rates of protein synthesis have been demonstrated to occur in multiple cell types during hypoxia and anoxia, including skeletal muscle (Koritzinsky et al., 2006; Land et al., 1993; Preedy et al., 1985; Preedy & Sugden, 1989; Shrieve et al., 1983). However, it is important to consider the severity of hypoxia in this context as some

groups have shown that muscle cells maintain protein synthesis under moderate (8-12% O_2) hypoxia (Arthur et al., 2000; Etheridge et al., 2011). Regarding actin dynamics, hypoxia has been demonstrated to alter the actin cytoskeleton (Zieseniss, 2014). Treadmilling – the replacement of actin subunits within actin filaments - occurs to maintain homeostatic regulation of the actin network (Carlier & Shekhar, 2017). However, in various species that have evolved to survive anoxia (e.g., the goldfish), downregulation of cytoskeletal activity (i.e. “cytoskeletal arrest”) has been reported as a protective mechanism to decrease in energy consumption during times of energetic stress (Myrka & Buck, 2021). Furthermore, pharmacological inhibition of actin filament turnover has been demonstrated to decrease ATP depletion by ~50% (Bernstein & Bamburg, 2003), Thus, cytoskeletal arrest would offer a similar energetic benefit to skeletal muscle when O_2 levels become limited. If a skeletal muscle were able to downregulate non-essential ATP-consuming reactions during hypoxia, the cell would ensure sufficient free energy for essential reactions such as ion transport to maintain membrane potential (Hochachka et al., 1996). Collectively, a balance between energetic supply and demand within the cell would be a critical phenotype of muscle hypoxia resistance.

Another critical aspect of hypoxia resistance would be an enhanced ability of the myocyte to buffer and/or reduce the production of ROS. A plausible option is the rerouting of reducing equivalents that accumulate due to mitochondrial ETS inhibition for participation in protective processes. For example, excess NADH could be converted to NADPH (Singh et al., 2008), which is a substrate for the production of glutathione – a critical antioxidant within skeletal muscle (Puskas et al., 2000). NADPH is also synthesized via the pentose phosphate pathway (PPP), and has been reported to increase up to 7-fold in response to hypoxia (Gupte et al., 2006). Importantly, the PPP does not require ATP or O_2 to take place (Jalloh et al., 2015) and has gained increasing attention in the skeletal muscle literature (Valentino et al., 2021). Increased PPP activity has been proposed as a protective mechanism against hypoxic muscle damage (Zaied et al., 2023),

resulting in greater NADPH and subsequent glutathione synthesis to augment protection of the muscle against redox stress (Chicco et al., 2018).

ii. Structural protection

For a skeletal muscle to survive a hypoxic insult the sarcolemma must be capable of withstanding disruption and prevent or attenuate Ca^{2+}-induced damage. Previous research in the rat extensor digitorum longus (EDL) has demonstrated a direct relationship between sarcolemmal damage and elevated $[Ca^{2+}]_i$ during hypoxia (Fredsted et al., 2005). Furthermore, the mouse soleus muscle exhibits an attenuated degree of membrane damage when Ca^{2+} is removed from the experimental buffer (Jones et al., 1984). The EDL and soleus exhibit distinct muscle phenotypes (Schiaffino & Reggiani, 2011), thus Ca^{2+} overload is a universal feature of hypoxic muscle damage. To achieve protection against Ca^{2+} overload the skeletal muscle plasma membrane repair (PMR) system must be robust.

Although the precise mechanism remains to be fully elucidated, skeletal muscle PMR involves several mechanisms where Ca^{2+} acts as a key signaling molecule. The literature posits two primary means of PMR in skeletal muscle: 1) the lipid raft and 2) lysosomal exocytosis. Upon sarcolemmal disruption, Ca^{2+} influx activates the cooperation of various PMR proteins to seal membrane lesions through the recruitment and aggregation of intracellular vesicles that contain dysferlin – the predominant skeletal muscle PMR protein – and are trafficked to the injury site by MG53 (Cai et al., 2009; Cárdenas et al., 2016). Fusion of dysferlin-containing vesicles with other components of the PMR system are further coordinated through Ca^{2+}-dependent interaction with annexins (Lennon et al., 2003). The annexins are a family of phospholipid-binding proteins, many of which participate in forming the lipid raft that ultimately patches the damaged membrane and allows for the export of excess cytosolic Ca^{2+} (Croissant et al., 2022; Draeger et al., 2011). Less characterized than the lipid raft response to membrane damage is the response of lysosomes. However, previous research suggests that lysosomes not only participate in vesicular aggregation

to form the lipid raft, but also contribute to decreasing membrane tension via exocytosis of damaged membrane components (lipids, proteins, etc.) (Barthélémy et al., 2018).

Protecting a muscle from hypoxic insults would require efficient PMR, which could occur by increasing the number of available PMR players and/or increasing the $[Ca^{2+}]_i$ sensitivity of the PMR system. Enhancing the activation properties of PMR proteins would enable the myocyte to repair membrane lesions in a timely and efficient manner as less Ca^{2+} would be required to initiate the PMR response. Thus, in theory an intracellular environment that is responsive to hypoxia by attenuating or preventing sarcolemmal damage would ameliorate the potential for cytosolic Ca^{2+} overload that likely contributes to the loss of muscle function exhibited during hypoxia exposure (Schmidt et al., 2018).

Discussion of the Literature

Although skeletal muscle is remarkably resilient during times of stress, even acute bouts of hypoxia exposure elicit substantial consequences to the tissue. Hypoxia initiates a cascade of intracellular events that synergistically enhance the onset of dysfunction and ultimately induce cell death. A collective assessment of the literature would suggest that regulation of energetic homeostasis and sarcolemmal structure are critical to the muscle's ability to survive hypoxia.

Following the onset of a hypoxic insult, reductions in cellular O_2 tension would contribute to an increase in ADP content likely due to reductions in ETS function. Increased ADP content can alter the energetic status of the cell and contribute to impaired physiological function. Coinciding with increases in [ADP] is an increase in ROS content either due to increased production and/or reduced buffering capacity, which results in reduced force production of the muscle cell due to oxidation of key contractile proteins. Hypoxia also can alter intracellular Ca^{2+} homeostasis due to loss of sarcolemmal stability and potentially due to dysregulation of SR function (Fredsted et al., 2005). Cytosolic Ca^{2+} overload leads to the loss of muscle function in part due to calpain activation, which results in the degradation of both contractile and membrane proteins (Pandurangan & Hwang, 2012; Smith et al., 2008). Overall, hypoxia damages skeletal

muscle in various ways, thus a multitude of protective mechanisms must be in place to survive an acute insult.

To the best of our knowledge, there are no therapeutic or preventive strategies for a skeletal muscle to resist hypoxic insults. Further, the field currently lacks a clear understanding of cellular properties that are necessary to confer survival during hypoxia. The ambiguity that exists in our knowledge is a consequence of skeletal muscle being sensitive to losses in O_2 tension. Here, the current understanding of the literature is utilized to propose critical mechanisms needed for skeletal muscle to survive hypoxia. Specifically, muscle hypoxia resistance must include an immediate ability for the cells to undergo bioenergetic reprogramming and provide structural protection. For example, it would be expected that the muscle cell contains an equivalent ability to match ATP demand and supply independent of the O_2 tension within the surrounding environment to prevent any accumulation of ADP. It could be predicted that the muscle requires a means to enhance flux through glycolysis, improve glycolytic efficiency, and/or reduce activity of systems that utilize large amounts of ATP. Additionally, perhaps the muscle could reroute substrates towards the PPP, which would provide NADPH for glutathione synthesis to strengthen the muscle antioxidant defense system. Finally, the muscle would require an augmented sarcolemmal repair system to seal membrane lesions and reduce the rate and/or amount of extracellular Ca^{2+} entry in order to limit calpain activation and/or other negative consequences induced by Ca^{2+} overload. In turn, physiological function of the muscle would be preserved for longer periods of time when faced with hypoxia exposure.

A goal for the field to consider is engineering a skeletal muscle to survive without O_2 as the knowledge gained from such a muscle would elicit multifaceted benefits. For example, scientists would be equipped with an improved ability to design therapeutics or interventions that limit cellular damage during hypoxia that is induced by different pathologies (e.g., peripheral artery disease, traumatic arterial occlusions, heart failure, total knee arthroplasty) or as a result of an environmental exposure (e.g., mountain sickness). Furthermore, the underlying mechanisms of

muscle hypoxia resistance could be leveraged in other tissues that are susceptible to hypoxic damage, thereby overcoming a critical gap that could offer long-term benefits to various populations.

CHAPTER 3: Hypoxia resistance is an inherent phenotype of the mouse flexor digitorum brevis skeletal muscle.

Adam J. Amorese[^1], Everett C. Minchew[^1], Michael D. Tarpey[1], Andrew T. Readyoff[5], Nicholas C. Williamson[1], Cameron A. Schmidt[2], Shawna L. McMillin[3], Emma J. Goldberg[1], Zoe S. Terwilliger[1], Quincy A. Spangenburg[1], Carol A. Witczak[6,7,8], Jeffrey J. Brault[6,7], E. Dale Abel[9], Joseph M. McClung[1,4,5], Kelsey H. Fisher-Wellman[1,4], Espen E. Spangenburg*[1,4]

1 – East Carolina University, Department of Physiology, Brody School of Medicine, Greenville, NC, USA, 27834
2 – East Carolina University, Department of Biology, Greenville, NC, USA, 27834
3 – East Carolina University, Department of Kinesiology, Greenville, NC, USA, 27858
4 – East Carolina University, Department of Cardiovascular Sciences, Brody School of Medicine, Greenville, NC, USA, 27834
5 – East Carolina Diabetes and Obesity Institute, East Carolina University, Greenville, NC, USA, 27834
6 – Indiana University School of Medicine, Department of Anatomy, Cell Biology, and Physiology, Indianapolis, IN, USA, 46202
7 – Indiana Center for Musculoskeletal Health, Indianapolis, IN, USA, 46202
8 – Indiana Center for Diabetes and Metabolic Diseases, Indianapolis, IN, USA, 46202
9 – University of California, David Geffen School of Medicine, Department of Medicine, Los Angeles, CA, USA, 90095
* – Corresponding Author
^These authors contributed equally to this work

*To whom correspondence should be addressed: Espen E. Spangenburg Ph.D., Department of Physiology, East Carolina Diabetes and Obesity Institute, Brody School of Medicine, 115 Heart Drive, East Carolina University, Greenville, NC 27834; spangenburge14@ecu.edu; Tel. 252-737-5035

Abstract

The various functions of skeletal muscle (movement, respiration, thermogenesis, etc.) require the presence of oxygen (O_2). Inadequate O_2 bioavailability (i.e., hypoxia) is detrimental to muscle function, and in chronic cases can result in muscle wasting. Current therapeutic interventions have proven largely ineffective to rescue skeletal muscle from hypoxic damage. However, our lab has identified a mammalian skeletal muscle that maintains proper physiological function in an environment depleted of O_2. Using mouse models of *in vivo* hindlimb ischemia and *ex vivo* anoxia exposure, we observed the preservation of force production in the flexor digitorum brevis (FDB) while in contrast the extensor digitorum longus (EDL) and soleus muscles suffered loss of force output. Unlike other muscles, we found that the FDB phenotype is not dependent on

mitochondria, which partially explains the hypoxia resistance. Muscle proteomes were interrogated using a discovery-based approach that identified significantly greater expression of the transmembrane glucose transporter GLUT1 in the FDB as compared to the EDL and soleus. Through loss-and-gain-of-function approaches, we determined that GLUT1 is necessary for the FDB to survive hypoxia, but overexpression of GLUT1 was insufficient to rescue other skeletal muscles from hypoxic damage. Collectively, the data demonstrate that the FDB is uniquely resistant to hypoxic insults. Defining the mechanisms that explain the phenotype may provide insight towards developing approaches for preventing hypoxia-induced tissue damage.

Introduction

Acute or extended bouts of hypoxia or anoxia can induce and/or exacerbate a skeletal muscle myopathy. This myopathy is characterized by the loss of muscle force-producing capacity that contributes directly to overall muscle weakness and potentially leads to reduced functional independence (Berru et al., 2019; Pipinos et al., 2008). During lengthy bouts of hypoxia, the inability of skeletal muscle to survive and function becomes a major predictor of mortality and associates with the development of a necrotic pathology (Chaillou et al., 2014; Fitzgerald et al., 2004). Hypoxia detrimentally affects skeletal muscle in numerous diseases including various dystrophies, peripheral artery disease, acute traumatic arterial injury/occlusion, heart failure, etc., as well as elective surgeries such as total knee arthroplasty (Mayer et al., 2017; Ryan et al., 2019; Strassburg et al., 2005). Thus, it is critical to define mechanisms and/or approaches that can attenuate hypoxia-induced loss of skeletal muscle function.

A critical gap in developing interventions and/or treatments for hypoxic muscle injury is that the field currently lacks knowledge of the properties reflective of hypoxia resistance. Therefore, the available information is insufficient to reverse engineer a muscle to survive without O_2. This gap is attributable to the fact that the most extensively studied skeletal muscles are sensitive to hypoxia and exhibit damage within minutes of a hypoxic insult (Fredsted et al., 2005; Shamsadeen & Duncan, 1989). Irrespective of muscle fiber type, skeletal muscle is dependent

upon a maintained cellular O_2 tension. O_2 serves as the terminal electron acceptor in the mitochondrial electron transport system (ETS), which is a critical component of meeting the energetic demand of the cell. The EDL muscle, for example, is composed predominantly of fast glycolytic fibers (i.e., IIb or IIx fibers) and yet requires O_2 to remain viable (Schmidt et al., 2020). Thus, O_2 dependency is a universal phenotype of skeletal muscle.

To induce hypoxia *in vivo* we employ an animal model in which the femoral artery in the lower limb is transected and ligated, resulting in loss of O_2 tension to distal skeletal muscles. In this model, we have documented complete loss of force production in the EDL and soleus muscles (Goldberg et al., 2019). Current dogma states that tissues located most distal to the site of an arterial occlusion suffer the greatest functional burden and necrotic pathology (Schmidt et al., 2018). However, we surprisingly discovered that the flexor digitorum brevis (FDB) – a muscle located at the bottom aspect of the foot that is among the most distal from the site of artery transection – exhibits a remarkable capacity to maintain function following the same hypoxic insult. Our *in vivo* findings were confirmed using an *ex vivo* approach during which muscle anoxia exposure significantly impaired function in the EDL and soleus but did not alter the force-producing capacity of the FDB.

Here we reveal that, unlike any other skeletal muscle, the FDB can function properly without O_2 for extended periods of time. Importantly, the FDB provides a unique model system from which the field can gain novel insight towards developing approaches for promoting tissue survival during hypoxia. In this study we provide a complete characterization of the FDB's ability to resist hypoxic insults and we present data concerning our initial attempts to uncover the underlying mechanism(s). We specifically hypothesized that the FDB relies on glycolytic metabolism to maintain physiological function and meet energetic demands during hypoxia.

Materials & Methods

Animals

The following mice were utilized in the described experiments: 10-12-week-old male

C57BL/6NJ mice (n=88, Jackson Laboratories) and 10-12-week-old male and female muscle-specific GLUT1 knockout (KO) mice generously provided by Dr. Carol Witczak (Indiana University) and Dr. E. Dale Abel (University of California, Los Angeles). GLUT1 fl/fl mice were bred with muscle creatine kinase Cre recombinase transgenic mice (MCK-Cre^{+}; C57BL/6J strain #005304; Jackson Laboratories) generating MCK-Cre^{+} (control), GLUT1 fl/fl (WT) or muscle-specific GLUT1 knockout (GLUT1 KO). For these studies both male and female GLUT1 KO or GLUT1 fl/fl and their wild-type/control littermates (n=6-8/group) were utilized. Genetic deletion of GLUT1 specifically in the skeletal muscle was confirmed previously by the Witczak lab (McMillin et al., 2022). Additionally, our lab confirmed the reduction of GLUT1 mRNA in single FDB muscle fibers via RT-PCR (PowerTrack SYBR Green #A46109, ThermoFisher) in a similar fashion as previously described using primer sequences for GLUT1 (SLC2A1) and HAGH(McMillin et al., 2022). No differences were detected in the FDB muscles between the MCK-Cre^{+} (control) and GLUT1 fl/fl (WT) in a preliminary investigation, thus GLUT1 fl/fl were used as WT mice for the present study.

Mice were housed in a temperature- (22°C) and light- (12/12 hr. light/dark) controlled facility and allowed *ad libitum* access to food and water. All animal procedures and usage were approved by the Institutional Review Committee at East Carolina University, and animal care complied with the Guide for the Care and Use of Laboratory Animals, Institute of Laboratory Animal Resources, Commission on Life Sciences, National Research Council (Washington: National Academy Press, 1996).

Model of acute hindlimb ischemia (HLI)

Acute hindlimb ischemia was induced in the lower limb as previously described (Schmidt et al., 2018). Briefly, to anesthetize the C57BL/6NJ mice an intraperitoneal injection of ketamine at 90 mg/kg body weight and xylazine at 10 mg/kg was administered. A small incision was made between the left inguinal fat pad and peritoneum to access the femoral artery, which was then isolated from the femoral vein. Ligatures were placed on the femoral artery in the region distal to

the inguinal ligament and the region proximal to the lateral circumflex branch. The femoral artery was subsequently transected at the area between the ligatures. For pain management, mice were administered a subcutaneous injection of buprenorphine at 0.5 mg/kg while recovering. Anesthetized mice were euthanized at various time points following induction of HLI for subsequent analysis.

Histology

Muscle morphology was assessed in control and ischemic muscles via standard hematoxylin & eosin staining methods. Briefly, EDL, soleus, and FDB muscles were frozen in optimal cutting temperature (OCT) media using isopentane submerged in liquid N_2. Transverse cryosections (10 μm) from the muscle mid-belly were cut using a cryostat (Leica 3050S) and adhered to charged glass slides. Sections were air-dried for 10 minutes prior to standard staining procedures. Following staining, sections were mounted, coverslipped, and imaged using an EVOS FL microscope (Life Technologies) through a 10X objective lens.

Blood perfusion of the limb and paw

Blood perfusion to the lower limb was assessed using laser Doppler perfusion imaging (LDPI) as previously described (Schmidt et al., 2018). Briefly, mice were anesthetized with ketamine/xylazine and placed on a heating pad at 37°C. Using a microshaver, fur was removed from the lower limb and both plantar paws (4 ms/pixel scan rate) and medial thighs (10 ms/pixel scan rate) were imaged using a LDI2-High Resolution System (830 nm) (Moor Instruments, Moor, Axminster, UK). LDPI was performed prior to HLI surgery, immediately following surgery, and at 24- and 48-hours following surgery prior to sacrifice.

Perfused vessel labeling

Quantification of total vessel and perfused vessel content was performed as previously described (Schmidt et al., 2018). Briefly, mice were administered a retro-orbital injection of *Griffonia simplicolia* isolectin-B_4 Dylight 594 conjugate (Vector Labs, Burlingame, CA) (50μL of

1mg/mL) immediately following the induction of HLI. At 6 hours post-HLI, EDL and FDB muscles were dissected and frozen in OCT compound (VWR). Transverse cryosections (10 μm) taken from the muscle midbelly were cut using a cryostat (Leica 3050S) and mounted on charged glass slides. Slides were fixed in 1:1 ice-cold methanol/acetone and incubated for 10 minutes at -20°C. Following 10 minutes of air drying, sections were rehydrated with ice-cold 1X phosphate buffered saline (PBS) for 5 minutes. PBS was subsequently removed, and sections were blocked with PBS-diluted 5% goat serum at room temperature in the dark for 1 hour. After removing goat serum, sections were incubated overnight with goat anti-rat CD31 (platelet endothelial cell adhesion molecule primary antibody (BioRad) (1:100) and anti-dystrophin primary antibody (Abcam ab15277) (1:100) at 4°C. The following day, primary antibodies were removed, and sections were washed three times with ice-cold 1X PBS for 5 minutes. Secondary antibodies (Alexa Fluor 488 goat anti-rat IgG, Thermo Fisher Scientific A-11006 and Alexa Fluor 647 goat anti-rabbit IgG, Thermo Fisher Scientific A-21244) were subsequently applied to sections (1:250) for incubation at room temperature in the dark for 1 hour. Following removal of secondary antibodies and a second round of washing at 3x5 minutes with ice-cold 1X PBS, sections were mounted with Vectashield (Vector Labs) and imaged using an EVOS FL microscope (Life Technologies) through a 20X objective lens. Image quantification was performed using ImageJ software by measuring the percentage area of Dylight 594 and CD31 positive signal within each image and, representing the data as a ratio of the signals.

Muscle dissection for contractile measurements

EDL, soleus, and FDB muscles were dissected as previously described (Tarpey et al., 2018). Briefly, mice were anesthetized via isoflurane (3-4%) and muscles dissected, with the mouse euthanized after the tissue was removed. During the dissection of the muscles 4-0 silk suture was used to tie a double square knot at distal and proximal tendons. Tendons were cut just above the knot, and muscles were submerged in a bath of oxygenated (95% O_2/5% CO_2) Krebs Ringer buffer (KRB) (119mM NaCl, 5mM KCl, 5mM $NaHCO_3$, 1.25mM $CaCl_2$, 1mM KH_2PO_4,

10mM HEPES, 1mM $MgSO_4$) at room temperature. To force the muscle to rely on stored substrates, the KRB did not contain any metabolic substrates (e.g., glucose). The muscles were dissected from each animal as quickly as possible and immediately placed in oxygenated KRB. Muscles were affixed to a force transducer apparatus (Aurora Scientific) and equilibrated in the oxygenated KRB bath for 10 minutes. Following equilibration, optimal muscle length (L_0) was determined by administering maximal twitch stimulations every 30 seconds and incrementally adjusting muscle length until peak twitch force was achieved.

Muscle contractile protocols

Following establishment of L_0, EDL, soleus, and FDB muscles were subjected to either a force-frequency protocol as previously described (Tarpey et al., 2018) or a 3-hour protocol of isometric muscle contraction. We have published a detailed description of the protocol for assessing contractile function of the FDB, EDL and soleus (Tarpey et al., 2018). Briefly silk suture was tied to the proximal and distal tendons of all muscles except for the FDB where suture is secured to the three medial toe tendons simultaneously. Force-frequency protocols were employed in the oxygenated (95% O_2/5% CO_2) KRB bath with isometric force measured via sequential administration of 200 ms pulse trains separated by 60 seconds at 10, 20, 40, 60, 80, 100, and 120Hz. For the 3-hour protocol, isometric force was measured with the administration of 200 ms pulse trains at 100Hz every 10 minutes over the course of 3 hours. To run the 3-hour protocol, the muscles were initially incubated in oxygenated KRB, and resting L_o was determined as described above. The muscles were either switched to a fresh solution of oxygenated (95% O_2/5% CO_2) KRB or nitrogenated (95%N_2/5%CO_2) KRB to simulate anoxia. Using a Clark electrode (Innovative Instruments, Inc), measurable O_2 concentration in the KRB was reduced to undetectable levels approximately 30 seconds after the KRB was bubbled with N_2. Following contractile protocols, L_0 was measured using digital calipers. Muscles were then removed from the force transducer and tendons were trimmed using micro-scissors. Muscles were blotted dry prior to measuring wet weights. Finally, muscles were flash frozen in liquid N_2. Specific muscle

force (N/cm^2) was determined as previously described (Minchew et al., 2022) using predetermined equations (Brooks & Faulkner, 1988; Tarpey et al., 2018).

Pharmacological Inhibition of mitochondrial respiration and glycolysis

To inhibit mitochondrial respiration during the 3-hour contractile protocols, muscles were incubated with potassium cyanide (KCN). Cyanide binds the heme-containing subunit of complex IV in the ETS, inhibiting O_2 utilization (Leavesley et al., 2008). Following muscle isolation, determination of L_o, and measurement of initial normoxic force production, either 2mM KCN or the equivalent KRB vehicle was added to the bath. Muscles were then subjected to anoxia (95% N_2/5% CO_2) and completed the 3-hour contractile protocol described above. The KCN concentration was determined based on previous work in murine contractile function experiments (Zhang et al., 2006). We also confirmed that this concentration completely abolished mitochondrial respiration in murine isolated fiber bundles (data not shown).

To inhibit glycolysis during 3-hour contractile protocols, muscles were incubated with bromopyruvate (BrP). BrP inhibits the activity of hexokinase and glyceraldehyde 3-phosphate dehydrogenase (GAPDH), (Shoshan, 2012). Following muscle isolation, determination of L_o, and measurement of initial normoxic force production, either 500 μM BrP or the equivalent KRB vehicle was added to the bath. Muscles were then subjected to anoxia (95% N_2/5% CO_2) and completed the 3-hour contractile protocol described above. Concentrations of BrP were tested incrementally between 100μM and 1mM based on previous studies (Jardim-Messeder et al., 2012; Park, 2017). 500 μM was the highest tolerable concentration that did not result in immediate signs of muscle toxicity. Other cell types have been incubated with BrP concentrations as low as 10 μM (Attia et al., 2015) and as high as 1000 μM (Ehrke et al., 2015) in previous research.

Adenine nucleotide measurements

Adenine nucleotides (ATP, ADP, AMP) and IMP concentrations in EDL, soleus, and FDB muscles were determined using ultra-performance liquid chromatography (UPLC) as previously

described (Brault et al., 2013; Davis et al., 2020). Briefly, muscles were dissected, incubated in oxygenated or nitrogenated KRB for 1 hour, and flash frozen in liquid N_2. Muscles were homogenized using a glass-on-glass homogenizer in cold 3.5% perchloric acid (PCA), and protein was removed via centrifugation. Homogenates were neutralized with 1M KOH, and adenine nucleotides and IMP concentrations were determined using an Acquity UPLC H class system (Waters, Milford, MA). IMP accumulation is reflective of a mismatch between ATP synthesis and degradation, while decreased ATP/AMP ratio is indicative of impaired cellular energy status (Baldwin et al., 1999; Hardie, 2003). Concentrations of adenine nucleotides and IMP were normalized to muscle wet weights (mg).

Muscle proteomics

The proteome of the EDL, soleus, and FDB muscles were characterized using methods described previously (McLaughlin et al., 2020) with slight modifications. Briefly, muscles from both limbs were dissected from two different male C57BL/6NJ mice and combined to ensure adequate protein yield. Four total muscles were added to 1mL of urea-based lysis buffer (8M Urea, 50mM Tris, 40mM NaCl, 2mM $MgCl_2$, 10mM $Na_4P_2O_7$, 50mM NaF, 50µL Halt protease inhibitor cocktail, 1 PhosSTOP tab), and homogenized on ice using a handheld homogenizer (Kinematica AG). This was repeated 4 times resulting in 4 different biological samples per muscle type. Samples were fractionated using the Pierce High pH Reversed-Phase Peptide Fractionation Kit (ThermoFisher Scientific, Cat#84868) and fractions were frozen on dry ice and lyophilized. Each fraction was resuspended in 0.1% formic acid at a concentration of 0.25µg/µL following peptide quantification (ThermoFisher Scientific, Cat#23275). *Nano*LC-MS/MS analysis was performed as previously described (Fisher-Wellman et al., 2019; McLaughlin et al., 2020). For data analysis, Proteome Discoverer 2.2 (PDv2.2) and MitoCarta 3.0 were used as previously described (McLaughlin et al., 2020) with significance set at $p<0.05$. A detailed description of these procedures is provided in the Supplement. All raw data have been deposited in ProteomeXchange (accession # PXD039811) and jPOST (accession # JPST002018) (Okuda et al., 2017).

Muscle glycogen content

Glycogen content was determined by acid hydrolysis and an enzyme-coupled assay to measure D-glucose concentrations as previously described (Schmidt et al., 2020). Briefly, segments (2-6mg) of frozen EDL, soleus, and FDB muscles were placed in 125µL of 2M HCl for acid hydrolysis and boiled on a heating block at 95°C for 2 hours. Over the course of the 2 hours, samples were vortexed every 30 minutes. Following acid hydrolysis, samples were neutralized with the addition of 125µL of 2N NaOH, and 5µL of Tris HCl pH 7.0 was added to act as a buffer. Samples were vortexed vigorously, and 10µL of each sample was added to a clear 96 well plate alongside 10µL of a glucose calibrator (Cima Scientific) and 10µL of water to act as a blank. 200µL of hexokinase reagent (ATP – 1.0 mM; Glucose-6-phosphate dehydrogenase (G6PDH) – 3250 u/L; Hexokinase (yeast) – 1000 u/L; NAD – 1.0 mM) (Cima Scientific) was added to each well and samples incubated at room temperature for 10 minutes. During this incubation, hexokinase used ATP to catalyze the phosphorylation of glucose to G6P, which is then oxidized with the concomitant reduction of NAD to NADH. Absorbance at 340nm was measured on a Cytation 5 microtiter plate reader (Biotek, Winooski, VT) to determine the concentration of NADH, which is directly proportional to the concentration of glucose. A linear standard curve (generated by the glucose calibrator) determined the D-glucose concentration in each sample, which was normalized to muscle wet weight (mg).

Muscle lactate content

Lactate content was determined using a lactate assay kit (Sigma). Briefly, segments (2-6mg) of frozen EDL, soleus, and FDB muscles were submerged in 75µL of 3M PCA maintained on dry ice. Samples were placed on ice for 15 minutes to allow the PCA to thaw and penetrate the muscle. Next, samples were incubated at 4°C for 5 minutes then refrozen on dry ice. Once the PCA was frozen, 125µL of 2M potassium bicarbonate was added to each sample while on dry ice and samples were centrifuged at 4000xg for 1 hour (4°C). Caps were left open to prevent pressure increases due to CO_2 buildup inside the centrifuge tubes. Following centrifugation, 10µL

of each sample were added to a 96 well plate alongside lactate standards (0, 2, 4, 6, 8, and 10 nmol/well). Lactate assay buffer (Sigma) was added to each well to achieve a final volume of 50µL. Next, 50µL of lactate master mix (46µL lactate assay buffer, 2µL lactate enzyme mix, 2µL lactate probe, Sigma) was added to each well. The plate was then covered for light protection and shaken for 30 minutes. Absorbance at 570nm was measured on a Cytation 5 microtiter plate reader (Biotek, Winooski, VT). A linear standard curve (generated by the lactate standards) determined the lactate concentration in each sample, which was normalized to muscle wet weight (mg).

Muscle ascorbate content

A colorimetric enzyme-based assay kit (Abcam, ab65656) was used to measure ascorbate content of the EDL, soleus, and FDB muscles. Briefly, muscles from GLUT1 KO (n=16) and age matched WT littermates (n=14) were dissected and snap-frozen in liquid N_2. Muscles from two mice were combined to ensure an adequate yield of muscle mass. Combined samples were resuspended in 20µL of deionized H_2O per mg of tissue and homogenized using a glass-on-glass homogenizer for 10-15 passes. Samples were then centrifuged at 500xg for 5 min (4º C) and supernatant was collected and transferred to a clean microcentrifuge tube. Following completion of the assay procedure, ascorbate content was measured using a 96-well microplate at 593 nm and normalized to total protein content determined by a Pierce BCA Protein Assay Kit (ThermoFisher Scientific) that was carried out in triplicate.

GLUT1 Overexpression

GLUT1 overexpression in the EDL was achieved by injecting GLUT1-GFP cDNA via AAV9 into the anterior compartment of the lower limb of male GLUT1 KO mice (10-12 weeks age, n=24 animals). We have previously shown this approach effectively transduces both the TA and EDL muscles [31,32]. Briefly, animals were anesthetized by isoflurane inhalation (3-4% or to effect) and after proper surgical depth was obtained a 29-gauge needle was used to deliver $1.5x10^{11}$ viral

genome particles suspended in 40 μL of sterile 1x PBS to the EDL. Contralateral limbs were injected with an equivalent volume of a PBS vehicle to serve as an internal control. We have previously found that AAV delivery of GFP alone does not affect force production (Tarpey et al., 2018). At 3-weeks post-injection, appropriate GLUT1 localization was determined via GFP signal colocalization with dystrophin staining. We repeated the 3-hour contractile protocol described above in EDL muscles from GLUT1 KO mice under the following conditions (n=8/group): GLUT1 alone, GLUT1 + 5 mM glucose, GLUT1 + 50 μM ascorbate (Sigma #A4034), and GLUT1 + 50 μM ascorbate + 50 mU/mL ascorbate oxidase (Sigma #A0157). Glucose, ascorbate, and ascorbate oxidase were added directly to fresh KRB that replaced unsupplemented KRB at the time of the experiments. The glucose concentration was based on circulating concentrations in a lean mouse and ascorbate concentrations were based on previously described cell culture experiments (Eccardt et al., 2017).

Statistical analysis

All data are presented as mean ± SEM. Statistical analyses were performed using GraphPad Prism (Version 9.0; DotMatics). One-way or two-way ANOVA with Tukey's multiple comparisons test were used for comparisons of group means when appropriate. Two-tailed t-tests were used when appropriate. For all statistical tests, $P < 0.05$ was considered statistically significant.

Results

Short term HLI does not cause functional or structural damage in the FDB.

Ex vivo isometric force production and muscle histomorphology were assessed in the EDL, soleus, and FDB following 48-hr of HLI. Previous work from our lab has demonstrated nearly a complete loss of force-producing capacity in skeletal muscles distal to the ligation site (Goldberg et al., 2019). In agreement, the EDL (Fig 1A, $p<0.00005$) and soleus (Fig 1B, $p<0.005$) exhibited a significant loss in specific force post-HLI compared to the muscles from the contralateral control

limb. In contrast, the FDB lacked any measurable loss in force output despite the same insult (Fig 1C). Histological assessment revealed the presence of severe myopathy in the ischemic EDL and soleus as demonstrated by fibrotic lesions within the interstitium and altered myofiber morphology (Fig 1D). The FDB, however, did not exhibit typical signatures of ischemia-induced myopathy at the same time point (Fig 1D).

Perfusion to the FDB is not detectable in the HLI model.

Blood flow to the paw as assessed by LDPI in the ischemic limb was reduced immediately after HLI surgery (0 hr., Fig 2A) and remained depressed through the 48-hr timepoint (Fig 2A-B). The paw, where the FDB is located, exhibited a significant loss in blood flow at all timepoints (Fig 2B). We have previously documented a complete loss of O_2 saturation in skeletal muscles distal to the ligation site following induction of HLI (Schmidt et al., 2018). Individual vessel perfusion at the tissue level was confirmed using GS-IB4 lectin delivery, which labels actively perfused vessels (Schmidt et al., 2018). HLI surgery eliminated tissue level vessel perfusion in the ischemic EDL and FDB but not within the contralateral control muscles (Fig 2C; orange). Quantification of GS-IB4 signal and normalization of GS-IB4 to the number $CD31^+$ vessels, (tissue endothelial cells), demonstrated consistent loss of perfusion to the ischemic EDL and FDB in the HLI limb (Fig 2D-F, $p<0.0005$).

The FDB retains force production during ex vivo anoxia exposure.

To further assess the FDB in a controlled environment, muscles were surgically removed and placed in either normoxic (O_2) or anoxic (N_2) Kreb's Ringer Buffer (KRB) within an *ex vivo* tissue bath system. The EDL and soleus exhibited a rapid loss in force output as early as 20 minutes of anoxia exposure when compared to oxygenated control conditions (Fig 3A-B). The FD^{50} (force drop 50) represents the time at which the muscle loses 50% of its initial normoxic force production and is a proxy of the muscle's sensitivity to hypoxia. The EDL and soleus muscles reached the FD^{50} at a similar timepoint (66.8 & 61.8 mins, respectively) during anoxia (Fig 3D).

Furthermore, a near-complete loss of force-producing capacity in these muscles was evident at approximately 2 hr following the onset of anoxia exposure (Fig 3A-B). In contrast, the FDB did not lose force output during the first 2 h of anoxia and maintained a similar percentage of initial force production between normoxic and anoxic conditions until 160 mins of the protocol (Fig 3C).

Nucleotide concentrations differ across anoxic skeletal muscles.

Mammalian skeletal muscle requires O_2 to derive chemical energy in the form of adenosine triphosphate (ATP). The total amount of ATP in a cell is not a driving factor of function, but rather the concentration of ATP ([ATP]) relative to the concentration of ADP ([ADP]). A lower [ATP]/[ADP] or [ATP]/[AMP] ratio is indicative of energetic stress in the tissue (Neufer, 2018). Higher [IMP] reflects energetic stress as well. Minimal changes were detected in [ATP] after anoxia exposure across muscles. However, the anoxic EDL and soleus exhibited significantly lower [ATP]/[ADP] and [ATP]/[AMP] ratios compared to contralateral oxygenated muscles (Table 1, $p<0.05$). Furthermore, IMP concentrations significantly increased in the EDL and soleus following anoxia exposure (Table 1, $p<0.05$). Remarkably, no differences in either the [ATP]/[ADP], the [ATP]/[AMP] ratio, or [IMP] were detected between normoxic and anoxic conditions in the FDB (Table 1).

Unlike other peripheral skeletal muscles, FDB function is not dependent upon mitochondria.

Preserved contractile function of the FDB under anoxic conditions suggests either that the muscle uniquely maintains O_2 tension or that the muscle is not dependent upon the mitochondria to regulate energetic charge. To test this question, we treated muscles with potassium cyanide (KCN) in the *ex vivo* bath to inhibit mitochondrial respiration and simultaneously limit oxygen availability during anoxia exposure. The addition of KCN increased the rate of force loss in the anoxic EDL and soleus as evidenced by a lower FD^{50} compared to anoxia exposure alone (Fig 4D). Significant differences in EDL (Fig 4A, $p<0.005$) and soleus (Fig 4B, $p<0.05$) force output

between KCN-treated and control conditions were observed as early as 10 mins of anoxia exposure. In the FDB, the FD^{50} did not occur until 150.2 mins after KCN treatment whereas the FD^{50}s of KCN-treated EDL and soleus muscles were 37.4 and 23 mins, respectively (Fig 4D). Significant differences in FDB force output between conditions were observed after 130 mins of anoxia exposure (Fig 4C, $p<0.05$).

Pharmacological inhibition of glycolytic enzymes decreases FDB force output during anoxia.

Since the FDB's maintenance of energetic charge during anoxia does not appear to rely on the mitochondria, our data would suggest that glycolysis is a major contributor to the function of the FDB. To test this hypothesis, we incubated FDBs with the glycolytic inhibitor bromopyruvate (BrP), which has been shown to inhibit multiple enzymes in the glycolytic pathway (Cardaci et al., 2012). During the 3-hour contractile protocol described above, the FD^{50} was reached at 38.7 mins in BrP-treated FDBs, which was similar to the EDL (30.2 mins) and soleus (23.4 mins) under the same conditions (Fig 4H). Significant differences in force output of all three BrP-treated muscles were observed after 10 mins of anoxia exposure (Fig 4E-G, $p<0.05$). In untreated muscles, we found significant differences in glycogen content between the FDB and EDL, but not the soleus (Fig 5A, $p=0.005$). To determine if anoxia exposure altered glycogen stores, we compared the glycogen content of BrP-treated and vehicle-treated EDL and FDB muscles following anoxia exposure. However, glycogen content did not decrease in either muscle between conditions (Fig 5B-C).

Comprehensive analysis of the FDB proteome compared to the EDL and soleus proteome.

To further delineate the unique phenotype of the FDB, we compared the proteome of the EDL, soleus, and FDB using TMT-labeled mass spectrometry and identified differential expression patterns of over 2000 proteins across muscles at a significance level of $p<0.05$ (Fig

6A-B, Table S1 (top 75 targets)). Calculation of the mitochondrial enrichment factor (MEF) found that mitochondrial protein content detected in the FDB was considerably less than that of the EDL and soleus (MEF; Fig 6C). The MEF represents the number of mitochondrial proteins identified by MitoCarta normalized to the total number of proteins identified by the Proteome Discoverer (more than 500 different mitochondrial proteins were identified and included in this factor). Heatmap analysis of ETS complex-specific content across muscles further suggests that mitochondrial respiratory capacity is lower in the FDB than the EDL and soleus (Fig 6D). To characterize mitochondrial function in the FDB, respiration rates were assessed under energetically clamped conditions in permeabilized muscle fiber bundles (PMFB) and in isolated mitochondria from EDL and FDB muscles (Supplemental Fig S1A-B). Across a range of physiologically-relevant [ATP]/[ADP] ratios, mitochondrial respiration rates were significantly lower in both PMFB and isolated mitochondria from the FDBs compared to the EDL muscles. These data are consistent with previously published work from our lab (Tarpey et al., 2018). Mitochondrial membrane potential ($\Delta\Psi$) was also significantly lower in mitochondria isolated from the FDB compared to the EDL (Fig S1C). Finally, efficiency of the ETS as assessed by plotting JO2 vs $\Delta\Psi$ was lower in FDB than EDL mitochondria (Fig S1D). The data suggest collectively that relative to mitochondria from the EDL, FDB mitochondria are inefficient and are not critical to overall function. Due to the FDB's relatively low MEF, we hypothesized that glycolytic protein abundance would be greatest in the FDB as compared to the EDL and soleus. However, the number of identified glycolytic proteins normalized to the total number of identified proteins was significantly higher in the EDL than the FDB, although the FDB did contain more glycolytic proteins than the soleus (Fig 6E). These findings were supported by heatmap analysis of identified glycolytic enzyme content across muscles (Fig 6F).

GLUT1 is necessary for the anoxia-resistant phenotype of the FDB.

We further refined the proteomics data by examining proteins that were approximately 2-fold greater and significantly higher in the FDB compared to the EDL and soleus. Considering the

deleterious effect of BrP on force output of the FDB, we focused on targets that might influence glycolytic function. Thus, we selected the transmembrane glucose transporter protein type 1 (GLUT1) as our first target. GLUT1 content in the FDB was 1.9- and 2.1-fold greater than the EDL ($p=9.4x10^{-5}$, Table S1) and soleus ($p=4.5x10^{-5}$, Table S1), respectively. To determine if GLUT1 plays a critical role in the FDB's resistance to anoxia, we employed a skeletal muscle-specific GLUT1 knockout mouse (GLUT1 KO). Skeletal muscle-specific loss of GLUT1 expression was confirmed via mRNA analysis of single fibers from the FDBs of GLUT1 KO mice (Fig 7A, $p<0.05$). However, no differences in GLUT1 mRNA were found between whole muscle homogenates of FDBs from GLUT1 KO and WT mice (Fig 7B), indicating that GLUT1 is expressed in non-muscle cells (Wertheimer et al., 1991). Our data confirm another lab's demonstration of GLUT1 deletion in skeletal muscle of the GLUT1 KO mice (McMillin et al., 2022). To determine whether GLUT1 is necessary for the FDB to maintain force output during anoxia, we repeated the 3-hour contractile protocol described above in WT and GLUT1 KO muscles. Deletion of GLUT1 in the FDB resulted in loss of force output as the FD^{50} in the KO group was reached at 135 mins of anoxia exposure whereas the FD^{50} did not occur in anoxic WT muscles (Fig 7C). Furthermore, FDB force production was significantly different between genotypes after 100 mins of anoxia exposure (Fig 7C, $p<0.05$) whereas no genotype effect was found under oxygenated conditions. Finally, no differences in EDL or soleus force output were found between genotypes compared within conditions (data not shown).

We next compared glycogen and lactate content between WT and GLUT1 KO FDBs during normoxia and anoxia with the hypothesis that the content of both metabolites would be lower in the KO than WT muscles. However, no differences were found between genotypes across conditions (Fig 8A-B). Furthermore, no changes in lactate efflux were found between the EDL and FDB following anoxia exposure (Fig S2). Another substrate imported by GLUT1 in skeletal muscle is the oxidized form of ascorbate – dehydroascorbate (Eccardt et al., 2017). Ascorbate content was significantly greater in the WT FDB compared to WT EDL and soleus muscles (Fig 8C,

p<0.0001), however no differences in ascorbate content were found between WT and GLUT1 KO FDBs (Fig 8C).

GLUT1 expression is insufficient to prevent anoxia-induced loss of force output of the EDL.

Following our determination that muscle-specific loss of GLUT1 increased the FDB's susceptibility to anoxia, we assessed whether increasing GLUT1 content in the EDL muscle of GLUT1 KO mice would prevent or attenuate anoxia-induced loss of contractile function in the EDL. GLUT1 overexpression in the EDL was achieved via AAV9-mediated delivery of GLUT1-GFP cDNA. At 3 weeks post-injection, GLUT1 was present at the sarcolemma as evidenced by the signal co-localization of GFP and dystrophin (Fig 9A). Using the gain-of-function approach, the sufficiency of GLUT1 for anoxia resistance in the EDL was assessed under four different conditions: GLUT1 overexpression alone, GLUT1 + glucose, GLUT1 + ascorbate, and GLUT1 + ascorbate + ascorbate oxidase. However, none of the conditions improved the ability of the EDL to retain force output during anoxia (Fig 9B-D; ascorbate oxidase data not shown).

Discussion

It is universally accepted that O_2 is essential to mammalian cell function and survival. Skeletal muscle is among the most metabolically active organ systems in which O_2 plays a critical role in meeting the high bioenergetic demands of the tissue. Accordingly, hypoxia exposure is a potent insult to muscle function (Godt & Nosek, 1989; Schmidt et al., 2020). HLI surgery results in functional and histomorphological disruption in the EDL and soleus muscles. In contrast, the FDB maintains force production and structural integrity despite the same loss of tissue vessel perfusion and O_2 tension. Consistent with *in vivo* findings, the FDB maintained force production during 3 hours of *ex vivo* anoxia exposure whereas the EDL and soleus muscles experienced significant force loss after only 20 mins. Using a discovery-based approach, we compared the proteome of the EDL, soleus and FDB. We found that GLUT1 content is higher in the FDB

compared to the EDL and soleus and confirmed that GLUT1 is necessary for the FDB phenotype using a skeletal muscle specific GLUT1 KO mouse. However, AAV-mediated overexpression of GLUT1 was unable to improve anoxia resistance in the EDL muscle. Collectively, our data indicate that the FDB contains a unique phenotype that is not seen more central skeletal muscles. It may be possible to leverage this phenotype to identify mechanisms that confer hypoxia resistance.

Loss of O_2 tension during hypoxia decreases flux of the mitochondrial ETS and consequently decreases the free energy available to perform cellular work due to a lower [ATP]/[ADP] ratio (Neufer, 2018). Unlike the EDL and soleus, the FDB is able to preserve cellular energy charge during anoxia exposure as evidenced by the lack of change in the [ATP]/[ADP] ratio. This ability suggests that bioenergetic regulation within the FDB is unique. Skeletal muscle fiber type analysis on the basis of myosin heavy chain (MHC) isoform prevalence is often associated with metabolic properties of a muscle. For example, IIx and IIb MHC are often linked with glycolytic metabolism while I and IIa MHC are linked with oxidative metabolism. The FDB is a mixed muscle comprised predominantly of IIa and IIx myofibers with few I and no IIb myofibers (Tarpey et al., 2018). Based on fiber type composition, one would predict that oxidative metabolism plays an integral role in the FDB. Surprisingly, however, our interrogation of basal mitochondrial function revealed that FDB respiration kinetics and $\Delta\Psi$ are far lower than those of the EDL (a fast glycolytic muscle). Furthermore, the EDL contains more mitochondrial proteins than the FDB as identified by discovery-based proteomics, suggesting that mitochondrial content is relatively low in the FDB. Supporting the notion that mitochondria do not play a key role in the FDB is the relatively small change in anoxic force production when KCN is added to the *ex vivo* bath. In contrast, the EDL and soleus muscles demonstrated significant loss in force output when exposed to KCN during anoxia. The longer time to reach the FD_{50} in the FDB shows that KCN sensitivity is much lower than that of the EDL and soleus. These data suggest the FDB has adopted a phenotype that does not depend upon the mitochondria to meet the energetic demand of the muscle and further does not reflect the muscle fiber type composition.

Inhibition of glycolysis with bromopyruvate (BrP) decreased force production of all three muscles during anoxia, suggesting that glycolysis is necessary for function across muscles. Importantly, the lack of differences in BrP sensitivity indicates that the FDB does not depend upon glycolysis more than other muscles. Interestingly, the sum of glycolytic proteins identified in the FDB was less than that of the EDL suggesting that the FDB is not upregulating the capacity to perform glycolysis. Discovery-based proteomic analysis determined that GLUT1 content is significantly higher in the FDB compared to the EDL and soleus. While GLUT4 is the predominant insulin- and exercise-responsive glucose transporter in skeletal muscle, GLUT1 is thought to be responsible for basal glucose uptake (Kraegen et al., 1993; Richter & Hargreaves, 2013). We hypothesized that glycogen content would differ across the three included muscles and found that the FDB contains more glycogen than the EDL but not the soleus muscle. We also measured glycogen content following the 3-hour contractile protocol during anoxia to assess whether the FDB would contain less glycogen than the EDL at completion. Neither muscle exhibited a large decrease in glycogen content, which was surprising in light of previous research that demonstrated a significant decrease in skeletal muscle glycogen content following anoxia exposure (Schmidt et al., 2020). A key difference in the study by Schmidt et al. (2020) is the greater work performed by the muscles during the contractile protocol as compared to our protocol, thus implying greater energetic demand, and potentially explaining lower glycogen content. Also surprisingly, McMillin et al. (2022) recently demonstrated that neither glucose uptake nor glycogen content is altered in skeletal muscles that lack GLUT1 expression suggesting a complicated role for GLUT1 in skeletal muscle. Our resulting data provide equivocal evidence that pharmacological inhibition of glycolysis via BrP results in loss of FDB force production during anoxia exposure, however the muscle does not appear to catabolize greater amounts of glucose. It is possible that BrP treatment affected other mechanisms necessary for force production that are independent of glycolysis. However, the literature largely suggests that BrP inhibits multiple

glycolytic enzymes (Shoshan, 2012). With that said, we cannot rule out any non-specific effects of BrP on force production.

GLUT1 protein levels in adult rodent hindlimb skeletal muscles have been demonstrated to increase during hypoxia (Xia et al., 1997). Such a response may be indicative of metabolic protection during times of limited energy availability. Our data demonstrate greater GLUT1 protein content in the FDB as compared to the soleus and EDL. Thus, to determine if GLUT1 provides for any portion of the protective phenotype in the FDB, we subjected muscles from WT and skeletal muscle-specific GLUT1 KO mice to the 3-hour contractile protocol. FDBs from GLUT1 KO mice exhibited an accelerated loss of force output during anoxia compared to FDBs from WT littermate mice, suggesting that GLUT1 is necessary in part to explain the FDB phenotype. Despite the lack of differences in glycogen content between GLUT1 KO and WT FDBs, we found that the WT FDB contains over 13x greater ascorbate than the WT EDL and soleus. We hypothesized that high levels of ascorbate might attenuate oxidative stress in the FDB during anoxia, however deletion of GLUT1 did not affect FDB ascorbate content. This suggests that another mechanism is responsible for high ascorbate levels in the FDB. GLUT10, for example, also transports oxidized ascorbate (Lee et al., 2010).

Previous research in smooth muscle cells has shown that GLUT1 overexpression prevents apoptosis during acute hypoxia exposure (Lin et al., 2000). This work is based on a protective effect of increased glucose uptake and glycolytic activity for cardiomyocyte survival under hypoxic conditions (Malhotra & Brosius, 1999). To assess if GLUT1 offers protection of other skeletal muscles during anoxia, we overexpressed GLUT1 in the EDL from GLUT1 KO mice using an AAV-mediated delivery. In these experiments EDLs with GLUT1 were placed in a bath with or without glucose or ascorbate and subjected to the 3-hour contractile protocol. To ensure that newly introduced ascorbate was oxidized in the *ex* vivo bath we also included experiments with added ascorbate oxidase. However, resistance to anoxia-induced loss of EDL force production was not achieved under any condition. Our results indicate that GLUT1 overexpression

alone is insufficient to create a protective phenotype in skeletal muscle during anoxia. Furthermore, the FDB phenotype reflects a molecular adaptation that includes increased GLUT1 content but likely requires additional components that are undefined at this time. We speculate that GLUT1 may synergize with other cellular components to protect the FDB during hypoxia.

To our knowledge, this study provides the first evidence of a skeletal muscle that is inherently adapted to maintain its function in the complete absence of O_2. We have thoroughly documented multiple aspects of the FDB phenotype which provide key evidence to uncovering the muscle's ability to resist hypoxia. Protecting a skeletal muscle from hypoxia is a critical need to improve tissue survival during states of acute hypoxia (e.g., altitude) or during various conditions and/or diseases that are associated with muscle atrophy or wasting (e.g., PAD, COPD, CHF, total knee arthroplasty). Identifying the mechanism(s) that confer the FDB phenotype will be instrumental in overcoming these challenges with the goal of leveraging the mechanism(s) in other muscles and potentially in other tissues that are susceptible to hypoxia. In addition, since no other known murine skeletal muscle can replicate this unique phenotype, the FDB muscle represents a unique opportunity to increase our understanding of skeletal muscle biology using a muscle with a distinct phenotype. Thus, the physiology of the FDB offers an auspicious opportunity to unlock novel approaches that may promote the viability of mammalian tissue in conditions of limited O_2 bioavailability.

Acknowledgements

This work was funded by support from the following grants: NIH AR078100 (EES), NIH AR066660 (EES), NIH HL157659 (JMM), NIH R01AR070200 (JJB), NIH R01DK103562 (CAW), NIH R21AR081593 (CAW).

Figure 1 (A-D)

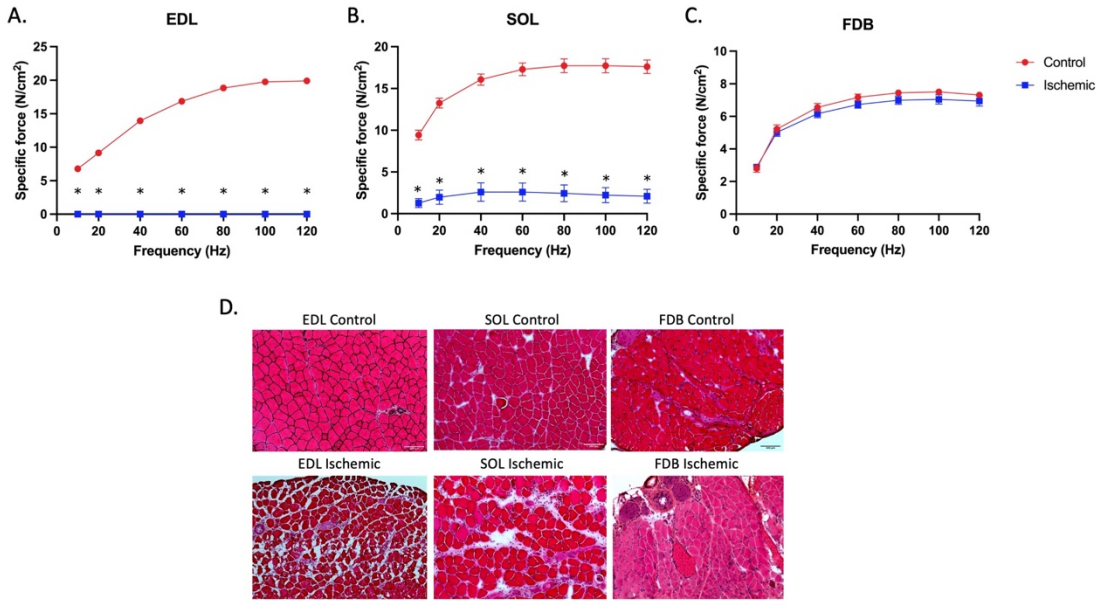

Figure 1. *In vivo* HLI causes functional & structural damage in the EDL & soleus, but not the FDB. Force-frequency curves from control (red) and ischemic (blue) EDL ($p<0.00005$ compared to contralateral control; A), soleus ($p<0.005$ compared to contralateral control; B), and FDB muscles (C) at 48 hours post-HLI. Muscles were stimulated to contract over a range of increasing frequencies, and force output was plotted at each stimulation. (D) Representative cross-sectional images of the EDL, soleus, and FDB stained with hematoxylin & eosin at 48 hours post-HLI.

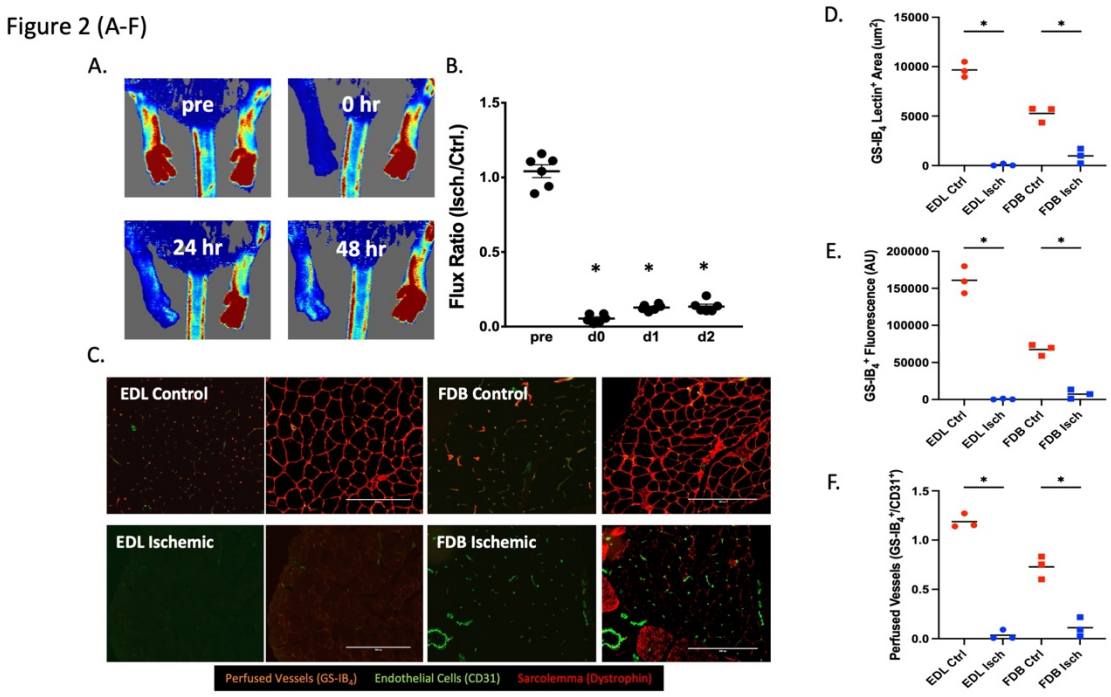

Figure 2. *In vivo* HLI causes loss of blood perfusion in skeletal muscles distal to the ligation site. Laser Doppler perfusion imaging (A) and quantification (B) of the paw in the prone position at various time points following induction of HLI. C) Representative immunofluorescent cross-sectional images of control and ischemic EDL and FDB muscles at 48 hours post-HLI. Sections were probed for GS-IB_4 lectin (orange) to label actively perfused vessels, CD31 (green) to label total endothelial cells, and dystrophin (red) to outline the sarcolemma. Loss of blood perfusion to the EDL and FDB was confirmed by measuring the area (D) and fluorescence (E) of GS-IB_4^+ vessels alongside plotting the signal ratio of GS-IB_4 to $CD31^+$ (F). * = $p<0.0005$ compared to contralateral control.

Figure 3 (A-C)

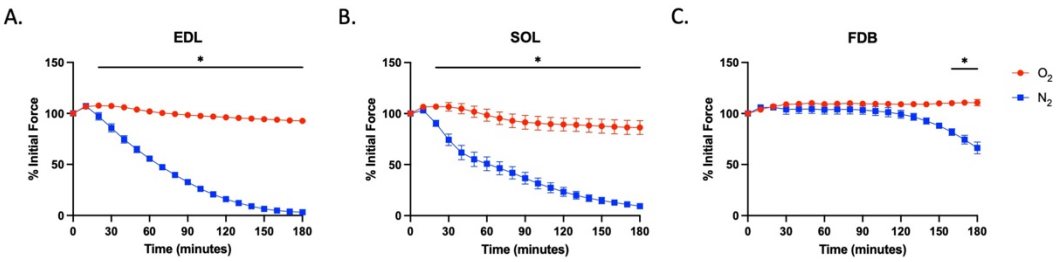

D.

FD^{50} (minutes) – N_2		
EDL	SOL	FDB
66.8	61.8	---

Figure 3. (A-C) *Ex vivo* anoxia exposure causes force loss in the EDL & soleus, but not the FDB. Initial force output was measured under oxygenated conditions. Muscles were then exposed to 95% O_2/5% CO_2 (normoxia) or 95% N_2/5% CO_2 (anoxia) for 180 mins. Muscles were stimulated maximally (100 Hz) every 10 mins and force output was measured and plotted as a percentage of the initial normoxic force. FD^{50} represents the time at which force output falls to 50% of the initial normoxic force. *$p<0.005$ compared to contralateral O_2 condition.

Figure 4 (A-H)

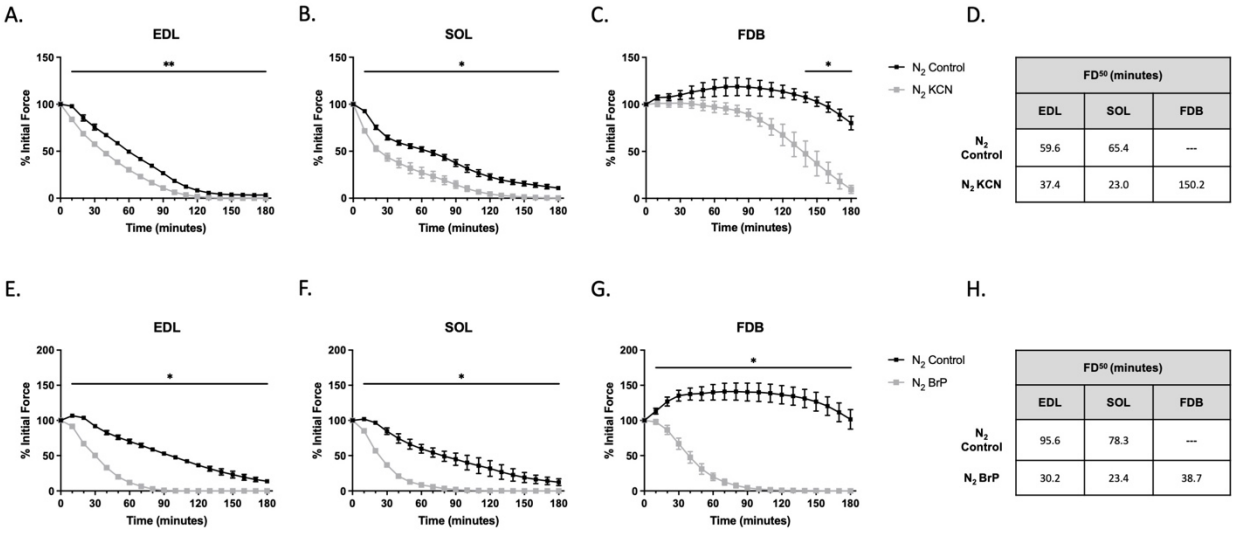

Figure 4. (A-D) Inhibition of mitochondrial respiration during *ex vivo* anoxia exposure accelerates force loss in the EDL and soleus, but not to the same extent in the FDB. Initial force output was measured under oxygenated conditions. Muscles were then exposed to 95% N_2/5% CO_2 (anoxia) for 180 mins with or without the addition of potassium cyanide (KCN) to the bath. Muscles were stimulated maximally (100 Hz) every 10 mins and force output was measured and plotted as a percentage of the initial normoxic force. *represents significant difference between N_2 control vs N_2 KCN condition EDL = $p<0.005$; *soleus = $p<0.05$; *FDB = $p<0.05$. (E-H) Inhibition of glycolysis during *ex vivo* anoxia exposure accelerates force loss in the EDL, soleus, and FDB**.** Initial force output was measured under oxygenated conditions. Muscles were then exposed to 95% N_2/5% CO_2 (anoxia) for 180 mins with or without the addition of bromopyruvate (BrP) to the bath. Muscles were stimulated maximally (100 Hz) every 10 mins and force output was measured and plotted as a percentage of the initial normoxic force. ** represents significant difference between N_2 control vs N_2 BrP condition EDL = $p<0.001$; * soleus = $p<0.05$; * FDB = $p<0.001$.

Figure 5 (A-C)

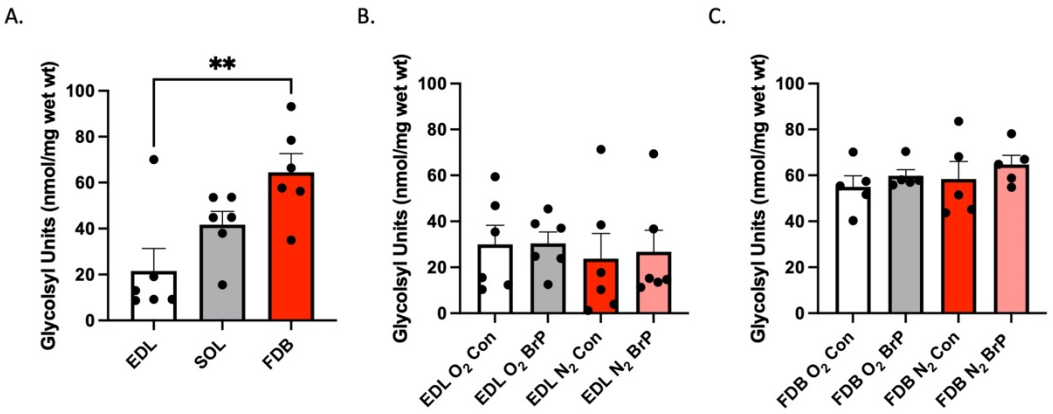

Figure 5. **(**A) Glycogen content in untreated EDL, soleus, and FDB muscles (**p=0.005). (B) Glycogen content in EDL muscles following the 3-hour contractile protocol during normoxia (O_2) or anoxia (N_2) with and without BrP treatment. (C) Glycogen content in FDB muscles following the 3-hour contractile protocol during normoxia (O2) or anoxia (N2) with and without BrP treatment.

Figure 6 (A-F)

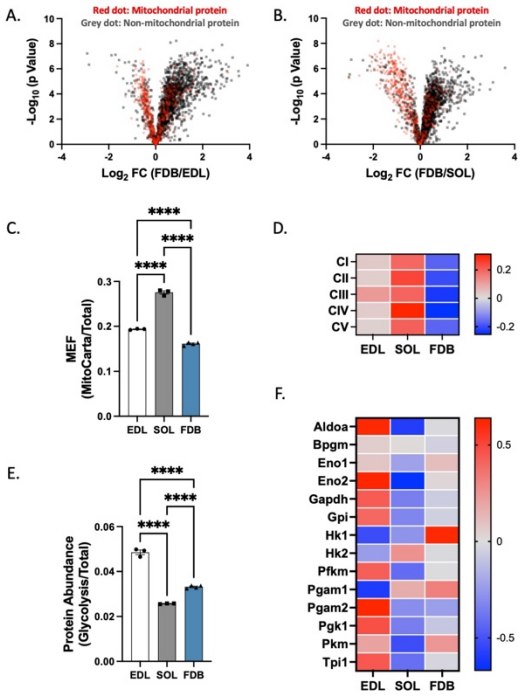

Figure 6. (A-B) Volcano plot of differentially expressed proteins between (A) EDL and FDB muscles and (B) soleus and FDB muscles. Red dots represent mitochondrial proteins while grey dots represent non-mitochondrial proteins. A leftward position of a dot indicates greater expression in the EDL or soleus while a rightward position of a dot indicates greater expression in the FDB. An upward position indicates a more significant difference in protein expression between muscles. (C) Quantification of the mitochondrial enrichment factor (MEF) in the EDL, soleus, and FDB muscles. The MEF represents the number of mitochondrial proteins identified by MitoCarta normalized to the total number of proteins identified by the Proteome Discoverer. (D) Heatmap analysis of mitochondrial ETS complex-specific content in the EDL, soleus, and FDB muscles. Red indicates greater content while blue indicates lower content. (E) Quantification of identified glycolytic proteins normalized to total proteins identified by the Proteome Discoverer in the EDL, soleus, and FDB muscles. (F) Heatmap analysis of 14 glycolytic enzymes detected in the EDL, soleus, and FDB muscles. Red indicates greater content while blue indicates lower content.

Figure 7 (A-C)

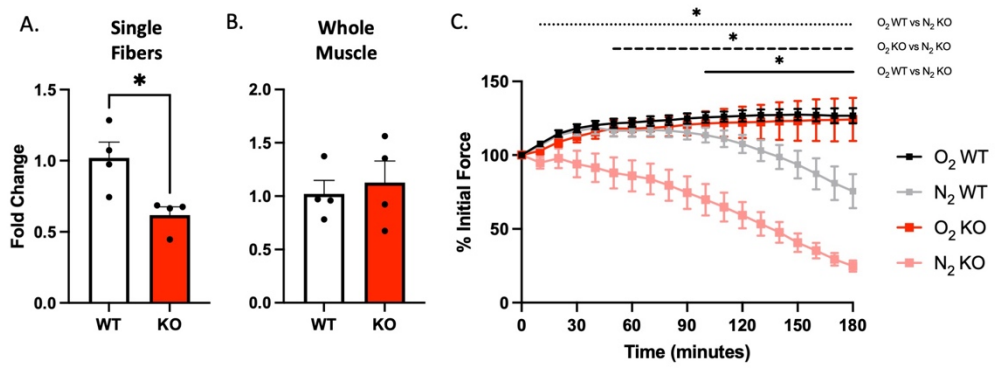

Figure 7. GLUT1 is necessary for the anoxia-resistant FDB phenotype.
(A) Validation of decreased GLUT1 mRNA via qRT-PCR analysis in single muscle fibers isolated from FDBs of GLUT1 KO mice as compared to that of WT FDBs ($p<0.05$ WT vs KO). (B) GLUT1 mRNA quantification via qRT-PCR analysis of whole FDB muscle homogenates from WT and GLUT1 KO mice. (C) Force-time curves of WT and GLUT1 KO FDBs during the 3-hour contractile protocol. Initial force output was measured under oxygenated conditions. Muscles were then exposed to 95% O_2/5% CO_2 (normoxia) or 95% N_2/5% CO_2 (anoxia) for 180 mins. Muscles were stimulated maximally (100 Hz) every 10 mins and force output was measured and plotted as a percentage of the initial normoxic force. *represents significantly different from N_2 KO $p<0.05$.

Figure 8 (A-C)

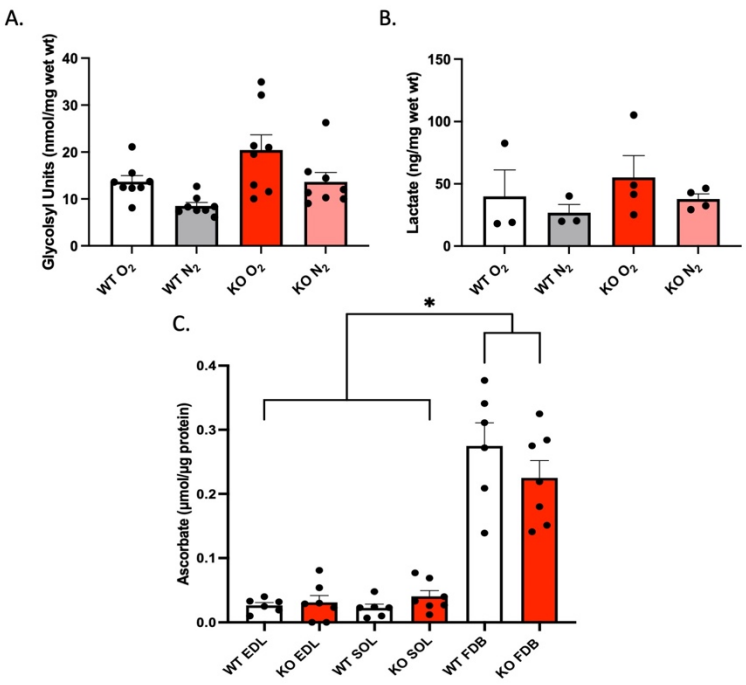

Figure 8. Glycogen (A) and lactate (B) content in FDBs from WT and GLUT1 KO mice following the 3-hour contractile protocol during normoxia (O_2) or anoxia (N_2). (C) Ascorbate content in EDL, soleus, and FDB muscles from WT and GLUT1 KO mice following the 3-hour contractile protocol during normoxia (O_2) or anoxia (N_2). * = main of effect of muscle type $p<0.0001$.

Figure 9 (A-D)

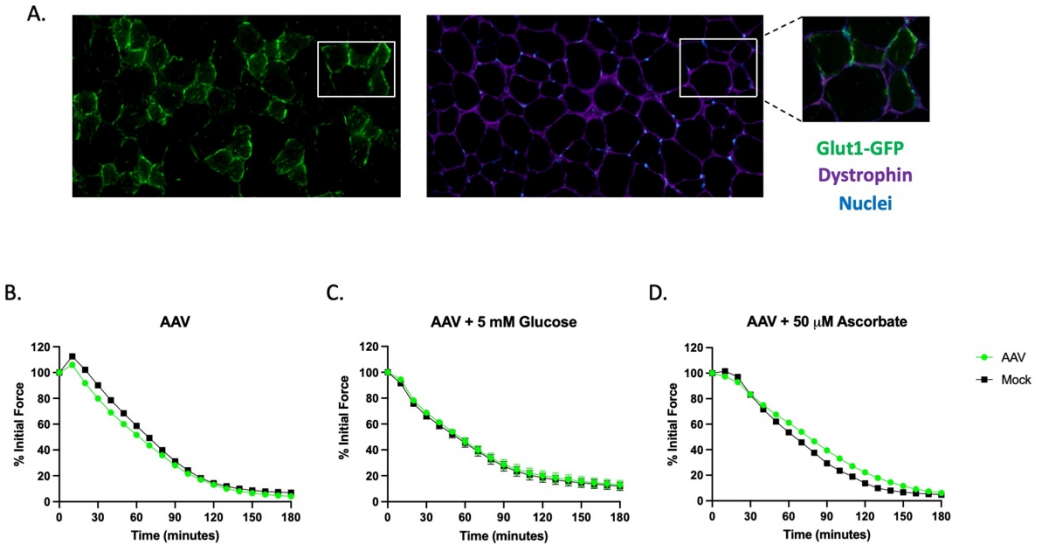

Figure 9. GLUT1 is insufficient to rescue the EDL from anoxic force loss.
(A) Representative cross-sectional image of an EDL with GLUT1-GFP overexpression. Sections were probed for nuclei (DAPI, blue) and dystrophin (purple) to confirm successful delivery of the GLUT1-GFP AAV. Note the dystrophin-GFP signal overlay at the sarcolemma. (B-D) Force-time curves of control EDLs (mock, black) and EDLs with GLUT1-GFP overexpression (AAV, green) during the 3-hour contractile protocol with anoxia exposure. Three conditions were employed: (B) GLUT1 AAV alone, (C) GLUT1 AAV + glucose, and (D) GLUT1 AAV + ascorbate.

Table 1

	ATP			ATP/ADP			ATP/AMP			IMP		
	EDL	SOL	FDB	EDL	SOL	FDB	EDL	SOL	FDB	EDL	SOL	FDB
O_2	6.1 ± 0.2	3.5 ± 0.7	2.1 ± 0.2	5.9 ± 0.3	4.5 ± 0.2	3.2 ± 0.2	505.8 ± 93	121 ± 19	56.7 ± 14.8	0.07 ± 0.02	0.03 ± 0.01	0.02 ± 0.001
N_2	6.1 ± 1	3.0 ± 0.8	2.2 ± 0.2	4.6 ± 0.3*	1.8 ± 0.3*	2.8 ± 0.2	176.3 ± 2.3*	16.6 ± 4.6*	51.5 ± 12.7	0.19 ± 0.04*	0.22 ± 0.07*	0.01 ± 0.003

Table 1. Nucleotide concentrations (μmol/g wet wt.) in different skeletal muscles following 1 hour of 95% O_2/5% CO_2 (normoxia) or 95% N_2/5% CO_2 (anoxia) exposure. * = $p<0.05$.

Supplement

Materials & Methods

Mitochondrial oxygen consumption and membrane potential

Mitochondrial O_2 consumption (JO_2) and membrane potential ($\Delta\Psi$) were measured as previously described (Tarpey et al., 2018, 2019). Briefly, muscle fiber bundles were isolated from the EDL, soleus, and FDB muscles and permeabilized with saponin (30 μg/mL). Glutamate- and malate-stimulated JO_2 was measured using the OROBOROS Oxygraph-2K high-resolution respirometer (Oroboros Instruments, Innsbruck, Austria) and normalized to muscle fiber bundle dry weight. In separate sets of experiments, EDL and FDB muscles were dissected from 8 different animals and placed in separate tubes. Muscles were minced and homogenized prior to differential centrifugation for mitochondrial isolation as previously described (Tarpey et al., 2019). All respiration measures in isolated mitochondria were normalized to mitochondrial protein, which was determined using a Pierce BCA Protein Assay Kit (ThermoFisher Scientific) that was carried out in quadruplicate. $\Delta\Psi$ was determined by quantifying the fluorescence of tetramethyl rhodamine methyl ester (TMRM; 0.2 uM) using a QuantaMaster spectrofluorometer (QM-400, Horiba Scientific, Kyoto, Japan). The excitation/emission ratio of 572/590 nm to 551/590 nm was used to measure TMRM fluorescence, which was subsequently converted to mV using a previously determined standard curve.

Detailed description of muscle proteomics

Samples were centrifuged at 500xg for 5 minutes (4°C) to remove large debris, and supernatants were transferred to fresh tubes. Protein concentrations of each sample were determined with a Pierce BCA Protein Assay Kit (ThermoFisher Scientific), and samples were prepared into aliquots of 500μg total protein in 200μL of urea lysis buffer. Samples were reduced by adding 2.02μL of 0.5M dithiothreitol (DTT) (final concentration of 5mM) and incubated at 32°C on a heat block for 30 minutes. After allowing samples to return to room temperature, alkylation

was performed by adding 6µL of 0.5M iodoacetamide (IAM) to each sample (final concentration of 15mM) and incubating at room temperature for 30 minutes in the dark. Unreacted IAM was quenched by adding 4.04µL of 0.5M DTT to each sample and incubating at room temperature for 10 minutes. Next, 4.5µL of Lys-C (0.5µg/µL) was added to each sample, and samples were incubated for 4 hours at 32°C on a heat block for 4 hours, vortexing occasionally. Samples were diluted to 1.5M urea by adding 845µL of 50mM (Tris pH 8.0) and 5mM $CaCl_2$. Sequence grade trypsin (Promega V511C) was added to each sample at 1:50 (10µg per sample), and samples were wrapped in parafilm and digested overnight at 32°C on a heat block. Samples were acidified to 0.5% v/v trifluoroacetic acid (TFA) by adding 50µL of 10% TFA to each sample and a pH of less than 2 was verified using pH strips. Undigested material was settled by centrifuging samples at 10,000xg for 10 minutes (room temperature). Supernatants containing soluble peptides were desalted via a 50 mg tC18 SEP-PAK solid phase extraction column (Waters, WAT054955), then eluted (500 µL 25% acetonitrile/0.1% TFA and 2 × 500 µL 50% acetonitrile/ 0.1% TFA). The eluate (1.5mL total) was then frozen on dry ice and lyophilized overnight. Following lyophilization, samples were centrifuged at 13,000xg for 10 minutes (room temperature). Tandem Mass Tag labeling was subsequently performed using a TMT10plex Isobaric Label Reagent Set (Thermo Fisher Scientific, Cat#90110) as previously described (Fisher-Wellman et al., 2019). Briefly, samples were resuspended in 100µL of 200mM triethylammonium bicarbonate and mixed with a unique 10plex TMT reagent (0.8 mg re-suspended in 50 µL100% acetonitrile). Samples were vortexed for 4 hours. Unreacted TMT reagent was quenched by adding 0.8µL of 50% hydroxylamine to each sample and vortexing samples for 15 minutes. All samples were combined into one tube, frozen on dry ice, and lyophilized overnight. The combined sample was resuspended in 1mL of 1mL 0.1% TFA and 42µL 10% TFA. Solid phase extraction was repeated with a 100 mg tC18 SEP-PAK SPE column (Waters; Cat# WAT023590), and the sample was frozen on dry ice and lyophilized overnight.

Lactate efflux

During incubation of the EDL and FDB in 95% O_2/5% CO_2 (normoxia) or 95% N_2/5% CO_2 (anoxia) for 1 hour (n=6/condition), 1 mL of KRB was collected at the start of the protocol and again every 20 minutes. KRB samples were flash frozen in liquid N_2 upon collection. Lactate concentrations (ng/mL) in the KRB samples were subsequently measured using the lactate assay described in the Methods section.

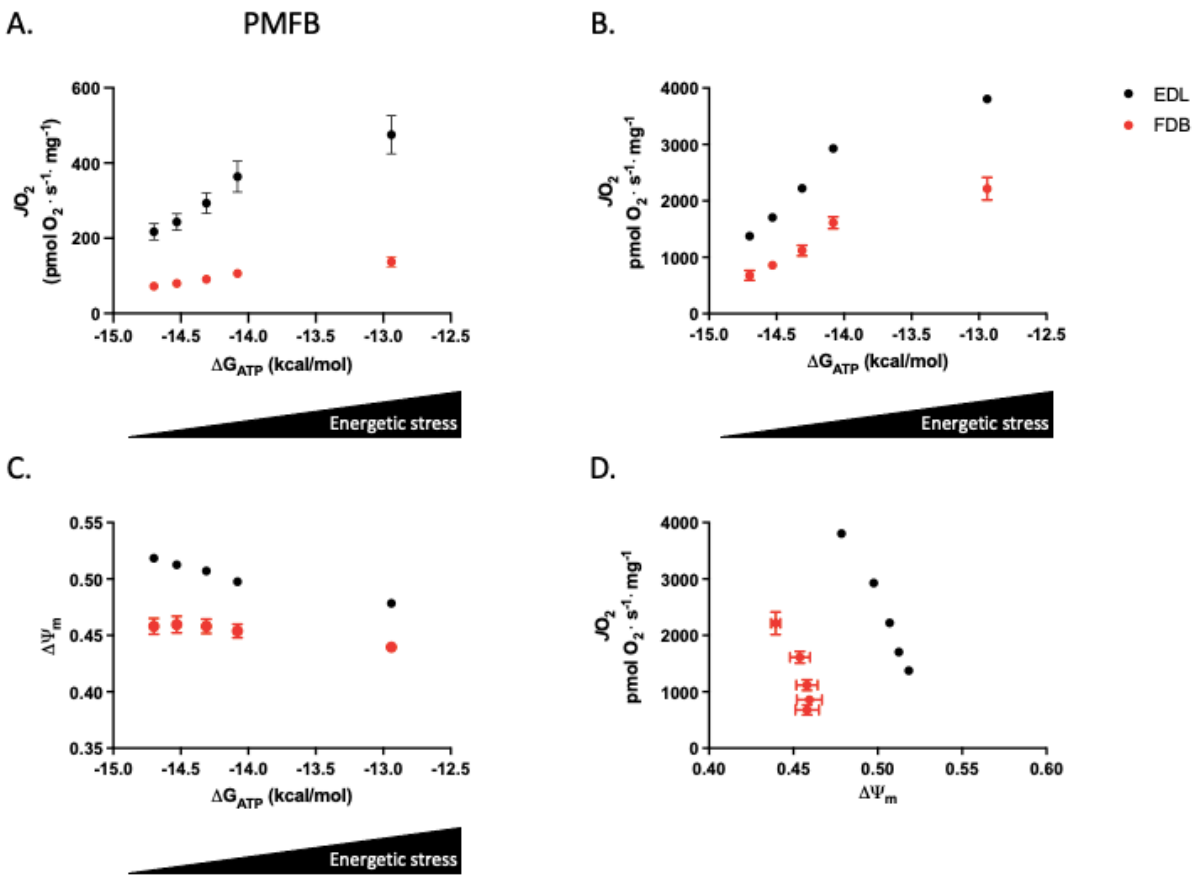

Figure S1. Basal mitochondrial function in the FDB is low relative to the EDL.
Mitochondrial respiration plotted against ATP free energy (ΔG_{ATP}) in (A) permeabilized muscle fiber bundles and (B) isolated mitochondria from EDL and FDB muscles. (C) Mitochondrial membrane potential ($\Delta\Psi$) plotted against ΔG_{ATP} in isolated mitochondria from EDL and FDB muscles. Note lower oxygen consumption (JO_2) and membrane potential in FDB mitochondria as compared to EDL mitochondria across the increasing values of ΔG_{ATP}, which represent greater energetic demands. (D) JO_2 plotted against $\Delta\Psi$ in isolated mitochondria from EDL and FDB muscles. A rightward shift in the graph indicates greater efficiency of the ETS.

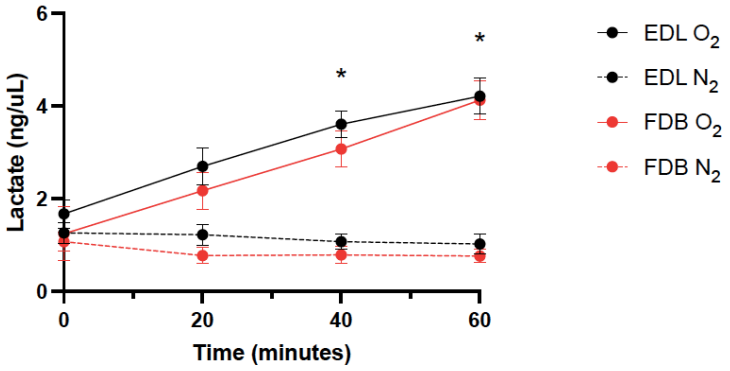

Figure S2. Lactate efflux from the EDL and FDB during 1 hour of normoxia and hypoxia. Lactate concentrations (ng/mL) were measured in KRB samples collected from the bath at the start of the protocol and every 20 minutes thereafter. * = significant differences between O_2 and N_2 conditions in both muscles ($p < 0.005$).

	FDB vs EDL			FDB vs SOL		
	Gene	**Log2FC**	**p-value**	**Gene**	**Log2FC**	**p-value**
1	Tnnt3	3.91390327	1.38855E-05	Tnnt3	3.59762554	2.05831E-05
2	Col3a1	3.54656866	3.89459E-05	Coch	3.08647474	9.28315E-05
3	Angptl7	3.52587433	2.35257E-05	Mybph	2.96183385	0.000219878
4	Coch	3.27555634	1.22489E-05	S100a4	2.59227825	1.0212E-05
5	Prph	3.22764817	6.04467E-05	Col3a1	2.54568105	0.000115454
6	Myl6b	3.1081665	1.61057E-05	Cnn1	2.50544662	0.000231309
7	Ca3	3.08531511	2.57117E-05	Anxa8	2.33913879	1.06192E-05
8	Plp1	3.05263546	5.02833E-05	Lgals3	2.25009756	6.74234E-05
9	Tpm2	3.03673556	2.35257E-05	Prph	2.24713577	0.00030069
10	Cnn1	3.01370337	7.05741E-05	Tagln	2.24216888	0.000165573
11	Tpm1	3.01021946	5.11212E-05	Angptl7	2.22579308	0.000394313
12	Uchl1	3.002694	1.38855E-05	Pvalb	2.19482894	5.78524E-05
13	Col1a1	2.92259875	0.000115233	Sod3	2.12315494	0.000417826
14	Tagln	2.86243599	4.41396E-05	Col1a1	2.1152661	0.000256954
15	Csrp3	2.84393895	1.83934E-05	Tpm2	2.06774745	0.00013439
16	S100a4	2.83043714	8.31105E-06	Tpm1	2.06501812	0.000203361
17	Csrp1	2.81896365	3.29223E-05	Cmbl	2.05317753	2.71146E-05
18	Lgals3	2.80834073	2.02531E-05	S100a6	2.02674829	2.77739E-05
19	Mbp	2.80197844	9.49756E-05	Col1a2	1.99506469	0.000313693
20	Comp	2.78074852	3.7452E-05	Sorbs2	1.98595507	9.34661E-05
21	Aspn	2.76502472	1.38855E-05	Csrp1	1.98293008	0.000146007
22	Col1a2	2.75700559	0.000143733	Plp1	1.92700833	0.001003893
23	Myoc	2.69888345	1.38855E-05	Uchl1	1.92671091	8.74662E-05
24	Nefl	2.62050083	7.14584E-05	Nefm	1.90673617	0.000289289
25	Sod3	2.59005895	6.33264E-05	Myoc	1.88515679	0.000316072
26	Col5a1	2.55963826	9.59241E-05	Slc2a1	1.88412226	9.37726E-05
27	Anxa8	2.55524881	1.38855E-05	Mustn1	1.87849224	0.000891484
28	Col2a1	2.55335682	0.000569715	Nefl	1.87515862	0.000377293
29	Col11a2	2.48104567	0.000294201	Cacng1	1.87164988	0.006895623
30	Cend1	2.4620941	0.000162673	Crip1	1.84167821	1.0212E-05
31	Igfbp7	2.45201141	0.000153815	Lum	1.80333097	2.15083E-05
32	Mt3	2.43569663	0.00020405	Cd9	1.80210991	0.000147403
33	Crip1	2.4323624	1.02878E-05	Cend1	1.77867861	0.000448897
34	Mpz	2.40999594	0.00048669	Vim	1.73659994	2.5856E-05
35	Myh11	2.39705438	0.000233502	Dstn	1.72841257	9.1152E-05
36	Fhl1	2.37557126	1.49033E-05	Mt3	1.72836304	0.000635504
37	Cnp	2.3581141	9.74619E-05	Mbp	1.72581884	0.000904946
38	Cd9	2.32981594	8.88946E-05	Tmem43	1.7082454	3.80609E-05
39	Rbm3	2.32783326	1.64494E-05	Col5a1	1.69937469	0.000235328
40	S100a6	2.31586379	1.38855E-05	Dcn	1.69918154	0.000128074
41	Kctd12	2.2825033	0.007807726	Tubb3	1.68778517	0.000903495

42	Tubb3	2.27852811	0.00015218	S100a10	1.68239478	4.30935E-05
43	Nefh	2.27328166	9.41742E-05	Cnp	1.67668875	0.000379732
44	Vim	2.24990831	1.66567E-05	Myh11	1.66862754	0.001133061
45	Prx	2.23991462	0.000135207	Dpt	1.63362342	1.73098E-05
46	Ppp1r12a	2.21165523	0.000102553	Flna	1.62602919	0.000443951
47	Dstn	2.19671187	8.80326E-05	Prx	1.62212643	0.000630786
48	Sorbs2	2.18601522	5.08075E-05	Mpz	1.61086526	0.002773612
49	Sh3bgrl	2.15773407	1.17614E-05	Aspn	1.60745468	4.46495E-05
50	Tuba1b	2.15259286	4.50959E-05	Inmt	1.60447054	2.38883E-05
51	Slc2a1	2.13936711	4.50959E-05	Tgfbi	1.59308696	5.52403E-05
52	Smtn	2.12951635	0.000402199	Col28a1	1.58547664	0.00117565
53	Thbs4	2.1145596	9.00276E-05	Rbm3	1.57904152	0.000120547
54	Myl9	2.11123724	0.000124473	Kctd12	1.56123925	0.029905775
55	Fbn2	2.0997099	4.64855E-05	Nefh	1.55240613	0.000590374
56	S100a10	2.09382908	1.5094E-05	Sh3bgrl	1.54224086	2.05831E-05
57	Myl6	2.07904528	5.26305E-05	Smtn	1.5419727	0.001270116
58	Entpd2	2.07603505	0.000395112	Anxa2	1.53321928	2.71146E-05
59	Flna	2.06271272	0.000147858	Prx	1.49490094	7.76721E-05
60	Sh3bgrl3	2.05949921	0.000165718	Pdlim3	1.49156832	0.00010311
61	Nefm	2.05816506	0.000110515	Entpd2	1.46647872	0.00031099
62	Mustn1	2.04612781	0.000281626	Krt10	1.44549965	0.063081795
63	Myh8	2.04434542	5.71375E-05	Ca3	1.44431633	0.000109703
64	Tnnc1	2.0337455	0.006037208	F13a1	1.44360022	0.000109703
65	Epb41l2	2.02130982	0.000143733	Myl6b	1.44127611	2.42014E-05
66	Prx	2.00392405	5.54131E-05	Col2a1	1.43782606	0.001393956
67	Fbn1	1.99485683	0.000123074	Col6a1	1.42428092	9.69176E-05
68	Ndrg1	1.98789048	0.000295407	Map1b	1.42057973	0.00037013
69	Lum	1.98505876	1.38855E-05	Anxa1	1.40236266	7.96605E-05
70	Tgfbi	1.97996265	4.41396E-05	Lmna	1.39868726	2.15083E-05
71	Lmna	1.97679969	1.38855E-05	Col6a2	1.38528031	0.000203361
72	Tubb2a	1.96820453	7.64326E-05	Thbs4	1.37535159	0.000150038
73	Cotl1	1.9583231	2.56052E-05	Apod	1.37368131	9.04347E-05
74	Serpinb1a	1.95253711	1.24445E-05	Krt2	1.37347326	0.077802118
75	Tmem43	1.9479535	1.02878E-05	Fmod	1.36423375	0.000291584

Table S1. 75 proteins with the greatest content detected by the Proteome Discoverer in the FDB vs EDL (left) and FDB vs soleus (right). GLUT1 (gene name – Slc2a1) is surrounded by red borders within the table.

CHAPTER 4: Innate or adapted? Sarcolemmal stability promotes hypoxia resistance in the mouse flexor digitorum brevis skeletal muscle

Everett C. Minchew[1], Andrew T. Readyoff[1], Adam J. Amorese[1], Nicholas C. Williamson[1], McLane M. Montgomery[1], Joseph M. McClung[1,2,3], Kelsey H. Fisher-Wellman[1,2], Espen E. Spangenburg*[1,2]

1 – East Carolina University, Department of Physiology, Brody School of Medicine, Greenville, NC, USA, 27834
2 – East Carolina Diabetes and Obesity Institute, East Carolina University, Greenville, NC, USA, 27834
3 – East Carolina University, Department of Cardiovascular Sciences, Brody School of Medicine, Greenville, NC, USA, 27834

* – Corresponding Author

*To whom correspondence should be addressed: Espen E. Spangenburg Ph.D., Department of Physiology, East Carolina Diabetes and Obesity Institute, Brody School of Medicine, 115 Heart Drive, East Carolina University, Greenville, NC 27834; spangenburge14@ecu.edu; Tel. 252-737-5035

Abstract

Hypoxia induces contractile failure in majority of mammalian skeletal muscles. However, we recently discovered that the murine flexor digitorum brevis (FDB) maintains physiological function in the complete absence of oxygen (O_2). To survive a hypoxic insult, structural integrity of the cell must be preserved. Accordingly, the FDB resists damage to the sarcolemma during hypoxia. Our proteomic analysis identified significantly greater expression of Annexin A2 and Col5a1 in the FDB as compared to the hypoxia-sensitive EDL and soleus muscles. Annexin A2 participates in sarcolemmal repair while Col5a1 contributes to collagen fibrillogenesis within the extracellular matrix (ECM), which is linked to the sarcolemma via the dystrophin-glycoprotein complex. Loss-of-function experiments indicated that elevated content of either protein does not explain the FDB phenotype. However, we found that the phenotype is adapted over time as FDBs from young mice exhibit damage under the same hypoxic conditions during which FDBs from adult mice survive. Upon our observations of the adaptation, we employed a comprehensive bioinformatics approach that interrogated the proteome of FDBs from adult and young mice and

integrated the results with our initial proteomics analysis of the FDB, EDL, and soleus. In turn, we have identified proteins that are differentially expressed between the FDB from adult mice and the other hypoxia-sensitive muscles. Subsequent literature-based assessments of the resulting proteins coupled with our data surrounding the adaptation of the phenotype suggest that the FDB from adult mice is protected against hypoxic damage partially due to stabilization of dystrophin.

Introduction

Skeletal muscle hypoxia occurs as a result of various diseases (e.g., DMD, PAD, CHF, COPD), elective surgeries (e.g., total knee arthroplasty, anterior cruciate ligament reconstruction), and/or environmental stimuli (e.g., altitude exposure, mountain sickness) (Bernard et al., 1998; D'Hulst & Deldicque, 2017; Mayer et al., 2017; Ryan et al., 2019; Strassburg et al., 2005). Hypoxia can induce and/or exacerbate a myopathy that is characterized by structural and functional damage, and increased morbidity and mortality (Chaillou et al., 2014; Fitzgerald et al., 2004; Pipinos et al., 2008). Current therapeutic interventions have largely failed to rescue skeletal muscle from hypoxia-induced injury (Biscetti et al., 2021; Kent et al., 2011). Thus, novel strategies are necessary to promote the survival of hypoxic muscle tissue.

A hallmark of hypoxic damage to skeletal muscle is disruption of the sarcolemma (Fredsted et al., 2005). Skeletal muscle cells are equipped with various plasma membrane repair (PMR) systems (Barthélémy et al., 2018; Demonbreun et al., 2016, 2019), however hypoxic sarcolemmal injury challenges myocyte survival by inducing membrane lesions that allow for the entry of extracellular molecules (Fredsted et al., 2005). Among the most damaging is extracellular calcium (Ca^{2+}), which activates cysteine proteases called calpains that degrade muscle proteins, including those localized to the plasma membrane (Huang & Forsberg, 1998; Smith et al., 2008). Ca^{2+} overload also induces excitotoxicity – a phenomenon that is characterized by a gradual increase in resting muscle tension over time (Wright et al., 2005).

We recently discovered that the murine FDB preserves physiological function under multiple forms of hypoxia (Amorese & Minchew et al., 2023). Here, we demonstrate that the

preservation of sarcolemmal stability underlies this unique phenotype. In contrast to the hypoxia-sensitive EDL muscle, the FDB resists the development of excitotoxicity and the loss of dystrophin during anoxia exposure. Dystrophin is an integral sarcolemmal protein that links the cytoskeleton to the ECM, and previous research has demonstrated that dystrophin is expression lost in the hypoxic EDL (Schmidt et al., 2018). Using a previously conducted proteomics analysis (Amorese & Minchew et al., 2023) we identified two proteins – Annexin A2 and Col5a1 – that regulate sarcolemmal stability and are elevated in the FDB as compared to the EDL and soleus. Annexin A2 participates in sarcolemmal repair while Col5a1 contributes to ECM fibrillogenesis, which we hypothesized confers structural protection of the FDB and promotes the maintenance of contractile function during hypoxia. Specifically, we reasoned that elevated Annexin A2 content enables the repair of sarcolemmal lesions prior to the induction of Ca^{2+} overload and calpain activation while elevated Col5a1 content ensures stability of the ECM and maintains the link to the sarcolemma via dystrophin.

Materials & Methods

Animals

Male and female C57/BL6NJ mice (4-, 10-, and 10-12-weeks-old) were utilized in the described experiments. For a small subset of experiments, we also employed 8-14-week-old male and female mice with global heterozygous (+/-) deletion of the type V collagen isoform *Col5a1* alongside wildtype (+/+) littermates of which expressed *Col5a1* on both alleles as determined via standard genotyping procedures. *Col5a1*$^{+/-}$ mice were kindly gifted to us by Dr. Louis J. Soslowsky (University of Pennsylvania). All mice were housed in a temperature- (22°C) and light- (12/12 hr. light/dark) controlled facility and allowed *ad libitum* access to food and water. All animal procedures and usage were approved by the Institutional Review Committee at East Carolina University, and animal care complied with the Guide for the Care and Use of Laboratory Animals, Institute of Laboratory Animal Resources, Commission on Life Sciences, National Research

Council (Washington: National Academy Press, 1996).

Muscle Dissection

EDL and FDB muscles were dissected as previously described (Tarpey et al., 2018). Briefly, mice were anesthetized via isoflurane (3-4%), muscles were dissected, and mice were euthanized after the tissue was removed. During the dissection of the muscles 4-0 silk suture was used to tie a double square knot at distal and proximal tendons. Tendons were cut just above the knot, and muscles were submerged in a bath of oxygenated (95% O_2/5% CO_2) Krebs Ringer buffer (KRB) (119mM NaCl, 5mM KCl, 5mM $NaHCO_3$, 1.25mM $CaCl_2$, 1mM KH_2PO_4, 10mM HEPES, 1mM $MgSO_4$) at room temperature. The muscles were dissected from each animal as quickly as possible and immediately placed in oxygenated KRB. Muscles were affixed to a force transducer apparatus (Aurora Scientific) and equilibrated in the oxygenated KRB bath for 10 minutes. Following equilibration, optimal muscle length (L_0) was determined by administering maximal 1 Hz twitch stimulations every 30 seconds and incrementally adjusting muscle length until peak twitch force was achieved.

Muscle Contractile Protocols

Following establishment of L_0, muscles were subjected to a 3-hour protocol of isometric muscle contraction as previously described (Amorese & Minchew et al., 2023). Briefly, muscles were initially incubated in oxygenated KRB, and resting L_o was determined as described above. Muscles were either switched to a fresh solution of oxygenated KRB or nitrogenated (95%N_2/5%CO_2) KRB to simulate anoxia. Using a Clark electrode (Innovative Instruments, Inc), measurable O_2 concentration in the KRB was reduced to undetectable levels approximately 30 seconds after the KRB was bubbled with N_2. Muscles were then subjected to a maximal 100 Hz contraction every 10 mins for 3 hours, and both baseline and maximal tension were measured and recorded. Following contractile protocols, L_0 was measured using digital calipers. Muscles were subsequently removed from the force transducer and tendons were trimmed using micro-

scissors. Muscles were blotted dry prior to measuring muscle mass, and subsequently embedded in optimal cutting temperature (OCT) medium and frozen in ice-cold isopentane using liquid N_2 for histology. Specific muscle force (N/cm^2) was determined as previously described (Minchew et al., 2022) using predetermined equations (Brooks & Faulkner, 1988; Tarpey et al., 2018).

RT-qPCR

PowerTrack SYBR Green real-time quantitative polymerase chain reaction (RT-qPCR) analysis was employed in samples from male and female mice (n=6 per group) to quantify and compare mRNA content of Annexin A2 and S100A10 (p11). In a separate set of experiments, RT-qPCR was also employed to validate the Col5a1 knockdown in male mice (n=3 per group). Primer sequences for each protein are listed below.

Protein	Forward	Reverse
Annexin A2	ACGCTGGAGTGAAGAGGAAA	ACAGGGGCTTGTTCTGAATG
p11	GCGACAAAGACCACTTGACA	TTCCCCTTCTGCTTCATGTT
Col5a1	AAGCGTGGGAAACTGCTCTCCTAT	AGCAGTTGTAGGTGACGTTCTGGT

Annexin A2 Knockdown

To decrease Annexin A2 expression in the FDB, we delivered a short hairpin RNA (shRNA) encased in AAV9 and tagged with GFP. 20 uL of the AAV ($3x10^{10}$ total viral particles) was injected into the FDB of one limb, and the contralateral FDB was mock-injected with 20 uL of sterile 1X PBS to serve as an internal control. To validate the Annexin A2-shRNA, RT-qPCR analysis of Annexin A2 mRNA (TaqMan #Mm01150673_m1, ThermoFisher) was employed at 3-weeks post injection (n=3, 10 weeks of age) using 18s RNA to normalize the data. As compared to control muscles, we confirmed approximately 60% reduction of Annexin A2 mRNA in shRNA-treated FDBs (Fig 3B). Following our validation of the shRNA, we employed loss-of-function contractile experiments surrounding Annexin A2. The shRNA was delivered to FDBs prior to 5 weeks of age, and at 10 weeks of age control and treated muscles were subjected to the 3-hour contractile

protocol described above under both normoxic and hypoxic conditions (n=4-8 muscles per group per condition). Following completion of the 3-hour contractile protocol, muscles were embedded in optimal cutting temperature (OCT) medium and frozen in ice-cold isopentane using liquid N_2 for histological analysis of dystrophin signal as described below.

Histology

Immunofluorescence

Transverse cryosections (10 μm) from the muscle mid-belly were cut using a cryostat (Leica 3050S) and adhered to charged glass slides. Sections were air-dried for 10 minutes and subsequently fixed in 1:1 ice-cold methanol/acetone for 10 minutes at -20°C. Following another 10 minutes of air drying, sections were rehydrated with ice-cold 1X phosphate buffered saline (PBS) for 5 minutes. PBS was removed, and sections were blocked with PBS-diluted 5% goat serum at room temperature in the dark for 1 hour. After removing goat serum, sections were incubated overnight with anti-dystrophin primary antibody (#PA5-32388, ThermoFisher, 1:100) at 4°C. The following day primary antibody was removed, and sections were washed three times with ice-cold 1X PBS for 5 minutes. Secondary antibody (Alexa Fluor 488 donkey anti-rabbit IgG, #A21206, ThermoFisher, 1:250) was subsequently applied to sections for incubation at room temperature in the dark for 1 hour. Following removal of the secondary antibody and a second round of washing for 3x5 minutes with ice-cold 1X PBS, sections were incubated in wheat germ agglutinin (WGA; #W7024, ThermoFisher, 1 μg/mL) for 10 minutes to visualize the entire sarcolemma. Following removal of WGA and a third round of washing for 3x5 minutes with ice-cold 1X PBS, sections were mounted with Vectashield (Vector Labs) and imaged using an EVOS FL microscope (Life Technologies).

ImageJ software was used to quantify the number of myofibers with a loss of dystrophin expression following anoxia exposure. Light parameters of the microscope (exposure, gain, etc.) remained constant for a consistent analysis of dystrophin signal across samples. Only myofibers

with a complete disruption in the dystrophin signal were counted as dystrophin-null, and the number of dystrophin-null myofibers were expressed as a percentage of the total number of fibers counted (n=100-150 fibers per muscle per condition). The same number of fibers were utilized to assess the percentage of fibers with centralized nuclei.

H&E

Gross muscle morphology was assessed in FDB muscles from adult and young mice via standard hematoxylin & eosin staining methods. Briefly, muscles were frozen in optimal cutting temperature (OCT) media using isopentane submerged in liquid N_2. Transverse cryosections (10 μm) from the muscle mid-belly were cut using a cryostat (Leica 3050S) and adhered to charged glass slides. Sections were air-dried for 10 minutes prior to standard staining procedures. Following staining, sections were mounted with CytoSeal, coverslipped, and imaged using an EVOS FL microscope (Life Technologies) through a 20X objective lens.

Myofiber and Whole Muscle Cross-sectional Area (CSA)

Myofiber CSA in FDBs from adult and young mice was assessed as described previously (Minchew et al., 2022) using muscle cryosections probed for dystrophin (n=100-150 fibers per muscle). Whole muscle CSA was assessed using 10X images of Sirius Red stained sections (described below). ImageJ software was employed to determine CSA in both analyses.

Sirius Red Staining, Collagen Quantification, and Myofiber Number Quantification

Sirius Red staining was employed as previously described (O'Brien et al., 2023). Briefly, 10 μm cryosections were incubated with or without a 1% SDS-PBS solution (#BP166-500, Thermo Fisher Scientific) for 15 mins. SDS was utilized to remove cytosolic material and isolate collagen within the extracellular matrix. SDS-treated sections were washed 3x with sterile 1x PBS for 5 mins prior to the application of Picro-Sirius Red Solution (#NC1873312; Abcam) for 1 hour. Slides were subsequently submerged in two different containers of 0.5% acetic acid solution, then

washed twice with 100% ethanol. Once dry, slides were mounted using Cytoseal and imaged using an EVOS FL microscope (Life Technologies) through 10X and 20X objective lenses.

SDS-treated sections were utilized to quantify the percentage of the total muscle area that contains collagen in FDB muscles from adult and young mice (n=6 per group). Collagen analysis was employed as described by https://imagej.nih.gov/ij/docs/examples/stained-sections4/ with slight modifications. The presented ImageJ macro was copied to the clipboard and altered to accurately set the scale as well as to prevent removal of the scale bar. SDS-treated sections imaged on the 10X objective were also utilized to quantify the total number of myofibers within FDB sections from adult and young mice.

Muscle Proteomics

The proteome of FDB muscles from adult and young mice was characterized via LC-MS/MS. Briefly, FDBs from both limbs were dissected from two different male and female C57BL/6NJ mice and combined to ensure adequate protein yield. This was repeated 2 times resulting in 2 different biological samples per sex per age group. Muscles were added to 1mL of urea-based lysis buffer (8M Urea, 50mM Tris, 40mM NaCl, 2mM $MgCl_2$, 10mM $Na_4P_2O_7$, 50mM NaF, 50µL Halt protease inhibitor cocktail, 1 PhosSTOP tab), and homogenized on ice using a handheld homogenizer (Kinematica AG). Samples were fractionated using the Pierce High pH Reversed-Phase Peptide Fractionation Kit (ThermoFisher Scientific, Cat#84868) and fractions were frozen on dry ice and lyophilized. Each fraction was resuspended in 0.1% formic acid at a concentration of 0.25µg/µL following peptide quantification (ThermoFisher Scientific, Cat#23275). *Nano*LC-MS/MS analysis was performed as previously described (Fisher-Wellman et al., 2019; McLaughlin et al., 2020). Proteome Discoverer 2.2 (PDv2.2) was used to analyze the data as previously described (McLaughlin et al., 2020) with significance set at $p<0.05$. We have previously published a detailed description of these procedures (Amorese & Minchew et al., 2023).

The results of our proteomics analysis of FDBs from adult and young mice were subsequently filtered to yield differentially expressed proteins (DEPs) with $p<0.01$. The resulting

DEPs were then cross-referenced with our initial proteomics analysis of the FDB, EDL, and soleus to identify proteins that are differentially expressed ($p<0.01$) in the same direction across datasets (i.e., proteins that are both greater and lower in the FDB from adult mice as compared to all other muscles). Finally, we interrogated the literature to determine the function of the overlapping DEPs, their sensitivity to hypoxia, and their implication towards the maintenance of structural stability in the FDB from adult mice during hypoxia.

Statistical Analysis

All data are presented as mean ± SEM. Statistical analyses were performed using GraphPad Prism (Version 9.0; DotMatics). One-way or two-way ANOVA with Tukey's multiple comparisons test were used for comparisons of group means when appropriate. Two-tailed t-tests were used when appropriate. For all statistical tests, $p < 0.05$ was considered significant.

Results

The FDB resists structural damage during anoxia exposure

Acute hypoxia leads to excitotoxicity in skeletal muscle due to an uncontrolled influx of Ca^{2+} that enters the cell through lesions created within the sarcolemma. As compared to oxygenated controls, EDL muscles demonstrated the development of excitotoxicity as evidenced by a 453.6% increase in resting tension at the completion of the 3-hour anoxia protocol with significant differences found after 60 mins (Fig 1A; $p<0.01$). In contrast, anoxic and normoxic FDBs lacked significant differences in resting tension at any time point (Fig 1B). To further investigate sarcolemmal protection in the FDB, dystrophin expression was assessed in cross-sections of anoxic and normoxic muscles. Dystrophin is a hypoxia-sensitive protein that links intracellular components of the cell to the ECM via the dystrophin-glycoprotein complex (DGC). Sections were additionally treated with wheat germ agglutinin (WGA) – a glycoprotein-binding lectin – as it interacts with multiple compartments of the sarcolemma. Thus, decreased dystrophin expression with a concomitant preservation of WGA signal would isolate dystrophin loss as a

component of anoxic sarcolemmal damage. Consistent with our excitotoxicity data, we found that anoxic EDLs exhibited significant loss of dystrophin content in 20.78% of analyzed myofibers compared to all other tested groups (Fig 1C-D). However, in response to hypoxia exposure FDBs did not demonstrate any differences dystrophin expression between conditions (Fig 1C-D), further supporting the notion of sarcolemmal stability. Finally, WGA signal was preserved consistently across all sections (Fig 1C).

Annexin A2 is dispensable to the anoxia-resistant FDB phenotype.

To assess how the FDB retains sarcolemmal stability, we referenced our discovery-based proteomics approach to identify differentially expressed proteins in the FDB compared to the EDL and soleus. Among the most abundant proteins in the FDB was the sarcolemmal repair protein Annexin A2 and its binding partner p11 (Fig 2A). In addition to protein content, we confirmed significantly greater Annexin A2 ($p<0.0005$) and p11 ($p<0.05$) mRNA in the FDB as compared to the EDL (Fig 2B). To determine the necessity of Annexin A2 for the FDB's ability to function without O_2, we delivered an Annexin A2-shRNA-AAV to the FDBs of one limb from; contralateral FDBs were mock-injected with PBS to serve as internal controls. FDBs from both groups were subjected to the 3-hour contractile protocol and subsequently assessed for dystrophin content. AAV-treated FDBs were found to contain ~60% less Annexin A2 mRNA than control muscles ($p<0.01$; Fig 2C). Although FDBs treated with the AAV suffered a slightly greater loss of force output during anoxia exposure as compared to control muscles, the FD^{50} was not reached in either group; significant differences between anoxic groups were not observed until after 140 mins of the protocol, suggesting that decreasing Annexin A2 in the FDB did not increase hypoxia sensitivity (Fig 2D). Furthermore, no differences in the susceptibility to excitotoxicity were found between groups, although both groups demonstrated a main effect between normoxic and anoxic conditions ($p<0.05$; Fig 2E). Finally, dystrophin expression was similar between groups following anoxia exposure (Fig 2F-G).

Col5a1 is dispensable to the anoxia-resistant FDB phenotype.

The type V collagen isoform Col5a1 is an ECM protein that is expressed at significantly greater levels in the FDB than the EDL and soleus (Fig 3A). Collagen fibrils comprise a substantial component of the ECM, which is connected to the cytoskeleton via the dystrophin-glycoprotein complex (DCG). Thus, we hypothesized that elevated Col5a1 content may confer structural protection of the FDB via stabilization of the ECM. We subjected FDBs from male and female mice with a heterozygous deletion of Col5a1 (*Col5a1*$^{+/-}$) and wildtype littermates (*Col5a1*$^{+/+}$) aged 8-14 weeks to the 3-hour anoxic contractile protocol. Homozygous deletion of Col5a1 results in embryonic lethality, thus only heterozygous mice could be utilized. We performed mRNA analysis of Col5a1, which demonstrated a ~6-fold difference between the FDB and the EDL ($p<0.01$; Fig 3B). Comparison of FDB Col5a1 mRNA between genotypes resulted in no significant difference in mRNA transcript levels in the *Col5a1*$^{+/-}$ group, however a *post hoc* statistical analysis indicated that more samples are required for sufficient power (Fig 3C). No differences in force output were found between genotypes under both normoxic and anoxic conditions (Fig 3D), suggesting that Col5a1 is not required for the FDB to resist anoxic damage. As expected, however, we observed a main effect of condition in each genotype (O_2 vs N_2; $p<0.05$). Significant differences in baseline tension were found between genotypes during the early portion of anoxia exposure ($p<0.05$), however not after 120 mins, suggesting a minimal difference in excitotoxicity susceptibility (Fig 3E). Consistent with our functional data, no differences in dystrophin expression were found between genotypes following anoxia exposure (Fig 3F-G).

Anoxia causes functional and structural damage in FDB muscles from young mice

Due to its anatomical location at the bottom aspect of the foot (Tarpey et al., 2018), the FDB is subjected to compressive stress during weight bearing and locomotion. We thus hypothesized that during the introduction of weight bearing and locomotion, the FDB adapts to its local environment over time and acquires the cellular machinery that is necessary to resist damage during hypoxia. To test our hypothesis that the FDB phenotype is adapted and not innate,

we subjected FDB muscles from young (4-week-old) mice to the 3-hr anoxia protocol. Contrary to their adult counterparts, FDBs from young mice demonstrated a significant loss in force production during anoxia exposure (Fig 4C). Our data from adult mice demonstrated that contractile function is lost in the EDL but preserved in the FDB during anoxia exposure. The FD^{50} represents the time at which the muscles lost 50% of the initial normoxic force output, which serves as a proxy of the muscle's sensitivity to anoxia. The adult EDL reached the FD^{50} at 66.8 mins whereas at no point does the adult FDB reach its FD^{50} (Fig 4A-B). However, the FD^{50} was reached at 74.1 mins in anoxic FDBs from young mice; significant differences in force production between anoxic and normoxic muscles were found after 110 mins of the protocol (Fig 4C; $p<0.0005$).

From an excitotoxicity perspective, FDBs from young mice appeared to respond to anoxia exposure in a similar fashion as their adult counterparts, reaching a ~200% increase in resting tension (Fig 5B-C). Significant differences between conditions were found after 120 mins of the protocol in young mice (Fig 5C; $p<0.05$). The histological assessment of dystrophin expression was repeated in muscles from young mice, which demonstrated dystrophin loss in 20.54% of analyzed myofibers from the anoxic EDL (Fig 5D-E; $p<0.0001$). In contrast to FDBs from adult mice, anoxic FDBs from young mice exhibited a significant loss of dystrophin content in 14.34% of fibers as compared to normoxic controls, (Fig 5D-E; $p<0.0001$). Similar to muscle sections from adult mice, WGA signal was preserved consistently across muscles (Fig 5D).

Myofiber, but not whole muscle size, is different between FDBs from adult and young mice

To further characterize phenotypical differences between FDBs from adult and young mice, we employed several measurements of muscle size and composition. No differences were found in muscle mass or whole muscle cross-sectional area (CSA) (Fig 6B-C), despite the significant difference in average body weight between adult (29.73g) and young (12.98g) mice ($p<0.0001$; Fig 6A). Individual muscle fiber CSA was assessed in all muscles, with significant differences detected when comparing the average fiber size of FDBs from young mice (CSA of

862.1 μm^2) to their adult counterparts (CSA of 1150.6 μm^2) (Fig 4D; $p<0.0001$). Accordingly, FDBs from young mice demonstrated a leftward shift in the myofiber CSA frequency distribution compared to their adult counterparts (Fig 5E).

Histological comparison of FDBs from adult and young mice

Upon gross examination of muscle morphology via standard H&E staining procedures (Fig 7A), we found that the FDB contains more centralized nuclei than other peripheral skeletal muscles. Thus, we utilized our immunofluorescent images of muscles probed for dystrophin and DAPI to quantify centronuclei and compare between groups. No differences in the percentage of myofibers with centronuclei were found between FDBs from adult (12.98%) and young (13.68%) mice (Fig 7B-C). Subsequently, the composition of collagen tissue in both groups was assessed using Sirius Red staining. The application of SDS was used to decellularize the cytosol and isolate the extracellular matrix, which was confirmed by the absence of yellow coloration in the representative images of Fig 5D. Collagen quantification was performed with SDS-treated sections. FDBs from adult mice exhibited a collagen composition of 13.39%, which was significantly greater than the 10.45% observed in FDBs from young mice (Fig 5E; $p<0.05$). Finally, we utilized to SDS-treated sections to quantify the total number of myofibers in each muscle. The average number of fibers found in FDBs from young mice (673) was significantly greater than that of adult counterparts (407) (Fig 7F; $p=0.003$).

Proteomics

With the goal of improving the precision of our target selection, we compared the proteome of FDBs from adult and young mice. Over 1300 proteins were identified, 112 of which were found to be differentially expressed between FDBs from adult and young mice at $p<0.01$. Mitochondrial content did not differ between age groups as reflected by a similar mitochondrial enrichment factor (MEF; Fig 6B). Next, we cross-referenced the differentially expressed proteins (DEPs) between FDBs from adult and young mice with our initial discovery-based screening of the FDB, EDL, and

soleus proteomes. In doing so, we have created a list of DEPs between a skeletal muscle that survives hypoxia (i.e., the FDB from adult mice) and skeletal muscles that suffer hypoxic damage (i.e., the FDB from young mice, the EDL, and the soleus). Of the 112 DEPs between FDBs from adult and young mice, 10 proteins were found to be consistent across the proteomics analyses – 8 proteins with greater expression and 2 proteins with lower expression in the FDB from adult mice as compared to other muscles (Table 1).

Discussion

Unlike any other known skeletal muscle, the FDB is uniquely resistant to functional and structural damage within a hypoxic environment. The present study demonstrates that stabilization of the sarcolemma confers the ability of the FDB to maintain physiological function during hypoxia – a feat that is adapted by the muscle over time in response to its local environment. Our previously published proteomics analysis identified Annexin A2 and Col5a1 as two proteins that regulate the sarcolemma and are significantly greater in the FDB than the EDL and soleus. However, FDB's lacking both proteins did not demonstrate greater susceptibility to hypoxic damage as compared to control muscles. Following our observatons that the FDB phenotype is adapted, we performed a secondary proteomics analysis of FDBs from adult and young mice. Through integrating these results with our initial proteomic analysis of the FDB, EDL, and soleus, we have improved the precision of our future selection of proteins that can be targeted in the FDB from adult mice and ultimately leveraged in other skeletal muscles to promote survival under conditions of limited O_2 bioavailability.

During hypoxia skeletal muscle cells suffer structural damage that involves the development of lesions within the sarcolemma (Fredsted et al., 2005). Such lesions enable unregulated cytosolic entry of extracellular molecules like Ca^{2+}, which causes further membrane degradation via calpain activation (Huang & Forsberg, 1998). Intracellular Ca^{2+} accumulation also induces excitotoxicity, which is evidenced by increased resting muscle tension over time. Consistent with the literature (Schmidt et al., 2018; Wright et al., 2005), we observed the

development of excitotoxicity and the loss of dystrophin in the EDL following anoxia exposure. However, the FDB did not exhibit excitotixicity or dystrophin loss under the same conditions, suggesting a unique ability to preserve structural stability when faced with a hypoxic insult.

Following our observation that the FDB resists structural damage during anoxia exposure, we employed loss-of-function experiments surrounding the sarcolemma. Our discovery-based proteomics analysis identified the sarcolemmal repair protein Annexin A2 and its binding partner p11 among the most significantly elevated proteins in the FDB as compared to the EDL and soleus (Amorese & Minchew et al., 2023). Annexin A2 upregulation has been demonstrated to promote the survival of endothelial cells during hypoxia (Jiang & Xu, 2019), thus it was selected as our first target. A member of the large family of Ca^{2+}-binding proteins named in light of their ability to aggregate (or 'annex') phospholipids, Annexin A2 plays a key role in skeletal muscle plasma membrane repair (PMR) via interaction with dysferlin, which is the predominant muscle PMR protein (Cárdenas et al., 2016; Draeger et al., 2011; Gerke et al., 2005; Lennon et al., 2003). Upon sarcolemmal rupture, such as that which occurs during hypoxia, Ca^{2+} influx triggers Annexin A2 translocation to the injury site where it binds membrane-localized dysferlin; Annexin A2 also binds cytosolic dysferlin-containing vesicles for membrane translocation (Bittel et al., 2020). Co-accumulation of Annexin A2 and dysferlin at cholesterol-rich regions of the sarcolemma contributes to the formation of a 'repair cap,' which patches damaged membrane and allows for export of excess cytosolic Ca^{2+} (Croissant et al., 2022; Demonbreun et al., 2016, 2019). P11 (also known as S100A10) belongs to the large family of S100 proteins that modulate target proteins in response to intracellular [Ca^{2+}] changes (Rescher & Gerke, 2007). Two Annexin A2 monomers can be bound by p11 to form a heterotetrameric protein complex that appears to promote the membrane repair process (Dempsey et al., 2012; Liu et al., 2015; Rezvanpour et al., 2011). For example, the binding of p11 to Annexin A2 leads to a conformational shape change that increases the affinity to bind membrane phospholipids (Bharadwaj et al., 2013). P11 also decreases the [Ca^{2+}] requirement for Annexin A2 membrane interaction from millimolar to micromolar

concentrations, thus less Ca^{2+} is required for sarcolemmal translocation and PMR initiation when A2 is bound to p11 (Bharadwaj et al., 2021).

To our surprise, we found that FDBs lacking Annexin A2 are capable of maintaining force output during anoxia exposure. Despite a slightly faster rate of force loss in FDBs treated with the Annexin A2 shRNA as compared to control muscles, the FD^{50} was not reached in either group. Furthermore, no differences in dystrophin expression were observed between control and shRNA-treated muscles. Perhaps the shRNA-mediated knockdown was insufficient to decrease Annexin A2 levels to an extent that would induce the loss of the phenotype. Furthermore, previous literature has demonstrated that dysferlin also interacts with Annexin A1 during skeletal muscle PMR (Lennon et al., 2003). Thus, it may be possible that the loss of Annexin A2 expression induced the upregulation of Annexin A1 in the FDB to prevent impairments in the PMR process.

Considering its connection to the sarcolemma via dystrophin, the ECM is a critical component of skeletal muscle cell structure (Henderson et al., 2017). Elevated Col5a1-mediated collagen deposition has been reported as a characteristic of the local environment in cancer cells, which are well-suited to survive hypoxia (Zhu et al., 2022). Thus, Col5a1 loss-of-function experiments were employed to assess the contribution of an external mediator of the sarcolemma to the FDB's ability to survive hypoxia. However, similar to the loss-of-function experiments surrounding Annexin A2, no differences in contractile function or dystrophin expression were found in anoxic FDBs lacking Col5a1. Since Col5a1 is one of many collagen isoforms within the ECM (Ricard-Blum, 2011), perhaps its specific contribution to the hypoxia-resistant phenotype of the FDB is minimal. Furthermore, considering the inability to utilize mice with homozygous Col5a1 deletion due to embryonic lethality, it is possible that heterozygous deletion of Col5a1 was insufficient to induce impairments in ECM regulation as transcript levels were similar between genotypes.

The results of the loss-of-function experiments surrounding Annexin A2 and Col5a1 led us to reconsider the FDB phenotype and develop alternative hypotheses about the underlying

mechanisms. We reasoned that the FDB must be capable of functioning within its local environment, which involves repeated bouts of compressive forces during weight bearing and locomotion. Furthermore, it is possible that O_2 delivery to the muscle is decreased by vascular compression, creating a local environment that is intermittently hypoxic. Thus, the FDB's preservation of structural integrity during hypoxia led us to hypothesize that the anatomical location of the muscle induces structural protection of the myocyte. Accordingly, the FDB likely adapts to its local environment over time following the introduction of body weight, which eventually confers the muscle's ability to function without O_2. To test this hypothesis, we subjected FDBs from 4-week-old mice to the 3-hr contractile protocol and observed a rapid loss of the hypoxia-resistant phenotype that is seen in adult mice. We found that FDBs from young mice reached the FD^{50} (a proxy of sensitivity to hypoxia) at 74.1 mins and exhibited dystrophin loss in 14.34% of fibers – responses that are similar to those of the EDL during hypoxia exposure, which suggest that hypoxia resistance is indeed adapted by the FDB over time. To further characterize the apparent adaptation of the phenotype, we performed various assessments of muscle size and composition in FDBs from adult and young mice. To our surprise, we did not observe differences in muscle mass or whole muscle cross-sectional area (CSA), despite the significantly greater body weight of adult mice. However, FDBs from young mice were found to contain a significantly lower mean myofiber CSA and a leftward shift in the CSA frequency distribution, which indicates a greater percentage of smaller myofibers than adult counterparts.

A similar whole muscle size between age groups coupled with smaller FDB fibers and lower body weight in young mice led us to assess the intramuscular composition of collagen across groups. The FDB contains substantial connective tissue, which is likely a result of being located superior to the plantar fascia (Tarpey et al., 2018). Thus, we hypothesized that FDBs from young mice would contain more collagen than their adult counterparts to compensate for the lack of difference in muscle size. However, we found that FDBs from young mice contain less collagen than their adult counterparts. To explain the similar FDB muscle size in light of significant

differences in body weight between adult and young mice, we found that FDBs from young mice contain more fibers than FDBs from adult mice, albeit smaller in size. Thus, it is possible that FDBs from young mice are comprised of a population of myofibers that are susceptible to hypoxic damage and become necrotic following hypoxia exposure, which could induce a remodeling period that preserves the fibers of which survive hypoxia. Over time, the death of necrotic fibers and the maintenance of preserved fibers would contribute to the adaptation of the hypoxia-resistant FDB phenotype while the growth of the preserved fibers would explain the larger fiber size that is observed in FDBs from adult mice.

Examination of gross muscle morphology via H&E staining indicated that the FDB contains a relatively greater number of centralized nuclei as compared to other skeletal muscles. Centronuclei are indicative of skeletal muscle remodeling, usually within a myopathic setting. The mdx mouse for example is a widely-utilized animal model of Duchenne muscular dystrophy, which involves a fatal X-linked mutation in the dystrophin gene that causes the decline of skeletal muscle function over time (Russell et al., 2023). Previous research has demonstrated that up to 50% of myofibers are centronucleated within limb skeletal muscles from 4-week-old mdx mice whereas those muscles from wildtype littermates contain <1% of centronucleated myofibers (Anderson et al., 2006; Karpati et al., 1988). Quantification of centronucleation in the FDB myofibers revealed a much higher percentage of fibers (~13%) exhibiting centralized nuclei than would be typically found in a peripheral skeletal muscle. Furthermore, the lack of difference in the percentage of fibers with centronuclei between age groups suggests that centronucleation occurs during development and persists throughout adulthood, which is likely unique to the FDB. Future studies will employ myonuclear tracing and single nucleus transcriptomics to investigate whether differences exist between centronuclear populations from the FDB and nuclear populations from other hypoxia-sensitive muscles like the EDL.

Following our characterization of FDB muscles from young and adult mice, we elected to shift our approach and leverage our proteomic data with the goal of improving the precision of our

target selection. We began by employing a proteomic analysis of FDBs from adult and young mice, which revealed a similar mitochondrial content between groups as evidenced by the mitochondrial enrichment factors. We have previously demonstrated that mitochondrial content in the FDB is significantly lower than that of the EDL and soleus (Amorese & Minchew et al., 2023). Thus, a similar mitochondrial content between FDBs from adult and young mice suggests that the muscle does alter mitochondrial density during post-natal growth. Furthermore, our data surrounding FDB mitochondria highlight limitations surrounding the predictive power of muscle fiber typing techniques. The FDB is comprised predominantly of Type IIa and IIx myofibers (Tarpey et al., 2018), which implies that the muscle utilizes both glycolytic and oxidative metabolism for physiological function. Under current dogma, it would be predicted that oxidative metabolism is more critical for the FDB than the EDL considering that the EDL contains mostly glycolytic Type IIx and IIb myofibers. However, FDBs treated with the mitochondrial ETS inhibitor KCN during hypoxia do not exhibit an accelerated loss of force output to the same extent as the EDL under the same conditions; in fact, force output is minimally affected in the KCN-treated FDB during hypoxia (Amorese & Minchew et al., 2023). Furthermore, basal mitochondrial respiration of the FDB is significantly lower than that of the EDL in both permeabilized muscle fiber bundles and isolated mitochondria, the latter of which controls for mitochondrial content (Tarpey et al., 2018). Overall, we predict that the contradiction between current dogma surrounding skeletal muscle fiber types and the hypoxia-resistant phenotype of the FDB is unique to the FDB itself.

Our initial proteomic analysis generated a list of proteins that are differentially expressed between the FDB and the EDL and soleus (Amorese & Minchew et al., 2023). Loss- and gain-of-function experiments that targeted the proteins of which were elevated in the FDB and related to our data surrounding hypoxia resistance revealed that an alternative approach was necessary to generate hypotheses. By integrating our proteomic analysis of FDBs from adult and young mice with our initial proteomics analysis of the FDB, EDL, and soleus, we have enhanced the power and precision of our future target selection. Our goal was to identify differentially expressed

proteins (DEPs) with similar expression relationships across the analyses. In other words, we searched for proteins that were consistently found to be both greater and lower in the FDB from adult mice as compared to other muscles. Following a literature search to determine the hypoxia sensitivity of the resulting DEPs, we focused on targets that relate to the preservation of structural integrity. As a result, we identified myocilin as a future protein target.

Myocilin is a proposed member of the DGC that participates in dystrophin trafficking, and *in vivo* myocilin overexpression has been demonstrated to enhance the interaction of DGC components with dystrophin (Joe et al., 2012). In addition to the loss of dystrophin expression in hypoxic skeletal muscles, previous research has demonstrated that myocilin is decreased by hypoxia exposure (Obazawa et al., 2004). Thus, it is likely that elevated myocilin content ensures proper dystrophin localization within the sarcolemma, which promotes the maintenance of structural integrity in the FDB during hypoxia. It is important to note that the effects of altered myocilin expression are contended. Some groups have proposed that myocilin solely affects the eye (Borrás, 2014), whereas other groups have demonstrated changes in skeletal muscle cells with altered myocilin expression (Joe et al., 2012; Judge et al., 2020; Milewska et al., 2019). Such considerations will be important when designing experiments that target myocilin in the FDB.

Overall, our data surrounding the FDB suggests that the muscle adapts to its local environment and acquires the cellular machinery that protects against structural damage and enables the preservation of physiological function during hypoxia. The mechanisms that we propose to explain the FDB phenotype are presented in Fig 9. Relatively low mitochondrial content in the FDB relieves the muscle's reliance on the mitochondria to synthesize the majority of cellular ATP. Furthermore, the bioenergetic compromise that occurs within the mitochondria during hypoxia is likely minimized, enabling the FDB to maintain energetic charge. On the other hand, glycolysis is indeed required for hypoxia resistance in the FDB, although the muscle does not appear to catabolize greater amounts of glucose than the hypoxia-sensitive EDL muscle (Amorese & Minchew et al., 2023). Furthermore, our discovery-based proteomics results

demonstrated that the FDB contains fewer glycolytic proteins than the EDL, suggesting that the muscle does not upregulate its glycolytic capacity to survive hypoxia. However, we found that the FDB contains more glycogen than the EDL, thus it is possible that the muscle mobilizes glucose stores to flux through both glycolytic and non-glycolytic pathways like the pentose phosphate pathway (PPP). Previous research has suggested that PPP-generated glyceraldehyde 3-phosphate can re-enter glycolysis (Chicco et al., 2018), which could occur in the FDB to maintain ATP supply and cellular energy charge. Future studies will employ carbon radiolabeling to trace the fate of glucose in the FDB.

Another benefit of elevated PPP flux is sufficient production of NADPH for glutathione synthesis, which likely contributes to the robust defense system against redox sress that enables the FDB to survive hypoxia. Other components that minimize ROS in the FDB include low mitochondrial content, which fundamentally decreases mitochondrial ROS production, and an abundance of antioxidants. We have previously demonstrated that ascorbate content in the FDB is more than 13x that of the EDL and soleus (Amorese & Minchew et al., 2023). Skeletal muscle ascorbate is recycled throughout the cell (Eccardt et al., 2017). Thus, it is likely that ascorbate detoxifies ROS in the extracellular space, becomes oxidized to dehydroascorbate, enters the cell via GLUT1, becomes reduced back to ascorbate, and is exported by the cell in a cyclical manner. Furthermore, dehydroascorbate has been demonstrated to stimulate the PPP in skeletal muscle (Puskas et al., 2000). Another extracellular antioxidant in the FDB is superoxide dismutase 3 (SOD3), which was identified by our proteomics analysis among the proteins that are significantly greater in the FDB as compared to the EDL and soleus. Overall, protection against free radical damage appears to be a critical aspect of the FDB phenotype.

A final key consideration of the FDB phenotype is the maintenance of sarcolemmal stability. As compared to other skeletal muscles, the FDB contains an abundance of sarcolemmal repair proteins, such as various annexins, which likely enable the muscle to seal membrane lesions in a timely manner prior to the induction of cell damage and/or death. Furthermore,

elevated content of myocilin likely ensures a stable connection between the ECM and the cytoskeleton through transmembrane protein dystrophin. The location of dystrophin is likely maintained by myocilin, while the integrity of dystrophin expression is likely protected against ROS-mediated damage by the FDB's antioxidant defense system and against calpain-mediated damage by the FDB's PMR system.

The present study elaborates on our lab's previously published data that demonstrates the FDB's remarkable ability to maintain physiological function during hypoxia. Here, we have provided evidence that hypoxia resistance in the FDB is adapted over time as FDB muscles from young mice exhibit a loss of the phenotype under the same hypoxic conditions during which FDBs from adult mice survive. We draw further insight towards the mechanisms that underlie this phenotype from the preservation of sarcolemmal stability during anoxia exposure in the FDB from adult mice, which is evidenced by resistance against excitotoxicity and dystrophin loss. Loss-of-function experiments surrounding intracellular (Annexin A2) and extracellular (Col5a1) regulators of the sarcolemma suggest that structural integrity in the anoxic FDB from adult mice is a result of mechanisms other than or in combination with Annexin A2-mediated membrane repair and Col5a1-mediated fibrillogenesis. To improve the precision of our target selection, we integrated our proteomic analyses of (1) the FDB from adult and young mice and (2) the FDB, EDL, and soleus. As a result, we have generated a list of DEPs between the hypoxia-resistant FDB from adult mice and the hypoxia-sensitive FDB from young mice, EDL, and soleus. Follow-up analysis of the hypoxia-sensitive DEPs identified myocilin as a protein target that likely mediates the FDB phenotype and will be investigated in future studies to define skeletal muscle hypoxia resistance. Rescuing and/or preventing the development of hypoxic myopathy remains a critical gap in the muscle biology field that can be bridged through reverse engineering the FDB's unique ability to survive and thrive during hypoxia.

Figure 1 (A-D)

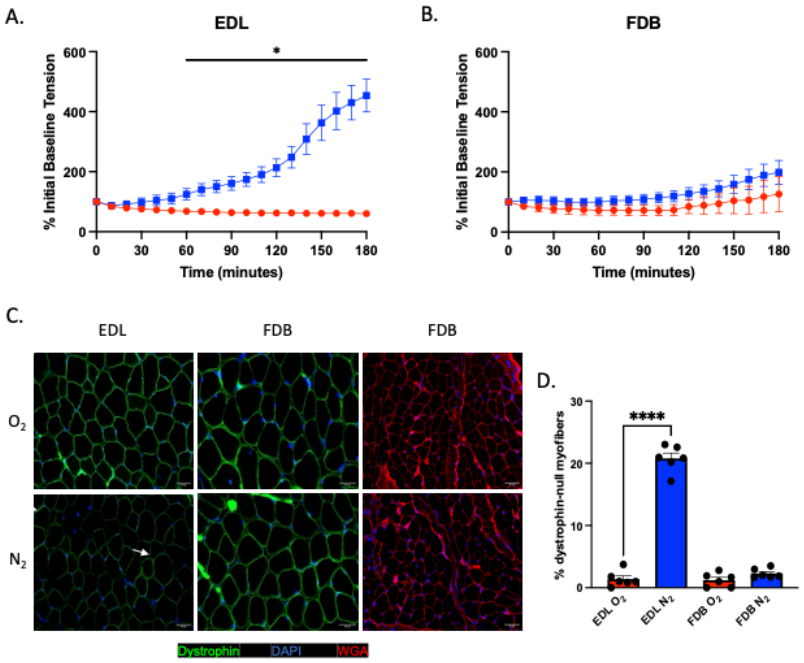

Figure 1. (A-D) The FDB, but not the EDL, suffers structural damage during anoxia exposure. Force-time curves of (A) the EDL and (B) the FDB during the 3-hour anoxia protocol. Initial force output was measured under oxygenated conditions. Muscles were then exposed to 95% O_2/5% CO_2 (normoxia) or 95% N_2/5% CO_2 (anoxia) for 180 mins. Muscles were stimulated maximally (100 Hz) every 10 mins and resting tension was measured and plotted as a percentage of the initial normoxic tension (n=6-8 per group). *$p<0.01$ compared to contralateral O_2 condition. (C) Representative images from normoxic (O_2) and anoxic (N_2) EDL and FDB cryosections probed for dystrophin (green), DAPI (nuclei, blue), and wheat germ agglutinin (WGA, red). WGA was utilized to outline the entire sarcolemma as it interacts with multiple components of the plasma membrane whereas dystrophin is a singular sarcolemmal marker. (D) Dystrophin expression was subsequently quantified across muscles for comparison between normoxic and anoxic conditions (n=6-8 per group). *$p<0.0005$ compared to O_2 condition.

Figure 2 (A-G)

A.

Protein	FDB/SOL (FC)	p-value	FDB/EDL (FC)	p-value
Annexin A2	1.533219	$2.71x10^{-5}$	1.909853	$1.39x10^{-5}$
p11	1.682395	$4.31x10^{-5}$	2.093829	$1.51x10^{-5}$

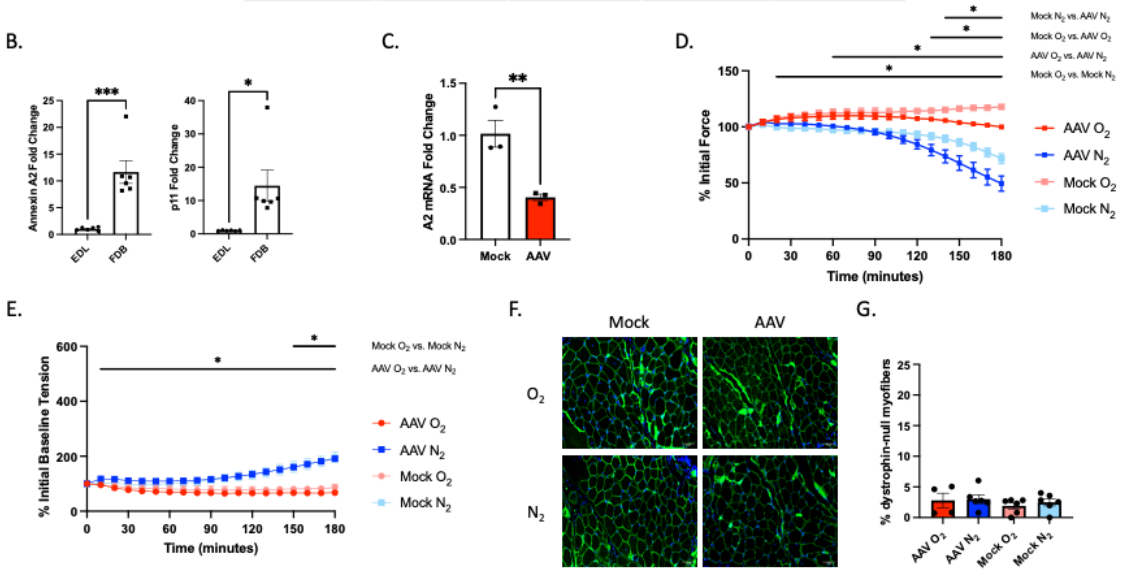

Figure 2. (A-G) Elevated content of Annexin A2 does not explain the FDB phenotype. (A) Table presenting expression fold differences of Annexin A2 and its binding partner p11 in the FDB compared to the EDL and soleus. (B) mRNA analysis of Annexin A2 and p11 confirmed the elevated protein expression in the FDB as compared to the EDL. (C) Validation of the Annexin A2-shRNA-AAV, which decreased Annexin A2 mRNA levels by ~60% in treated FDBs. (D) Force output and (E) resting tension of AAV-treated and mock-injected (PBS controls) FDBs during the 3-hour contractile protocol under normoxic and anoxic conditions (O_2 – n=4; N_2 – n=10). Initial force output was measured under oxygenated conditions. Muscles were then exposed to 95% O_2/5% CO_2 (normoxia) or 95% N_2/5% CO_2 (anoxia) for 180 mins. Muscles were stimulated maximally (100 Hz) every 10 mins; force output and resting tension were measured and plotted as a percentage of the respective initial force and baseline tension (*p<0.05). (F) Representative cross-sectional images of PBS-treated (control) and AAV-treated FDBs probed for dystrophin (sarcolemma, green) and DAPI (nuclei, blue). (G) Quantification of dystrophin expression in FDBs following the contractile protocols (O_2 – n=4; N_2 – n=10).

Figure 3 (A-G)

A.

Protein	FDB/SOL (FC)	p-value	FDB/EDL (FC)	p-value
Col5a1	1.699375	0.000235	2.559638	9.59×10^{-5}

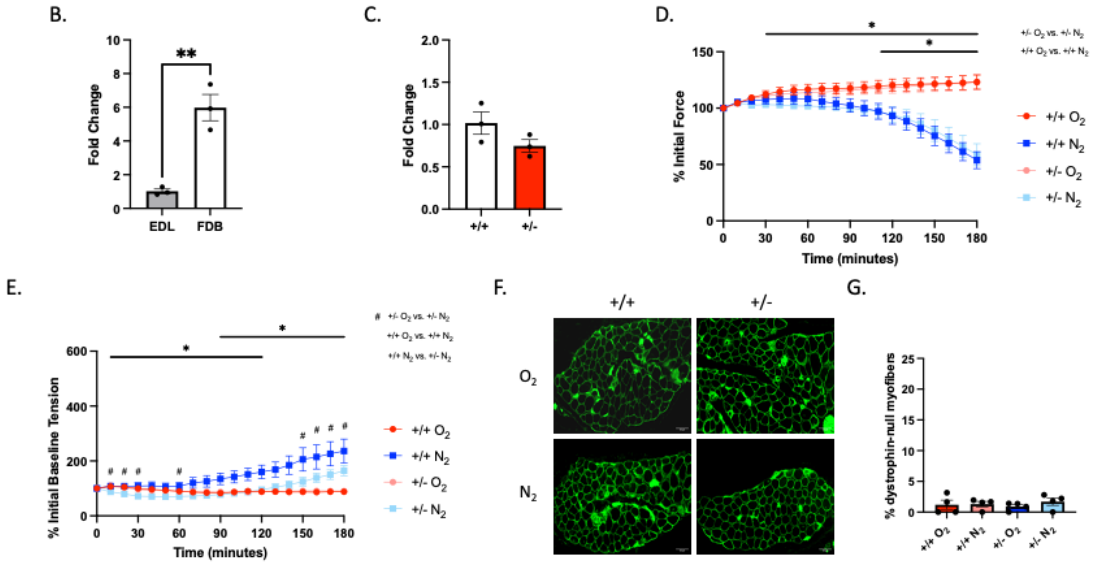

Figure 3. (A-G) Elevated content of Col5a1 does not explain the FDB phenotype.
(A) Table presenting fold difference of Col5a1 expression in the FDB compared to the EDL and soleus. (B) mRNA analysis of Col5a1 confirmed the elevated protein expression in the FDB as compared to the EDL (n=3 per group). (C) mRNA analysis of Col5a1 in the FDB from heterozygous Col5a1 knockout mice (+/-) and WT littermates (+/+), which demonstrated a trend towards lower mRNA in the +/- muscles (n=3 per group). (D) Force output and (E) resting tension of +/+ and +/- FDBs during the 3-hour contractile protocol under normoxic and anoxic conditions (n=8 per group). Initial force output was measured under oxygenated conditions. Muscles were then exposed to 95% O_2/5% CO_2 (normoxia) or 95% N_2/5% CO_2 (anoxia) for 180 mins. Muscles were stimulated maximally (100 Hz) every 10 mins; force output and resting tension were measured and plotted as a percentage of the respective initial force and baseline tension (*p<0.05). (F) Representative cross-sectional images of +/+ and +/- FDBs probed for dystrophin (sarcolemma, green). (G) Quantification of dystrophin expression in FDBs following the contractile protocols (n=8 per group).

Figure 4 (A-C)

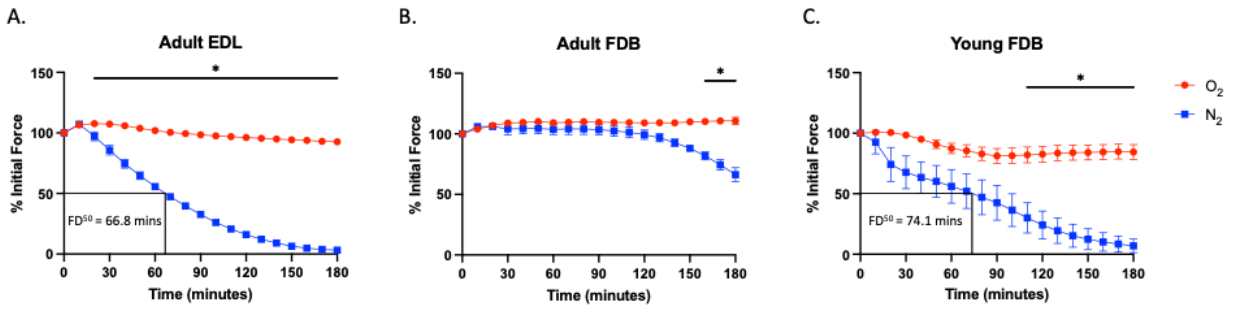

Figure 4. (A-C) Force-time curves of EDLs from adult mice and FDBs from adult and young mice during anoxia exposure.
Initial force output was measured under oxygenated conditions. Muscles were then exposed to 95% O_2/5% CO_2 (normoxia) or 95% N_2/5% CO_2 (anoxia) for 180 mins. Muscles were stimulated maximally (100 Hz) every 10 mins and resting tension was measured and plotted as a percentage of the initial baseline tension at each stimulation (n=6-8 per group). FD^{50} represents the time at which force output falls to 50% of the initial normoxic force. *$p<0.05$ compared to contralateral O_2 condition.

Figure 5 (A-E)

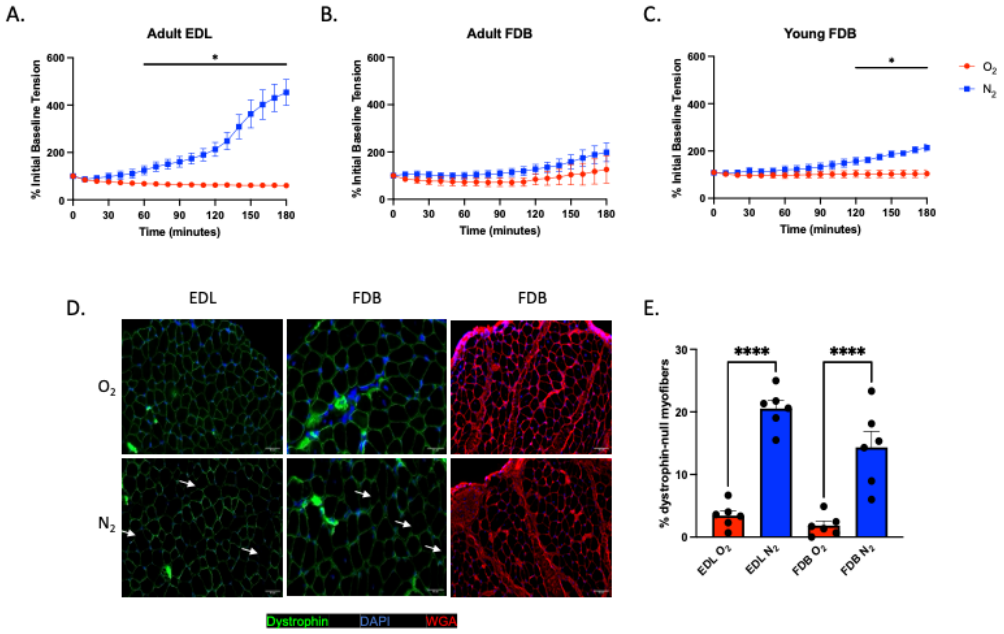

Figure 5. (A-E) FDBs from young mice are susceptible to hypoxic structural damage. (A-C) Resting tension of EDLs from adult mice and FDBs from adult and young mice during anoxia exposure. Initial force output was measured under oxygenated conditions. Muscles were then exposed to 95% O_2/5% CO_2 (normoxia) or 95% N_2/5% CO_2 (anoxia) for 180 mins. Muscles were stimulated maximally (100 Hz) every 10 mins and resting tension was measured and plotted as a percentage of the initial baseline tension at each stimulation (n=6-8 per group). *p<0.05 compared to contralateral O_2 condition. (D-E) Representative images from EDL and FDB muscles from young mice. Cryosections probed for dystrophin (green), DAPI (nuclei, blue), and wheat germ agglutinin (WGA, red). WGA was utilized to outline the entire sarcolemma as it interacts with multiple components of the plasma membrane whereas dystrophin is a singular sarcolemmal marker. (E) Dystrophin expression was subsequently quantified across muscles for comparison between normoxic and anoxic conditions (n=6-8 per group). *p<0.0005 compared to O_2 condition.

Figure 6 (A-E)

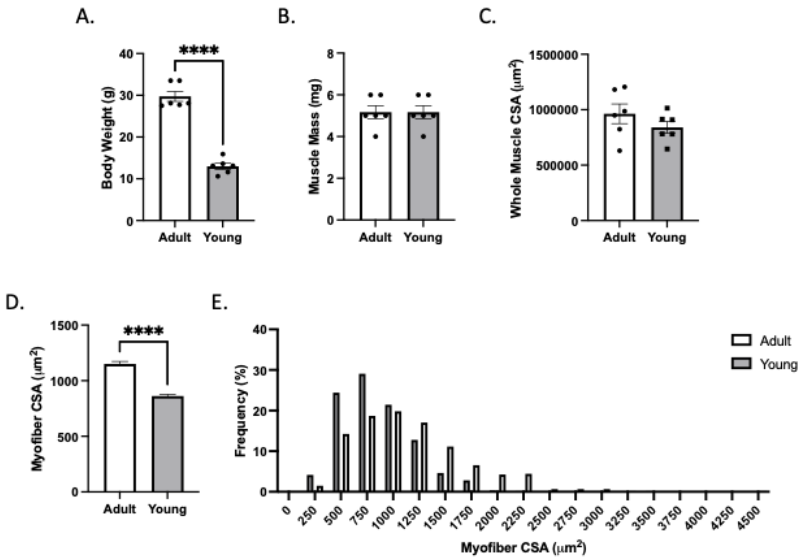

Figure 6. (A-E) Myofiber size, but not whole muscle size, is smaller in FDBs from young mice as compared to adult counterparts.
(A) Body weights of adult and young mice (n=6 per group). (B) Whole muscle mass and (C) whole muscle cross-sectional area (CSA) of FDBs from adult and young mice. (D) Comparison of mean fiber CSA demonstrates significantly smaller fibers in the FDBs from young mice (*p<0.0001), which is accompanied by (E) a leftward shift in the frequency distribution of myofiber CSA.

Figure 7 (A-F)

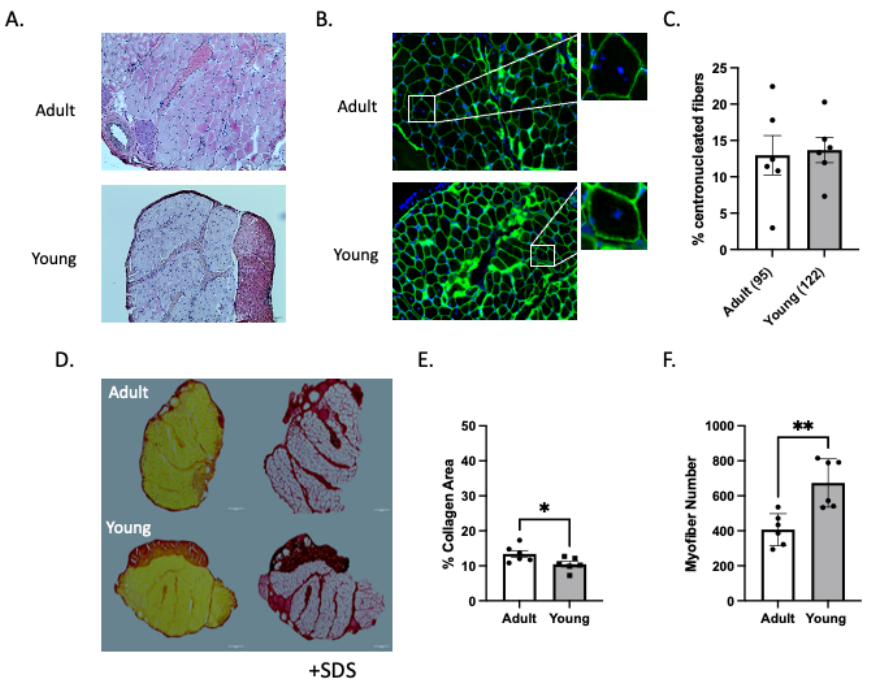

Figure 7. (A-F) Histological comparison of FDB muscles from adult and young mice. (A) Representative cross-sectional images of H&E-stained FDBs (n=6 per group). (B) Representative cross-sectional images of FDBs probed for dystrophin (sarcolemma, green) and DAPI (nuclei, blue). (C) Immunofluorescence was utilized to quantify the percentage of fibers with centralized nuclei with the total number of centronuclei presented in parentheses on the x-axis. (D) Representative cross-sectional images of Sirius red-stained FDBs to compare the collagen composition between muscles at different ages. The application of SDS was utilized to deplete cells of cytosolic material, which was confirmed by the absence of yellow coloration in the right figure panels. (E) Collagen quantification demonstrates a significantly lower composition in FDBs from young mice ($p<0.05$). (F) Myofiber quantification demonstrates a greater number of fibers in FDBs from young mice ($p=0.003$).

Figure 8 (A-B)

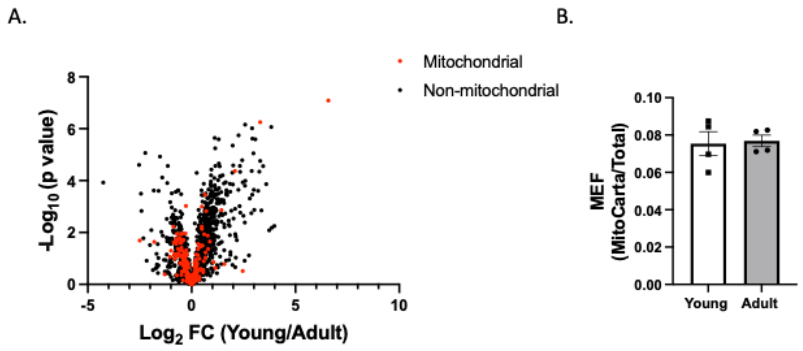

Figure 8. (A-B) Proteomic analysis of FDBs from adult and young mice.
(A) Volcano plot of differentially expressed proteins between FDB muscles from adult and young mice (n=2 biological replicates per sex per group). Red dots represent mitochondrial proteins while grey dots represent non-mitochondrial proteins. A leftward dot position indicates greater expression in the adult FDB while a rightward dot position indicates greater expression in the young FDB. An upward dot position indicates a more significant difference in protein expression between muscles. (B) Quantification of the mitochondrial enrichment factor (MEF) in FDB muscles from adult and young mice. The MEF represents the number of mitochondrial proteins identified by MitoCarta normalized to the total number of proteins identified by the Proteome Discoverer.

GREATER IN ADULT FDB

Gene	Adult FDB/Young FDB (Log2FC)	p-adjusted	FDB/EDL (Log2FC)	p-adjusted	FDB/SOL (Log2FC)	p-adjusted
Apod*	2.227972517	0.0008457	1.277417045	9.047E-05	1.373681315	9.0435E-05
Ca3*	0.643458864	0.0048122	3.085315115	2.5712E-05	1.444316334	0.0001097
Coch	4.250394563	0.0036067	3.275556342	1.2249E-05	3.086474735	9.2832E-05
Hspb2*	0.759331121	0.00506489	1.112074007	2.2834E-05	0.630931435	0.00083231
Mustn1	0.954393998	0.00534371	2.046127814	0.00028163	1.878492238	0.00089148
Myoc*	2.530871659	0.00149936	2.698883447	1.3886E-05	1.885156786	0.00031607
Prelp	1.1716129	0.00365609	1.821916386	3.0994E-05	1.317694838	7.3176E-05
Synm	0.503712321	0.00547965	0.14754018	0.00909075	0.690412861	2.0704E-05

LOWER IN ADULT FDB

Gene	Young FDB/Adult FDB (Log2FC)	p-adjusted	EDL/FDB (Log2FC)	p-adjusted	SOL/FDB (Log2FC)	p-adjusted
Crat	6.584572227	0.00010901	0.633524297	1.3886E-05	1.371012996	1.0212E-05
Fabp3	0.564447173	0.00554171	0.775184267	0.00464227	3.035196644	5.0415E-05

Table 1. Differentially expressed proteins in the FDB from adult mice as compared to the FDB from young mice, the EDL, and the soleus ($p<0.01$). Gene names for each protein are listed alongside the fold difference in protein expression between muscles as identified by LC-MS/MS and the adjusted p-value as determined by Bonferroni correction. Hypoxia-sensitive proteins are labeled with * as determined by independent literature searches.

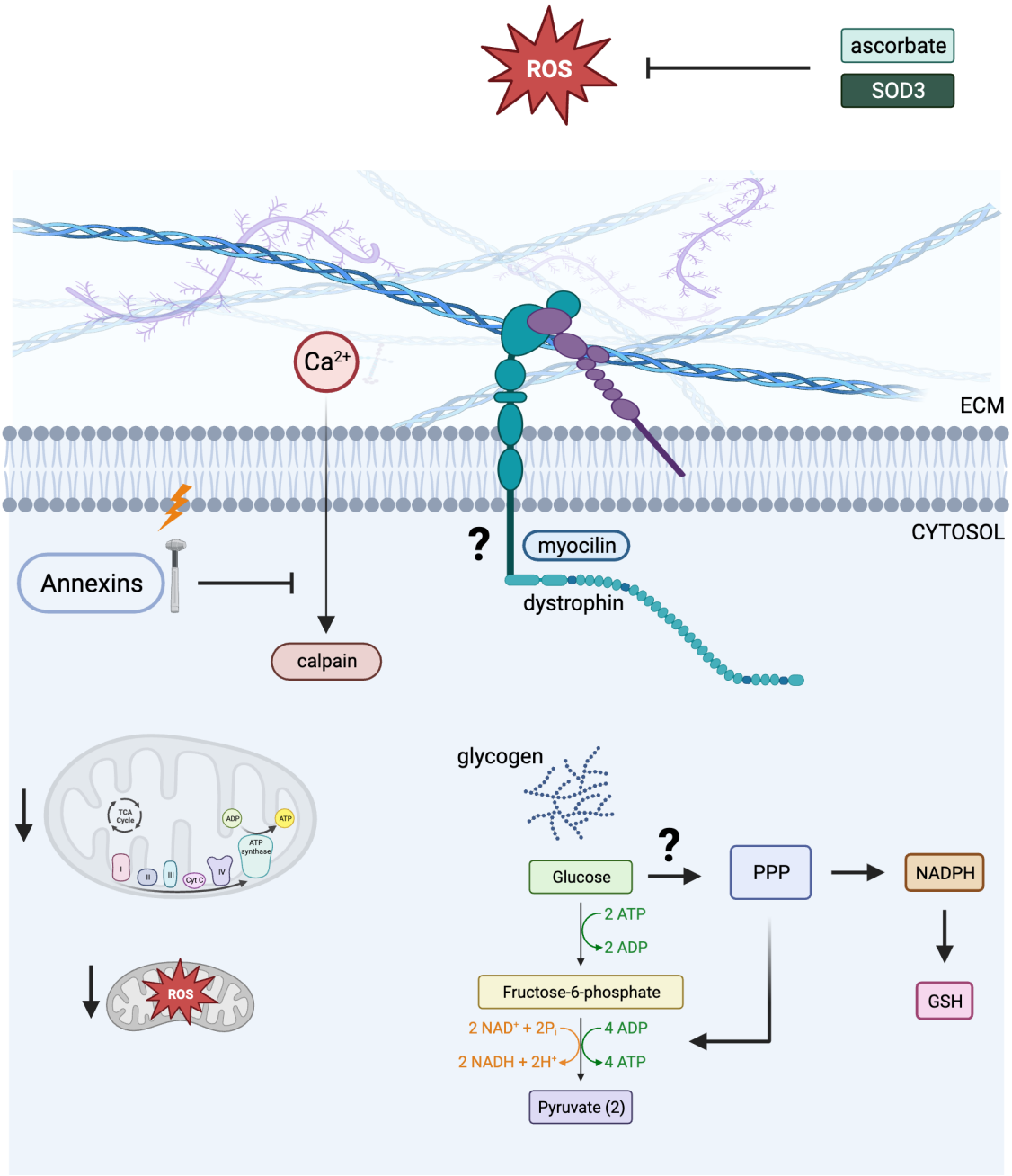

Figure 9. Summary schematic of the proposed mechanisms that explain the FDB phenotype. Relatively low mitochondrial content relieves the energetic burden that is placed on the mitochondria during hypoxia and concomitantly minimizes mitochondrial-derived ROS production. High glycogen stores support flux through glycolysis to maintain an adequate supply of ATP and potentially through the PPP to generate NADPH for glutathione (GSH) synthesis. Extracellular antioxidants like ascorbate and SOD3 minimize free radical damage while an abundance of sarcolemmal repair proteins (e.g., annexins) ensures the repair of membrane lesions prior to Ca^{2+} overload and calpain activation. Sarcolemmal stability is further promoted by myocilin-mediated dystrophin localization. Collectively, these mechanisms alongside other unidentified processes likely synergize and enable the FDB to maintain physiological function during hypoxia.

CHAPTER 5: Summary and Future Directions

Summary

In stark contrast to current dogma surrounding the relationship between skeletal muscle physiology and O_2 homeostasis, the murine flexor digitorum brevis (FDB) is uniquely resistant to hypoxia. Using both *in vivo* and *ex vivo* models of hypoxia exposure, our lab has performed a comprehensive analysis of the FDB through which we have documented various aspects of the muscle's remarkable ability to maintain physiological structure and function in an environment depleted of O_2. Key features of the FDB phenotype include the preservation of sarcolemmal stability and force output, both of which are lost in other skeletal muscles during hypoxia.

The present dissertation set to define the mechanisms that enable the FDB to survive hypoxia with the goal of identifying novel targets that can be leveraged in other skeletal muscles to promote hypoxia resistance. The first specific aim focused on determining whether unique bioenergetic regulation confers the FDB phenotype. We found that the FDB does not rely on the mitochondria to function during hypoxia as FDB muscles treated with the electron transport system inhibitor KCN maintained force output for a significantly longer period of time as compared to KCN-treated EDL and soleus muscles. Furthermore, investigation of basal mitochondrial function across muscles demonstrated that mitochondrial respiration is relatively low in the FDB. However, inhibition of glycolysis with BrP revealed that the FDB requires glycolysis to function during hypoxia. Accordingly, the FDB was found to contain significantly greater glycogen stores than the EDL, but not the soleus.

Our initial approach to define the precise mechanisms that confer the phenotype involved employing an unbiased, discovery-based proteomics analysis of which compared the proteome of the FDB with that of the EDL and soleus muscles. Considering the requirement of glycolysis for the FDB phenotype, we selected the transmembrane glucose transporter GLUT1 as our first target. Loss-of-function experiments surrounding GLUT1 involved subjecting FDB muscles from

mice with skeletal muscle-specific deletion of GLUT1 ($GLUT1^{-/-}$) to the 3-hour anoxia protocol. FDBs from $GLUT1^{-/-}$ mice demonstrated an accelerated loss of force output during anoxia as compared to FDBs from wildtype littermates, indicating that GLUT1 is necessary for the phenotype. However, AAV-mediated overexpression of GLUT1 in the EDL failed to attenuate force loss during anoxia, suggesting that GLUT1 is insufficient to rescue other skeletal muscles from hypoxic damage. It is important to note that in addition to glucose, GLUT1 imports the oxidized form of ascorbate – dehydroascorbate – within skeletal muscle cells. We found that ascorbate content in the FDB is more than 13x that of the EDL and soleus. Ascorbate is a potent extracellular antioxidant that becomes oxidized by accepting electrons from ROS, thus it is likely a key factor within the FDB's antioxidant defense system.

The second specific aim of the present dissertation focused on determining whether unique structural protection confers the FDB phenotype. We found that alongside the maintenance of force output, the FDB preserves stability of the sarcolemma during hypoxia exposure whereas other muscles suffer sarcolemmal damage. Evidence supporting sarcolemmal stability includes resistance against excitotoxity and the preservation of dystrophin expression when faced with the 3-hour anoxia protocol. In contrast, the EDL muscle exhibited the development of excitotoxicity and the loss of dystrophin expression under the same anoxic conditions. Following this observation, we hypothesized that the muscle requires structural protection to function within its local environment. Considering its anatomical location at the bottom aspect of the foot, the FDB is likely subjected to repeated bouts of compressive forces during weight bearing and locomotion. Thus, the muscle likely adapts to preserve its structure under stressful conditions like hypoxia. Upon testing this hypothesis, we generated substantial evidence that hypoxia resistance is adapted by the FDB over time as opposed to an innate phenotype that is induced during development. FDB muscles from young (4-week-old) mice were subjected to the 3-hour anoxia protocol and demonstrated the loss of force output and

sarcolemmal stability as evidenced by a similar FD^{50} and percentage of fibers with dystrophin loss as the EDL muscle.

Our first loss-of-function experiment surrounding the sarcolemma targeted Annexin A2, which was identified alongside its binding partner p11 among the proteins that are significantly elevated in the FDB as compared to the EDL and soleus. Annexin A2 interacts with the predominant sarcolemmal repair protein dysferlin to seal membrane lesions – a process that is activated by the accumulation of intracellular Ca^{2+} (Bittel et al., 2020). P11 enhances Annexin A2's Ca^{2+} sensitivity (Bharadwaj et al., 2021), thus elevated content of both proteins would likely enable the FDB to repair the sarcolemma prior to the induction of calpain-mediated damage. However, FDBs injected with an AAV containing an Annexin A2-shRNA did not exhibit greater sensitivity to hypoxic damage as compared to mock-injected muscles considering that neither muscle reached the FD^{50}. Furthermore, no differences in the susceptibility to excitotoxicity or the percentage of fibers with dystrophin loss were found between groups. Following loss-of-function experiments surrounding an intracellular regulator of the sarcolemma (Annexin A2), we selected an external regulator of the sarcolemma from our proteomics results – Col5a1. An isoform of Type V collagen, Col5a1 participates in the formation of collagen fibrils within the ECM (Sun et al., 2011), which is connected to the cytoskeleton via the transmembrane protein dysferlin. Col5a1 loss-of-function experiments involved subjecting FDBs from mice with a heterozygous deletion of Col5a1 and wildtype littermates to the 3-hour anoxia protocol. No differences in force output, excitotoxicity, or dystrophin loss were found between genotypes.

Ultimately, the described loss- and gain-of-function experiments failed to identify an effective target that could be leveraged in other skeletal muscles to promote survival during hypoxia. Thus, we placed our focus on further characterizing differences between FDBs from adult and young mice. No differences were found in whole muscle mass or CSA, however FDBs from young mice were found to contain smaller myofibers and less collagen than their adult counterparts despite lower body weight. To improve the precision of our target selection, we

employed a large-scale bioinformatics approach that integrated our initial proteomics analysis of the FDB, EDL, and soleus with a secondary proteomic comparison of FDB muscles from adult and young mice. Follow-up analysis of the hypoxia-sensitive differentially expressed proteins between FDBs from adult mice and other muscles suggest that dystrophin stabilization is a critical aspect of the FDB phenotype that will be investigated in future studies.

Future Directions

The fundamental finding of the present dissertation is that the FDB adapts to its local environment over time, which ultimately confers the ability to preserve structural integrity and maintain physiological function during hypoxia. Future studies of the FDB should investigate the fates of glucose, the presence of centronuclei under oxygenated conditions, the role of myocilin, the age at which the phenotype is fully adapted, and the potential for reversal of the adaptation. Carbon radiolabeling would be a useful tool to determine non-glycolysis fates of glucose (e.g., PPP), and whether those fates are implicated towards hypoxia resistance. Similarly, myonuclear labeling could be employed to track the fate of individual myonuclei. Myonuclear imaging has been traditionally carried out in post-mortem muscle tissue. However, recent research has demonstrated the efficacy of the "RG mouse," which is a transgenic model that tags myonuclei with a red fluorescent label and facilitates *in vivo* myonuclear imaging (Hastings et al., 2020). The RG mouse would be useful to track FDB myonuclei from birth. Subsequently, laser-mediated micro dissection could be used to isolate centronuclei from the FDB and single nucleus transcriptomics could be employed to determine if differences exist between FDB centronuclei and resident myonuclear populations from other skeletal muscles like the EDL. The results of these experiments could provide insight towards whether or not the centronucleation phenomenon is implicated towards the FDB phenotype. In addition to investigating centronuclei in the FDB, transgenic manipulation could also be used to assess the necessity of myocilin for the FDB phenotype (Judge et al., 2020). Similar to the loss-of-function experiments surrounding Col5a1, FDBs from mice with myocilin deletion could be subjected to the described functional and

structural experiments. Finally, it will be critical to determine the age of mice at which the FDB fully develops hypoxia resistance and whether or not the adaptation can be reversed. Future studies should involve subjecting FDBs from mice of different ages between 5 and 10 weeks to the described functional and structural experiments. Furthermore, hindlimb unloading and/or limb immobilization should be employed in adult mice to assess whether the loss of a mechanical stimulus is sufficient to induce the loss of hypoxia resistance. The insight gained from these experiments would provide further information about the conditions that are required for a skeletal muscle to survive hypoxia. As we deepen our understanding of the mechanisms that confer the unique ability of the FDB to function during hypoxia, we will be better informed to uncover novel targets that can be leveraged in other skeletal muscles to promote hypoxia resistance. In turn, patients who suffer from diseases and/or conditions that are associated with hypoxic myopathy could benefit from decreased morbidity and mortality, and potentially an improved degree of functional independence and quality of life.

References

Allen, J. F., & Martin, W. (2007). Out of thin air. *Nature*, *445*(7128), Article 7128. https://doi.org/10.1038/445610a

Amorese, A. J., Minchew, E. C., Tarpey, M. D., Readyoff, A. T., Williamson, N. C., Schmidt, C. A., McMillin, S. L., Goldberg, E. J., Terwilliger, Z. S., Spangenburg, Q. A., Witczak, C. A., Brault, J. J., Abel, E. D., McClung, J. M., Fisher-Wellman, K. H., & Spangenburg, E. E. (2023). Hypoxia Resistance Is An Inherent Phenotype of The Mouse Flexor Digitorum Brevis Skeletal Muscle. *Function*, zqad012. https://doi.org/10.1093/function/zqad012

Anderson, C. L., Repentigny, Y. D., Cifelli, C., Marshall, P., Renaud, J.-M., Worton, R. G., & Kothary, R. (2006). The Mouse Dystrophin Muscle Promoter/Enhancer Drives Expression of Mini-dystrophin in Transgenic mdx Mice and Rescues the Dystrophy in These Mice. *Molecular Therapy*, *14*(5), 724–734. https://doi.org/10.1016/j.ymthe.2006.04.013

Arthur, P. G., Giles, J. J., & Wakeford, C. M. (2000). Protein synthesis during oxygen conformance and severe hypoxia in the mouse muscle cell line C2C12. *Biochimica et Biophysica Acta (BBA) - General Subjects*, *1475*(1), 83–89. https://doi.org/10.1016/S0304-4165(00)00046-5

Attia, Y. M., EL-Abhar, H. S., Al Marzabani, M. M., & Shouman, S. A. (2015). Targeting glycolysis by 3-bromopyruvate improves tamoxifen cytotoxicity of breast cancer cell lines. *BMC Cancer*, *15*(1), 838. https://doi.org/10.1186/s12885-015-1850-4

Baldwin, J., Snow, R. J., Carey, M. F., & Febbraio, M. A. (1999). Muscle IMP accumulation during fatiguing submaximal exercise in endurance trained and untrained men. *American Journal of Physiology - Regulatory Integrative and Comparative Physiology*. https://doi.org/10.1152/ajpregu.1999.277.1.r295

Barthélémy, F., Defour, A., Lévy, N., Krahn, M., & Bartoli, M. (2018). Muscle Cells Fix Breaches by Orchestrating a Membrane Repair Ballet. *Journal of Neuromuscular Diseases*, *5*(1), 21–28. https://doi.org/10.3233/JND-170251

Baudry, N., Laemmel, E., & Vicaut, E. (2008). In vivo reactive oxygen species production induced by ischemia in muscle arterioles of mice: Involvement of xanthine oxidase and mitochondria. *American Journal of Physiology-Heart and Circulatory Physiology*, *294*(2), H821–H828. https://doi.org/10.1152/ajpheart.00378.2007

Berchtold, M. W., Brinkmeier, H., & Müntener, M. (2000). Calcium Ion in Skeletal Muscle: Its Crucial Role for Muscle Function, Plasticity, and Disease. *Physiological Reviews*, *80*(3), 1215–1265. https://doi.org/10.1152/physrev.2000.80.3.1215

Bernard, S., LeBlanc, P., Whittom, F., Carrier, G., Jobin, J., Belleau, R., & Maltais, F. (1998). Peripheral muscle weakness in patients with chronic obstructive pulmonary disease. *American Journal of Respiratory and Critical Care Medicine*, *158*(2), 629–634. https://doi.org/10.1164/ajrccm.158.2.9711023

Bernstein, B. W., & Bamburg, J. R. (2003). Actin-ATP hydrolysis is a major energy drain for neurons. *The Journal of Neuroscience: The Official Journal of the Society for Neuroscience*, *23*(1), 1–6. https://doi.org/10.1523/JNEUROSCI.23-01-00002.2003

Berru, F. N., Gray, S. E., Thome, T., Kumar, R. A., Salyers, Z. R., Coleman, M., Dennis Le, O'Malley, K., Ferreira, L. F., Berceli, S. A., Scali, S. T., & Ryan, T. E. (2019). Chronic kidney disease exacerbates ischemic limb myopathy in mice via altered mitochondrial energetics. *Scientific Reports*, *9*(1), Article 1. https://doi.org/10.1038/s41598-019-52107-7

Bharadwaj, A., Bydoun, M., Holloway, R., & Waisman, D. (2013). Annexin A2 Heterotetramer: Structure and Function. *International Journal of Molecular Sciences*, *14*(3), 6259–6305. https://doi.org/10.3390/ijms14036259

Bharadwaj, A., Kempster, E., & Waisman, D. M. (2021). The Annexin A2/S100A10 Complex: The Mutualistic Symbiosis of Two Distinct Proteins. *Biomolecules*, *11*(12), 1849. https://doi.org/10.3390/biom11121849

Biscetti, F., Nardella, E., Rando, M. M., Cecchini, A. L., Gasbarrini, A., Massetti, M., & Flex, A. (2021). Outcomes of Lower Extremity Endovascular Revascularization: Potential Predictors and Prevention Strategies. *International Journal of Molecular Sciences*, *22*(4), 2002. https://doi.org/10.3390/ijms22042002

Bittel, D. C., Chandra, G., Tirunagri, L. M. S., Deora, A. B., Medikayala, S., Scheffer, L., Defour, A., & Jaiswal, J. K. (2020). Annexin A2 Mediates Dysferlin Accumulation and Muscle Cell Membrane Repair. *Cells*, *9*(9), 1919. https://doi.org/10.3390/cells9091919

Borrás, T. (2014). The effects of myocilin expression on functionally relevant trabecular meshwork genes: A mini-review. *Journal of Ocular Pharmacology and Therapeutics: The Official Journal of the Association for Ocular Pharmacology and Therapeutics*, *30*(2–3), 202–212. https://doi.org/10.1089/jop.2013.0218

Brault, J. J., Pizzimenti, N. M., Dentel, J. N., & Wiseman, R. W. (2013). Selective inhibition of ATPase activity during contraction alters the activation of p38 MAP kinase isoforms in skeletal muscle. *Journal of Cellular Biochemistry*, *114*(6), 1445–1455. https://doi.org/10.1002/jcb.24486

Brooks, S. V., & Faulkner, J. A. (1988). Contractile properties of skeletal muscles from young, adult and aged mice. *The Journal of Physiology*, *404*(1), 71–82. https://doi.org/10.1113/jphysiol.1988.sp017279

Cai, C., Masumiya, H., Weisleder, N., Matsuda, N., Nishi, M., Hwang, M., Ko, J.-K., Lin, P., Thornton, A., Zhao, X., Pan, Z., Komazaki, S., Brotto, M., Takeshima, H., & Ma, J. (2009). MG53 nucleates assembly of cell membrane repair machinery. *Nature Cell Biology*, *11*(1), Article 1. https://doi.org/10.1038/ncb1812

Calderón, J. C., Bolaños, P., & Caputo, C. (2014). The excitation–contraction coupling mechanism in skeletal muscle. *Biophysical Reviews*, *6*(1), 133–160. https://doi.org/10.1007/s12551-013-0135-x

Cardaci, S., Desideri, E., & Ciriolo, M. R. (2012). Targeting aerobic glycolysis: 3-bromopyruvate as a promising anticancer drug. *Journal of Bioenergetics and Biomembranes*, *44*(1), 17–29. https://doi.org/10.1007/s10863-012-9422-7

Cárdenas, A. M., González-Jamett, A. M., Cea, L. A., Bevilacqua, J. A., & Caviedes, P. (2016). Dysferlin function in skeletal muscle: Possible pathological mechanisms and therapeutical targets in dysferlinopathies. *Experimental Neurology*, *283*(Pt A), 246–254. https://doi.org/10.1016/j.expneurol.2016.06.026

Carlier, M.-F., & Shekhar, S. (2017). Global treadmilling coordinates actin turnover and controls the size of actin networks. *Nature Reviews Molecular Cell Biology*, *18*(6), Article 6. https://doi.org/10.1038/nrm.2016.172

Chaillou, T., Koulmann, N., Meunier, A., Pugnière, P., McCarthy, J. J., Beaudry, M., & Bigard, X. (2014). Ambient hypoxia enhances the loss of muscle mass after extensive injury. *Pflugers Archiv : European Journal of Physiology*, *466*(3), 587–598. https://doi.org/10.1007/s00424-013-1336-7

Chicco, A. J., Le, C. H., Gnaiger, E., Dreyer, H. C., Muyskens, J. B., D'Alessandro, A., Nemkov, T., Hocker, A. D., Prenni, J. E., Wolfe, L. M., Sindt, N. M., Lovering, A. T., Subudhi, A. W., & Roach, R. C. (2018). Adaptive remodeling of skeletal muscle energy metabolism in high-altitude hypoxia: Lessons from AltitudeOmics. *The Journal of Biological Chemistry*, *293*(18), 6659–6671. https://doi.org/10.1074/jbc.RA117.000470

Clanton, T. L. (2007). Hypoxia-induced reactive oxygen species formation in skeletal muscle. *Journal of Applied Physiology*, *102*(6), 2379–2388. https://doi.org/10.1152/japplphysiol.01298.2006

Clanton, T. L., & Klawitter, P. F. (2001). Invited Review: Adaptive responses of skeletal muscle to intermittent hypoxia: the known and the unknown. *Journal of Applied Physiology*, *90*(6), 2476–2487. https://doi.org/10.1152/jappl.2001.90.6.2476

Collins, J.-A., Rudenski, A., Gibson, J., Howard, L., & O'Driscoll, R. (2015). Relating oxygen partial pressure, saturation and content: The haemoglobin–oxygen dissociation curve. *Breathe*, *11*(3), 194–201. https://doi.org/10.1183/20734735.001415

Croissant, C., Gounou, C., Bouvet, F., Tan, S., & Bouter, A. (2022). Trafficking of Annexins during Membrane Repair in Human Skeletal Muscle Cells. *Membranes*, *12*(2), 153. https://doi.org/10.3390/membranes12020153

Davis, P. R., Miller, S. G., Verhoeven, N. A., Morgan, J. S., Tulis, D. A., Witczak, C. A., & Brault, J. J. (2020). Increased AMP deaminase activity decreases ATP content and slows protein degradation in cultured skeletal muscle. *Metabolism: Clinical and Experimental*. https://doi.org/10.1016/j.metabol.2020.154257

Demonbreun, A. R., Fallon, K. S., Oosterbaan, C. C., Bogdanovic, E., Warner, J. L., Sell, J. J., Page, P. G., Quattrocelli, M., Barefield, D. Y., & McNally, E. M. (2019). Recombinant annexin A6 promotes membrane repair and protects against muscle injury. *Journal of Clinical Investigation*, *129*(11), 4657–4670. https://doi.org/10.1172/JCI128840

Demonbreun, A. R., Quattrocelli, M., Barefield, D. Y., Allen, M. V., Swanson, K. E., & McNally, E. M. (2016). An actin-dependent annexin complex mediates plasma membrane repair in muscle. *Journal of Cell Biology*, *213*(6), 705–718. https://doi.org/10.1083/jcb.201512022

Dempsey, B. R., Rezvanpour, A., Lee, T.-W., Barber, K. R., Junop, M. S., & Shaw, G. S. (2012). Structure of an Asymmetric Ternary Protein Complex Provides Insight for Membrane Interaction. *Structure*, *20*(10), 1737–1745. https://doi.org/10.1016/j.str.2012.08.004

D'Hulst, G., & Deldicque, L. (2017). Human skeletal muscle wasting in hypoxia: A matter of hypoxic dose? *Journal of Applied Physiology*, *122*(2), 406–408. https://doi.org/10.1152/japplphysiol.00264.2016

Donnelly, C., Schmitt, S., Cecatto, C., Cardoso, L., Komlódi, T., Place, N., Kayser, B., & Gnaiger, E. (2022). The ABC of hypoxia – what is the norm. *Bioenergetics Communications*, *2022*, 12–12. https://doi.org/10.26124/bec:2022-0012.v2

Draeger, A., Monastyrskaya, K., & Babiychuk, E. B. (2011). Plasma membrane repair and cellular damage control: The annexin survival kit. *Biochemical Pharmacology*, *81*(6), 703–712. https://doi.org/10.1016/j.bcp.2010.12.027

Eccardt, A., Bell, T., Mattathil, L., Prasad, R., Kelly, S., & Fisher, J. (2017). Trans-Plasma Membrane Electron Transport and Ascorbate Efflux by Skeletal Muscle. *Antioxidants*, *6*(4), 89. https://doi.org/10.3390/antiox6040089

Ehrke, E., Arend, C., & Dringen, R. (2015). 3-bromopyruvate inhibits glycolysis, depletes cellular glutathione, and compromises the viability of cultured primary rat astrocytes. *Journal of Neuroscience Research*, *93*(7), 1138–1146. https://doi.org/10.1002/jnr.23474

Eliason, J. L., & Wakefield, T. W. (2009). Metabolic Consequences of Acute Limb Ischemia and Their Clinical Implications. *Seminars in Vascular Surgery*, *22*(1), 29–33. https://doi.org/10.1053/j.semvascsurg.2009.01.001

Etheridge, T., Atherton, P. J., Wilkinson, D., Selby, A., Rankin, D., Webborn, N., Smith, K., & Watt, P. W. (2011). Effects of hypoxia on muscle protein synthesis and anabolic signaling at rest and in response to acute resistance exercise. *American Journal of Physiology - Endocrinology and Metabolism*, *301*(4), E697–E702. https://doi.org/10.1152/ajpendo.00276.2011

Fisher-Wellman, K. H., Davidson, M. T., Narowski, T. M., Lin, C.-T., Koves, T. R., & Muoio, D. M. (2018). Mitochondrial Diagnostics: A Multiplexed Assay Platform for Comprehensive Assessment of Mitochondrial Energy Fluxes. *Cell Reports*, *24*(13), 3593-3606.e10. https://doi.org/10.1016/j.celrep.2018.08.091

Fisher-Wellman, K. H., Draper, J. A., Davidson, M. T., Williams, A. S., Narowski, T. M., Slentz, D. H., Ilkayeva, O. R., Stevens, R. D., Wagner, G. R., Najjar, R., Hirschey, M. D.,

Thompson, J. W., Olson, D. P., Kelly, D. P., Koves, T. R., Grimsrud, P. A., & Muoio, D. M. (2019). Respiratory Phenomics across Multiple Models of Protein Hyperacylation in Cardiac Mitochondria Reveals a Marginal Impact on Bioenergetics. *Cell Reports*. https://doi.org/10.1016/j.celrep.2019.01.057

Fitzgerald, S., Barlow, C., Kampert, J., Morrow, J., Jackson, A., Blair, S., Fitzgerald, S., Barlow, C., Kampert, J., & Blair, S. (2004). Muscular Fitness and All-Cause Mortality: Prospective Observations. *J Phys Act Health*, *1*. https://doi.org/10.1123/jpah.1.1.7

Fredsted, A., Mikkelsen, U. R., Gissel, H., & Clausen, T. (2005). Anoxia induces Ca2+ influx and loss of cell membrane integrity in rat extensor digitorum longus muscle. *Experimental Physiology*, *90*(5), 703–714. https://doi.org/10.1113/expphysiol.2005.030247

Frontera, W. R., & Ochala, J. (2015). Skeletal Muscle: A Brief Review of Structure and Function. *Calcified Tissue International*, *96*(3), 183–195. https://doi.org/10.1007/s00223-014-9915-y

Gao, Q., & McNally, E. M. (2015). The Dystrophin Complex: Structure, function and implications for therapy. *Comprehensive Physiology*, *5*(3), 1223–1239. https://doi.org/10.1002/cphy.c140048

Gerke, V., Creutz, C. E., & Moss, S. E. (2005). Annexins: Linking Ca2+ signalling to membrane dynamics. *Nature Reviews. Molecular Cell Biology*, *6*(6), 449–461. https://doi.org/10.1038/nrm1661

Godt, R. E., & Nosek, T. M. (1989). Changes of intracellular milieu with fatigue or hypoxia depress contraction of skinned rabbit skeletal and cardiac muscle. *The Journal of Physiology*, *412*, 155–180.

Goldberg, E. J., Schmidt, C. A., Green, T. D., Karnekar, R., Yamaguchi, D. J., Spangenberg, E. E., & McClung, J. M. (2019). Temporal Association Between Ischemic Muscle Perfusion Recovery and the Restoration of Muscle Contractile Function After Hindlimb Ischemia.

Frontiers in Physiology, *10*. https://www.frontiersin.org/articles/10.3389/fphys.2019.00804

Grocott, M., Montgomery, H., & Vercueil, A. (2007). High-altitude physiology and pathophysiology: Implications and relevance for intensive care medicine. *Critical Care*, *11*(1), 203. https://doi.org/10.1186/cc5142

Guimarães-Ferreira, L. (2014). Role of the phosphocreatine system on energetic homeostasis in skeletal and cardiac muscles. *Einstein*, *12*(1), 126. https://doi.org/10.1590/S1679-45082014RB2741

Gupte, S. A., Okada, T., McMurtry, I. F., & Oka, M. (2006). Role of pentose phosphate pathway-derived NADPH in hypoxic pulmonary vasoconstriction. *Pulmonary Pharmacology & Therapeutics*, *19*(4), 303–309. https://doi.org/10.1016/j.pupt.2005.08.002

Hardie, D. G. (2003). Minireview: The AMP-Activated Protein Kinase Cascade: The Key Sensor of Cellular Energy Status. In *Endocrinology* (Vol. 144, Issue 12, pp. 5179–5183). https://doi.org/10.1210/en.2003-0982

Harman, J. W. (1947). A Histological Study of Skeletal Muscle in Acute Ischemia. *The American Journal of Pathology*, *23*(4), 551–565.

Hastings, R. L., Massopust, R. T., Haddix, S. G., Lee, Y. il, & Thompson, W. J. (2020). Exclusive vital labeling of myonuclei for studying myonuclear arrangement in mouse skeletal muscle tissue. *Skeletal Muscle*, *10*, 15. https://doi.org/10.1186/s13395-020-00233-6

Henderson, C. A., Gomez, C. G., Novak, S. M., Mi-Mi, L., & Gregorio, C. C. (2017). Overview of the Muscle Cytoskeleton. *Comprehensive Physiology*, *7*(3), 891–944. https://doi.org/10.1002/cphy.c160033

Hitchcock-DeGregori, S. E., & Irving, T. C. (2014). Hugh E. Huxley: The Compleat Biophysicist. *Biophysical Journal*, *107*(7), 1493–1501. https://doi.org/10.1016/j.bpj.2014.07.069

Hochachka, P. W., Buck, L. T., Doll, C. J., & Land, S. C. (1996). Unifying theory of hypoxia tolerance: Molecular/metabolic defense and rescue mechanisms for surviving oxygen

lack. *Proceedings of the National Academy of Sciences*, *93*(18), 9493–9498. https://doi.org/10.1073/pnas.93.18.9493

Hoppeler, H., Vogt, M., Weibel, E. R., & Flück, M. (2003). Response of skeletal muscle mitochondria to hypoxia. *Experimental Physiology*, *88*(1), 109–119. https://doi.org/10.1113/eph8802513

Huang, J., & Forsberg, N. E. (1998). Role of calpain in skeletal-muscle protein degradation. *Proceedings of the National Academy of Sciences of the United States of America*, *95*(21), 12100–12105. https://doi.org/10.1073/pnas.95.21.12100

Inserte, J., Hernando, V., & Garcia-Dorado, D. (2012). Contribution of calpains to myocardial ischaemia/reperfusion injury. *Cardiovascular Research*, *96*(1), 23–31. https://doi.org/10.1093/cvr/cvs232

Ivanics, T., Miklós, Z., Ruttner, Z., Bátkai, S., Slaaf, D. W., Reneman, R. S., Tóth, A., & Ligeti, L. (2000). Ischemia/reperfusion-induced changes in intracellular free Ca2+ levels in rat skeletal muscle fibers – an in vivo study. *Pflügers Archiv*, *440*(2), 302–308. https://doi.org/10.1007/s004240000287

Jalloh, I., Carpenter, K. L. H., Grice, P., Howe, D. J., Mason, A., Gallagher, C. N., Helmy, A., Murphy, M. P., Menon, D. K., Carpenter, T. A., Pickard, J. D., & Hutchinson, P. J. (2015). Glycolysis and the pentose phosphate pathway after human traumatic brain injury: Microdialysis studies using 1,2-13C2 glucose. *Journal of Cerebral Blood Flow & Metabolism*, *35*(1), 111–120. https://doi.org/10.1038/jcbfm.2014.177

Jardim-Messeder, D., Camacho-Pereira, J., & Galina, A. (2012). 3-Bromopyruvate inhibits calcium uptake by sarcoplasmic reticulum vesicles but not SERCA ATP hydrolysis activity. *International Journal of Biochemistry and Cell Biology*. https://doi.org/10.1016/j.biocel.2012.02.002

Jiang, S., & Xu, Y. (2019). Annexin A2 upregulation protects human retinal endothelial cells from oxygen-glucose deprivation injury by activating autophagy. *Experimental and Therapeutic Medicine*, *18*(4), 2901–2908. https://doi.org/10.3892/etm.2019.7909

Joe, M. K., Kee, C., & Tomarev, S. I. (2012). Myocilin Interacts with Syntrophins and Is Member of Dystrophin-associated Protein Complex. *The Journal of Biological Chemistry*, *287*(16), 13216–13227. https://doi.org/10.1074/jbc.M111.224063

Jones, D. A., Jackson, M. J., McPhail, G., & Edwards, R. H. (1984). Experimental mouse muscle damage: The importance of external calcium. *Clinical Science (London, England: 1979)*, *66*(3), 317–322. https://doi.org/10.1042/cs0660317

Judge, S. M., Deyhle, M. R., Neyroud, D., Nosacka, R. L., D'Lugos, A. C., Cameron, M. E., Vohra, R. S., Smuder, A. J., Roberts, B. M., Callaway, C. S., Underwood, P. W., Chrzanowski, S. M., Batra, A., Murphy, M. E., Heaven, J. D., Walter, G. A., Trevino, J. G., & Judge, A. R. (2020). MEF2c-dependent downregulation of Myocilin mediates cancer-induced muscle wasting and associates with cachexia in cancer patients. *Cancer Research*, *80*(9), 1861–1874. https://doi.org/10.1158/0008-5472.CAN-19-1558

Karpati, G., Carpenter, S., & Prescott, S. (1988). Small-caliber skeletal muscle fibers do not suffer necrosis in mdx mouse dystrophy. *Muscle & Nerve*, *11*(8), 795–803. https://doi.org/10.1002/mus.880110802

Kent, B. D., Mitchell, P. D., & McNicholas, W. T. (2011). Hypoxemia in patients with COPD: Cause, effects, and disease progression. *International Journal of Chronic Obstructive Pulmonary Disease*, *6*, 199–208. https://doi.org/10.2147/COPD.S10611

Knowles, R., Carter, J., Jebb, S. A., Bennett, D., Lewington, S., & Piernas, C. (2021). Associations of Skeletal Muscle Mass and Fat Mass With Incident Cardiovascular Disease and All-Cause Mortality: A Prospective Cohort Study of UK Biobank Participants. *Journal of the American Heart Association*, *10*(9), e019337. https://doi.org/10.1161/JAHA.120.019337

Koritzinsky, M., Magagnin, M. G., van den Beucken, T., Seigneuric, R., Savelkouls, K., Dostie, J., Pyronnet, S., Kaufman, R. J., Weppler, S. A., Voncken, J. W., Lambin, P., Koumenis, C., Sonenberg, N., & Wouters, B. G. (2006). Gene expression during acute and prolonged hypoxia is regulated by distinct mechanisms of translational control. *The EMBO Journal*, *25*(5), 1114–1125. https://doi.org/10.1038/sj.emboj.7600998

Kraegen, E. W., Sowden, J. A., Halstead, M. B., Clark, P. W., Rodnick, K. J., Chisholm, D. J., & James, D. E. (1993). Glucose transporters and in vivo glucose uptake in skeletal and cardiac muscle: Fasting, insulin stimulation and immunoisolation studies of GLUT1 and GLUT4. *The Biochemical Journal*, *295 (Pt 1)*(Pt 1), 287–293. https://doi.org/10.1042/bj2950287

Land, S. C., Buck, L. T., & Hochachka, P. W. (1993). Response of protein synthesis to anoxia and recovery in anoxia-tolerant hepatocytes. *The American Journal of Physiology*, *265*(1 Pt 2), R41-48. https://doi.org/10.1152/ajpregu.1993.265.1.R41

Leavesley, H. B., Li, L., Prabhakaran, K., Borowitz, J. L., & Isom, G. E. (2008). Interaction of Cyanide and Nitric Oxide with Cytochrome c Oxidase: Implications for Acute Cyanide Toxicity. *Toxicological Sciences*, *101*(1), 101–111. https://doi.org/10.1093/toxsci/kfm254

Lee, Y.-C., Huang, H.-Y., Chang, C.-J., Cheng, C.-H., & Chen, Y.-T. (2010). Mitochondrial GLUT10 facilitates dehydroascorbic acid import and protects cells against oxidative stress: Mechanistic insight into arterial tortuosity syndrome. *Human Molecular Genetics*, *19*(19), 3721–3733. https://doi.org/10.1093/hmg/ddq286

Lennon, N. J., Kho, A., Bacskai, B. J., Perlmutter, S. L., Hyman, B. T., & Brown, R. H. (2003). Dysferlin Interacts with Annexins A1 and A2 and Mediates Sarcolemmal Wound-healing. *Journal of Biological Chemistry*, *278*(50), 50466–50473. https://doi.org/10.1074/jbc.M307247200

Li, R., Xia, J., Zhang, X., Gathirua-Mwangi, W. G., Guo, J., Li, Y., McKenzie, S., & Song, Y. (2018). Associations of Muscle Mass and Strength with All-Cause Mortality among US

Older Adults. *Medicine and Science in Sports and Exercise*, *50*(3), 458–467. https://doi.org/10.1249/MSS.0000000000001448

Lin, Z., Weinberg, J. M., Malhotra, R., Merritt, S. E., Holzman, L. B., & Brosius, F. C. (2000). GLUT-1 reduces hypoxia-induced apoptosis and JNK pathway activation. *American Journal of Physiology-Endocrinology and Metabolism*, *278*(5), E958–E966. https://doi.org/10.1152/ajpendo.2000.278.5.E958

Lindahl, S. G. E. (2008). Oxygen and Life on Earth. *Anesthesiology*, *109*(1), 7–13. https://doi.org/10.1097/ALN.0b013e31817b5a7e

Liu, Y., Myrvang, H. K., & Dekker, L. V. (2015). Annexin A2 complexes with S100 proteins: Structure, function and pharmacological manipulation: Annexin A2-S100 complexes. *British Journal of Pharmacology*, *172*(7), 1664–1676. https://doi.org/10.1111/bph.12978

Magalhães, J., Ascensão, A., Soares, J. M. C., Ferreira, R., Neuparth, M. J., Marques, F., & Duarte, J. A. (2005). Acute and severe hypobaric hypoxia increases oxidative stress and impairs mitochondrial function in mouse skeletal muscle. *Journal of Applied Physiology*, *99*(4), 1247–1253. https://doi.org/10.1152/japplphysiol.01324.2004

Malhotra, R., & Brosius, F. C. (1999). Glucose uptake and glycolysis reduce hypoxia-induced apoptosis in cultured neonatal rat cardiac myocytes. *The Journal of Biological Chemistry*, *274*(18), 12567–12575. https://doi.org/10.1074/jbc.274.18.12567

Mayer, C., Franz, A., Harmsen, J.-F., Queitsch, F., Behringer, M., Beckmann, J., Krauspe, R., & Zilkens, C. (2017). Soft-tissue damage during total knee arthroplasty: Focus on tourniquet-induced metabolic and ionic muscle impairment. *Journal of Orthopaedics*, *14*(3), 347–353. https://doi.org/10.1016/j.jor.2017.06.015

McCall, K. E., & Duncan, C. J. (1989). Independent pathways causing cellular damage in mouse soleus muscle under hypoxia. *Comparative Biochemistry and Physiology Part A: Physiology*, *94*(4), 799–804. https://doi.org/10.1016/0300-9629(89)90637-3

McClung, J. M., McCord, T. J., Ryan, T. E., Schmidt, C. A., Green, T. D., Southerland, K. W., Reinardy, J. L., Mueller, S. B., Venkatraman, T. N., Lascola, C. D., Keum, S., Marchuk, D. A., Spangenburg, E. E., Dokun, A., Annex, B. H., & Kontos, C. D. (2017). A BAG3 Coding Variant in Mice Determines Susceptibility to Ischemic Limb Muscle Myopathy by Directing Autophagy. *Circulation*, *136*(3), 281–296. https://doi.org/10.1161/CIRCULATIONAHA.116.024873

McLaughlin, K. L., Kew, K. A., McClung, J. M., & Fisher-Wellman, K. H. (2020). Subcellular proteomics combined with bioenergetic phenotyping reveals protein biomarkers of respiratory insufficiency in the setting of proofreading-deficient mitochondrial polymerase. *Scientific Reports*. https://doi.org/10.1038/s41598-020-60536-y

McMillin, S. L., Evans, P. L., Taylor, W. M., Weyrauch, L. A., Sermersheim, T. J., Welc, S. S., Heitmeier, M. R., Hresko, R. C., Hruz, P. W., Koumanov, F., Holman, G. D., Abel, E. D., & Witczak, C. A. (2022). Muscle-Specific Ablation of Glucose Transporter 1 (GLUT1) Does Not Impair Basal or Overload-Stimulated Skeletal Muscle Glucose Uptake. *Biomolecules*, *12*(12), Article 12. https://doi.org/10.3390/biom12121734

Melkonian, E. A., & Schury, M. P. (2022). Biochemistry, Anaerobic Glycolysis. In *StatPearls*. StatPearls Publishing. http://www.ncbi.nlm.nih.gov/books/NBK546695/

Milewska, M., Domoradzki, T., Majewska, A., Błaszczyk, M., Gajewska, M., Hulanicka, M., Ciecierska, A., & Grzelkowska-Kowalczyk, K. (2019). Interleukin-8 enhances myocilin expression, Akt-FoxO3 signaling and myogenic differentiation in rat skeletal muscle cells. *Journal of Cellular Physiology*, *234*(11), 19675–19690. https://doi.org/10.1002/jcp.28568

Minchew, E. C., Williamson, N. C., Readyoff, A. T., McClung, J. M., & Spangenburg, E. E. (2022). Isometric skeletal muscle contractile properties in common strains of male laboratory mice. *Frontiers in Physiology*, *13*. https://www.frontiersin.org/articles/10.3389/fphys.2022.937132

Myrka, A., & Buck, L. (2021). Cytoskeletal Arrest: An Anoxia Tolerance Mechanism. *Metabolites*, *11*(8), 561. https://doi.org/10.3390/metabo11080561

Neufer, P. D. (2018). The Bioenergetics of Exercise. *Cold Spring Harbor Perspectives in Medicine*, *8*(5), a029678. https://doi.org/10.1101/cshperspect.a029678

Nicholls, D. G. (2013). *Bioenergetics*. Academic Press.

Obazawa, M., Mashima, Y., Sanuki, N., Noda, S., Kudoh, J., Shimizu, N., Oguchi, Y., Tanaka, Y., & Iwata, T. (2004). Analysis of Porcine Optineurin and Myocilin Expression in Trabecular Meshwork Cells and Astrocytes from Optic Nerve Head. *Investigative Ophthalmology & Visual Science*, *45*(8), 2652–2659. https://doi.org/10.1167/iovs.03-0572

O'Brien, J. G., Willis, A. B., Long, A. M., Kwon, J., Lee, G., Li, F., Page, P. G. T., Vo, A. H., Hadhazy, M., Crosbie, R. H., Demonbreun, A. R., & McNally, E. M. (2023). The super-healing MRL strain promotes muscle growth in muscular dystrophy through a regenerative extracellular matrix. *bioRxiv: The Preprint Server for Biology*, 2023.06.29.547098. https://doi.org/10.1101/2023.06.29.547098

Okuda, S., Watanabe, Y., Moriya, Y., Kawano, S., Yamamoto, T., Matsumoto, M., Takami, T., Kobayashi, D., Araki, N., Yoshizawa, A. C., Tabata, T., Sugiyama, N., Goto, S., & Ishihama, Y. (2017). jPOSTrepo: An international standard data repository for proteomes. *Nucleic Acids Research*, *45*(D1), D1107–D1111. https://doi.org/10.1093/nar/gkw1080

Orrenius, S., Zhivotovsky, B., & Nicotera, P. (2003). Regulation of cell death: The calcium–apoptosis link. *Nature Reviews Molecular Cell Biology*, *4*(7), Article 7. https://doi.org/10.1038/nrm1150

Pandurangan, M., & Hwang, I. (2012). The role of calpain in skeletal muscle. *Animal Cells and Systems*, *16*(6), 431–437. https://doi.org/10.1080/19768354.2012.724708

Paradis, S., Charles, A.-L., Meyer, A., Lejay, A., Scholey, J. W., Chakfé, N., Zoll, J., & Geny, B. (2016). Chronology of mitochondrial and cellular events during skeletal muscle ischemia-

reperfusion. *American Journal of Physiology-Cell Physiology*, *310*(11), C968–C982. https://doi.org/10.1152/ajpcell.00356.2015

Park, D.-R. (2017). Glycolysis Mediated Sarcoplasmic Reticulum Ca^{2+} Signal Regulates Mitochondria Ca^{2+} during Skeletal Muscle Contraction. *Exercise Science*. https://doi.org/10.15857/ksep.2017.26.3.229

Pipinos, I. I., Judge, A. R., Selsby, J. T., Zhu, Z., Swanson, S. A., Nella, A. A., & Dodd, S. L. (2008). Basic Science Review: The Myopathy of Peripheral Arterial Occlusive Disease: Part 2. Oxidative Stress, Neuropathy, and Shift in Muscle Fiber Type. *Vascular and Endovascular Surgery*, *42*(2), 101–112. https://doi.org/10.1177/1538574408315995

Pittman, R. N. (2011). *Regulation of Tissue Oxygenation*. Morgan & Claypool Life Sciences. http://www.ncbi.nlm.nih.gov/books/NBK54104/

Preedy, V. R., Smith, D. M., & Sugden, P. H. (1985). The effects of 6 hours of hypoxia on protein synthesis in rat tissues in vivo and in vitro. *The Biochemical Journal*, *228*(1), 179–185. https://doi.org/10.1042/bj2280179

Preedy, V. R., & Sugden, P. H. (1989). The effects of fasting or hypoxia on rates of protein synthesis in vivo in subcellular fractions of rat heart and gastrocnemius muscle. *The Biochemical Journal*, *257*(2), 519–527. https://doi.org/10.1042/bj2570519

Purves, D., Augustine, G. J., Fitzpatrick, D., Katz, L. C., LaMantia, A.-S., McNamara, J. O., & Williams, S. M. (2001). The Motor Unit. In *Neuroscience. 2nd edition*. Sinauer Associates. https://www.ncbi.nlm.nih.gov/books/NBK10874/

Puskas, F., Gergely, P., Banki, K., & Perl, A. (2000). Stimulation of the pentose phosphate pathway and glutathione levels by dehydroascorbate, the oxidized form of vitamin C. *The FASEB Journal*, *14*(10), 1352–1361. https://doi.org/10.1096/fasebj.14.10.1352

Qaisar, R., Bhaskaran, S., Premkumar, P., Ranjit, R., Natarajan, K. S., Ahn, B., Riddle, K., Claflin, D. R., Richardson, A., Brooks, S. V., & Van Remmen, H. (2018). Oxidative stress-induced dysregulation of excitation–contraction coupling contributes to muscle

weakness. *Journal of Cachexia, Sarcopenia and Muscle*, *9*(5), 1003–1017. https://doi.org/10.1002/jcsm.12339

Rebbeck, R. T., Karunasekara, Y., Board, P. G., Beard, N. A., Casarotto, M. G., & Dulhunty, A. F. (2014). Skeletal muscle excitation-contraction coupling: Who are the dancing partners? *The International Journal of Biochemistry & Cell Biology*, *48*, 28–38. https://doi.org/10.1016/j.biocel.2013.12.001

Rescher, U., & Gerke, V. (2007). S100A10/p11: Family, friends and functions. *Pflügers Archiv - European Journal of Physiology*, *455*(4), 575–582. https://doi.org/10.1007/s00424-007-0313-4

Rezvanpour, A., Santamaria-Kisiel, L., & Shaw, G. S. (2011). The S100A10-Annexin A2 Complex Provides a Novel Asymmetric Platform for Membrane Repair. *Journal of Biological Chemistry*, *286*(46), 40174–40183. https://doi.org/10.1074/jbc.M111.244038

Ricard-Blum, S. (2011). The Collagen Family. *Cold Spring Harbor Perspectives in Biology*, *3*(1), a004978. https://doi.org/10.1101/cshperspect.a004978

Richter, E. A., & Hargreaves, M. (2013). Exercise, GLUT4, and skeletal muscle glucose uptake. *Physiological Reviews*, *93*(3), 993–1017. https://doi.org/10.1152/physrev.00038.2012

Russell, A. J., DuVall, M., Barthel, B., Qian, Y., Peter, A. K., Newell-Stamper, B. L., Hunt, K., Lehman, S., Madden, M., Schlachter, S., Robertson, B., Deusen, A. V., Rodriguez, H. M., Vera, C., Su, Y., Claflin, D. R., Brooks, S. V., Nghiem, P., Rutledge, A., … Koch, K. (2023). Modulating fast skeletal muscle contraction protects skeletal muscle in animal models of Duchenne muscular dystrophy. *The Journal of Clinical Investigation*, *133*(10). https://doi.org/10.1172/JCI153837

Ryan, T. E., Schmidt, C. A., Tarpey, M. D., Amorese, A. J., Yamaguchi, D. J., Goldberg, E. J., Iñigo, M. M. R., Karnekar, R., O'Rourke, A., Ervasti, J. M., Brophy, P., Green, T. D., Neufer, P. D., Fisher-Wellman, K., Spangenburg, E. E., & McClung, J. M. (2020).

PFKFB3-mediated glycolysis rescues myopathic outcomes in the ischemic limb. *JCI Insight*, *5*(18). https://doi.org/10.1172/jci.insight.139628

Ryan, T. E., Yamaguchi, D. J., Schmidt, C. A., Zeczycki, T. N., Shaikh, S. R., Brophy, P., Green, T. D., Tarpey, M. D., Karnekar, R., Goldberg, E. J., Sparagna, G. C., Torres, M. J., Annex, B. H., Neufer, P. D., Spangenburg, E. E., & McClung, J. M. (2019, August 20). *Extensive skeletal muscle cell mitochondriopathy distinguishes critical limb ischemia patients from claudicants*. American Society for Clinical Investigation. https://doi.org/10.1172/jci.insight.123235

Salin, K., Auer, S. K., Rey, B., Selman, C., & Metcalfe, N. B. (2015). Variation in the link between oxygen consumption and ATP production, and its relevance for animal performance. *Proceedings of the Royal Society B: Biological Sciences*, *282*(1812), 20151028. https://doi.org/10.1098/rspb.2015.1028

Schiaffino, S., & Reggiani, C. (2011). Fiber Types in Mammalian Skeletal Muscles. *Physiological Reviews*, *91*(4), 1447–1531. https://doi.org/10.1152/physrev.00031.2010

Schmidt, C. A., Amorese, A. J., Ryan, T. E., Goldberg, E. J., Tarpey, M. D., Green, T. D., Karnekar, R. R., Yamaguchi, D. J., Spangenburg, E. E., & McClung, J. M. (2018). Strain-Dependent Variation in Acute Ischemic Muscle Injury. *The American Journal of Pathology*, *188*(5), 1246–1262. https://doi.org/10.1016/j.ajpath.2018.01.008

Schmidt, C. A., Fisher-Wellman, K. H., & Neufer, P. D. (2021). From OCR and ECAR to energy: Perspectives on the design and interpretation of bioenergetics studies. *The Journal of Biological Chemistry*, *297*(4), 101140. https://doi.org/10.1016/j.jbc.2021.101140

Schmidt, C. A., Goldberg, E. J., Green, T. D., Karnekar, R. R., Brault, J. J., Miller, S. G., Amorese, A. J., Yamaguchi, D. J., Spangenburg, E. E., & McClung, J. M. (2020). Effects of fasting on isolated murine skeletal muscle contractile function during acute hypoxia. *PLoS ONE*. https://doi.org/10.1371/journal.pone.0225922

Shamsadeen, N. M., & Duncan, C. J. (1989). Effects of anoxia on cellular damage in the incubated mouse diaphragm. *Tissue and Cell*, *21*(6), 857–861. https://doi.org/10.1016/0040-8166(89)90037-2

Shishmarev, D. (2020). Excitation-contraction coupling in skeletal muscle: Recent progress and unanswered questions. *Biophysical Reviews*, *12*(1), 143–153. https://doi.org/10.1007/s12551-020-00610-x

Shoshan, M. C. (2012). 3-bromopyruvate: Targets and outcomes. In *Journal of Bioenergetics and Biomembranes*. https://doi.org/10.1007/s10863-012-9419-2

Shrieve, D. C., Deen, D. F., & Harris, J. W. (1983). Effects of extreme hypoxia on the growth and viability of EMT6/SF mouse tumor cells in vitro. *Cancer Research*, *43*(8), 3521–3527.

Singh, R., Lemire, J., Mailloux, R. J., & Appanna, V. D. (2008). A Novel Strategy Involved Anti-Oxidative Defense: The Conversion of NADH into NADPH by a Metabolic Network. *PLoS ONE*, *3*(7), e2682. https://doi.org/10.1371/journal.pone.0002682

Smith, I. J., Lecker, S. H., & Hasselgren, P.-O. (2008). Calpain activity and muscle wasting in sepsis. *American Journal of Physiology - Endocrinology and Metabolism*, *295*(4), E762–E771. https://doi.org/10.1152/ajpendo.90226.2008

Srikanthan, P., & Karlamangla, A. S. (2014). Muscle mass index as a predictor of longevity in older adults. *The American Journal of Medicine*, *127*(6), 547–553. https://doi.org/10.1016/j.amjmed.2014.02.007

Stamati, K., Mudera, V., & Cheema, U. (2011). Evolution of oxygen utilization in multicellular organisms and implications for cell signalling in tissue engineering. *Journal of Tissue Engineering*, *2*(1), 2041731411432365. https://doi.org/10.1177/2041731411432365

Strassburg, S., Springer, J., & Anker, S. D. (2005). Muscle wasting in cardiac cachexia. *The International Journal of Biochemistry & Cell Biology*, *37*(10), 1938–1947. https://doi.org/10.1016/j.biocel.2005.03.013

Sun, M., Chen, S., Adams, S. M., Florer, J. B., Liu, H., Kao, W. W.-Y., Wenstrup, R. J., & Birk, D. E. (2011). Collagen V is a dominant regulator of collagen fibrillogenesis: Dysfunctional regulation of structure and function in a corneal-stroma-specific Col5a1-null mouse model. *Journal of Cell Science*, *124*(23), 4096–4105. https://doi.org/10.1242/jcs.091363

Tarpey, M. D., Amorese, A. J., Balestrieri, N. P., Fisher-Wellman, K. H., & Spangenburg, E. E. (2019). Doxorubicin causes lesions in the electron transport system of skeletal muscle mitochondria that are associated with a loss of contractile function. *Journal of Biological Chemistry*. https://doi.org/10.1074/jbc.RA119.008426

Tarpey, M. D., Amorese, A. J., Balestrieri, N. P., Ryan, T. E., Schmidt, C. A., McClung, J. M., & Spangenburg, E. E. (2018). Characterization and utilization of the flexor digitorum brevis for assessing skeletal muscle function. *Skeletal Muscle*, *8*(1), 14. https://doi.org/10.1186/s13395-018-0160-3

Thaveau, F., Zoll, J., Rouyer, O., Chafke, N., Kretz, J. G., Piquard, F., & Geny, B. (2007). Ischemic preconditioning specifically restores complexes I and II activities of the mitochondrial respiratory chain in ischemic skeletal muscle. *Journal of Vascular Surgery*, *46*(3), 541–547. https://doi.org/10.1016/j.jvs.2007.04.075

Valentino, T., Figueiredo, V. C., Mobley, C. B., McCarthy, J. J., & Vechetti, I. J. (2021). Evidence of myomiR regulation of the pentose phosphate pathway during mechanical load-induced hypertrophy. *Physiological Reports*, *9*(23), e15137. https://doi.org/10.14814/phy2.15137

Wang, H., Hai, S., Liu, Y., Liu, Y., & Dong, B. (2019). Skeletal Muscle Mass as a Mortality Predictor among Nonagenarians and Centenarians: A Prospective Cohort Study. *Scientific Reports*, *9*(1), Article 1. https://doi.org/10.1038/s41598-019-38893-0

Wertheimer, E., Sasson, S., Cerasi, E., & Ben-Neriah, Y. (1991). The ubiquitous glucose transporter GLUT-1 belongs to the glucose-regulated protein family of stress-inducible

proteins. *Proceedings of the National Academy of Sciences*, *88*(6), 2525–2529. https://doi.org/10.1073/pnas.88.6.2525

Wright, V. P., Klawitter, P. F., Iscru, D. F., Merola, A. J., & Clanton, T. L. (2005). Superoxide scavengers augment contractile but not energetic responses to hypoxia in rat diaphragm. *Journal of Applied Physiology (Bethesda, Md.: 1985)*, *98*(5), 1753–1760. https://doi.org/10.1152/japplphysiol.01022.2004

Xia, Y., Warshaw, J. B., & Haddad, G. G. (1997). Effect of chronic hypoxia on glucose transporters in heart and skeletal muscle of immature and adult rats. *American Journal of Physiology-Regulatory, Integrative and Comparative Physiology*, *273*(5), R1734–R1741. https://doi.org/10.1152/ajpregu.1997.273.5.R1734

Xu, H., & Van Remmen, H. (2021). The SarcoEndoplasmic Reticulum Calcium ATPase (SERCA) pump: A potential target for intervention in aging and skeletal muscle pathologies. *Skeletal Muscle*, *11*, 25. https://doi.org/10.1186/s13395-021-00280-7

Zaied, A. A., Ushio-Fukai, M., Fukai, T., Kovacs-Kasa, A., Alhusban, S., Sudhahar, V., Ganta, V. C., & Annex, B. H. (2023). Pentose Pathway Activation Is Superior to Increased Glycolysis for Therapeutic Angiogenesis in Peripheral Arterial Disease. *Journal of the American Heart Association*, *12*(7), e027986. https://doi.org/10.1161/JAHA.122.027986

Zhang, S. J., Andersson, D. C., Sandström, M. E., Westerblad, H., & Katz, A. (2006). Cross bridges account for only 20% of total ATP consumption during submaximal isometric contraction in mouse fast-twitch skeletal muscle. *American Journal of Physiology - Cell Physiology*. https://doi.org/10.1152/ajpcell.00578.2005

Zhu, H., Hu, X., Feng, S., Jian, Z., Xu, X., Gu, L., & Xiong, X. (2022). The Hypoxia-Related Gene COL5A1 Is a Prognostic and Immunological Biomarker for Multiple Human Tumors. *Oxidative Medicine and Cellular Longevity*, *2022*, 6419695. https://doi.org/10.1155/2022/6419695

Zieseniss, A. (2014). Hypoxia and the modulation of the actin cytoskeleton – emerging interrelations. *Hypoxia*, *2*, 11–21. https://doi.org/10.2147/HP.S53575

Appendix

Animal Care and Use Committee
003 Ed Warren Life Sciences Building | East Carolina University | Greenville NC 27834 – 4354
252-744-2436 office | 252-744-2355 fax

September 28, 2022

Espen Spangenburg, Ph.D.
Department of Physiology, ECU

Subject: Protocol Q337b, original approval date 06/25/2021.

Dear Dr. Spangenburg:

The amendment#3 to your Animal Use Protocol entitled, “Defining mechanisms of skeletal muscle function” (AUP#Q337b) was reviewed by this institution's Animal Care and Use Committee on 09/27/2022. The following action was taken by the Committee:

"Approved as submitted"

Please contact Aaron Hinkle prior to any hazard use

A copy of the protocols is enclosed for your laboratory files. Please be reminded that all animal procedures must be conducted as described in the approved Animal Use Protocol. Modifications of these procedures cannot be performed without prior approval of the ACUC. The Animal Welfare Act and Public Health Service Guidelines require the ACUC to suspend activities not in accordance with approved procedures and report such activities to the responsible University Official (Vice Chancellor for Health Sciences or Vice Chancellor for Academic Affairs) and appropriate federal Agencies. Please ensure that all personnel associated with this protocol have access to this approved copy of the AUP/Amendment and are familiar with its contents.

Sincerely yours,

Susan McRae, Ph.D.
Chair, Animal Care and Use Committee

SM/GD

enclosure